2007

A ray technique to calculate the multiple reflected and transmitted waves in layered media

Jeff Sadler
University of Windsor

A Ray Technique to Calculate the Multiple Reflected and Transmitted Waves in Layered Media

by
Jeff Sadler

A Dissertation
Submitted to the Faculty of Graduate Studies
though the Department of Physics
in Partial Fulfilment of the Requirements for
the Degree of Doctor of Philosophy at the
University of Windsor

Windsor, Ontario, Canada
2007

Your file Votre référence
ISBN: 978-0-494-35077-5
Our file Notre référence
ISBN: 978-0-494-35077-5

Abstract

In this thesis we consider the problem of calculating the propagation of acoustic waves within an ideal solid isotropic multilayer plate structure. In such a situation the process of mode conversion as the wave interacts with each interface of the plate creating an increasing number of waves to track, and to perform calculations on as the wave propagates within the layered media. We choose to explore this problem by examining the ray paths of the multiple reflections within the plate structure, and show that upon careful consideration many of these paths will travel equivalent distances in time and space becoming coincident. The principle of superposition can then be used to combine these coincident paths; this reduces the number of waves to track, and simplifies the problem so that the necessary calculations can be performed in a time efficient manner. In addition the use of the a ray model gives initial results which are independent of properties of the incident acoustic waves

In the first part of this thesis the theoretical basis of the ray technique will be overviewed, and the existence of equivalent and coincident paths in the single and multi-layer plate structure is examined. Next it will be described how a second set of calculations can be used to consider the attenuation of the media, recalculate the time of flight and horizontal distances of the rays due to altering the thickness of the layers of the plate, and extend the ray based results to more realistic acoustic waves. By including these factors as a separate set of calculations creates a more flexible technique, as the attenuation, thickness of the plate, or acoustic wave's space-time domain properties can be changed without recalculating the initial amplitude results, as long as the other features of the theoretical sample remain constant. Finally, the results of this thesis will examine various cases for validation, comparison to experimental results, and the examination of options for the detection of bonding or disbonding within a typical bonded plate sample.

To my family for their support through the years.

Table of Contents

List of Figures

List of Tables

List of Main Symbols and Notation

A	Amplitude of Wave
α	Attenuation Coefficient
b	Shear Vertical Velocity
c	Longitudinal Velocity
d	Plate Thickness
L	Longitudinal Polarized Wave Path
N	Number of Reflections
ρ	Density
R	Reflection Coefficient
S	Combined Reflection and Transmission Coefficient
T	Transmission Coefficient
tof	Time of Flight
θ	Angle of Wave's Propagation
V	Shear Vertical Polarized Wave Path
v_x	Horizontal Velocity ($v_x = x/tof$)
ω	Angular Frequency
x	Horizontal Distance
χ	Total Distance
Z	Acoustic Impedance

Superscripts And Subscripts

$1, 2, 3..n$	Numerical Layer of Plate
L	Longitudinal Polarized Wave Path
V	Shear Vertical Polarized Wave Path

Chapter 1: Introduction

1.1 Opening Remarks

As a most general description this thesis examines the propagation of waves through a layered plate structure; specifically the multiple reflections and transmissions of ultrasonic waves in a multilayered plate made up of isotropic solid materials. While the focus of this thesis will consider the propagation of ultrasonic waves in the layered plate structure, the problem is also of interest in the area of Optics [1] where electromagnetic waves (i.e. visible light, ultraviolet light, or infrared light) may also travel through a layered plate structure. In either field a variety of theoretical studies have examined the propagation of waves within the layered plate in cases where only a single wave is reflected and transmitted at each interface between the layers of the plate; such as cases of waves travelling at normal incidence, acoustic waves travelling through liquid layers, or acoustic waves with shear horizontal polarization travelling through isotropic solids. In acoustics however, the isotropic solid case requires two waves to be reflected and transmitted at each interface between the layers of the plate. This larger number of waves causes difficulty in the analysis of the problem, and typically one simplifies the problem by using approximations such as assuming plane waves, thin solid layers, or restricting the number and type of reflections to examine in the plate. This problem of examining the propagation of waves within a plate structure is not simply only of academic interest, but is also of practical interest. One such examination of a multilayered structure is found in the study of Oceanography where the sea floor can be analyzed as a Water-Sediment-Bedrock layered

structure. A second is found in the area of acoustics and non destructive testing, where a typical bonded material can be analyzed as a Metal-Adhesive-Metal layered structure. Being able to calculate results for such cases allows for validation of experimental results, and a well as to serve as a guide for experimental results by predicting results and aiding in focusing an experimental study.

1.2 Overview of the Problem

As previously mentioned, in this thesis we will consider the general case of ultrasonic waves travelling at non-normal incidence through a single, or multilayer, ideal plate structure made of isotropic solids. We wish to formulate a method to calculate the multiple reflections and transmissions of the acoustic waves within the plate structure, as well as the acoustic waves transmitted from the plate to a surrounding media. In doing so we do not wish to be restricted to cases such as examining only normal incidence, liquid layers, thin layers, specific material configurations, or examining only a specific reflection and transmission paths. Yet, in addition we wish that the calculation of the acoustic wave's propagation in the plate be completed in a relatively timely manner, thus it would be beneficial if these calculations can be completed on a typical modern computer, and not require the processing power of multiple supercomputers, at least for the cases of a single layer and two layer plate samples. As well as the creation of the technique, this thesis will also examine the practical side of being able to calculate such results. Here we will compare the results of the ray based technique with experimental results, showing how

these results can provide a theoretical basis for comparison with experimental results, as well as being able to explain results which are initially unexpected from the experimental setup. In addition, we examine the specific application of the non destructive evaluation of the bonding in a typical bonded plate (Section 6.3), where one is interested in the detection of the bonding, or disbonding, between the Metal-Adhesive, and Adhesive-Metal interfaces.

The goal of creating this technique will be achieved by treating the acoustic waves in the multilayer plate structure as rays, as initially described by Sadler and Maev in references [2] and [3]. Here the time and space distribution of the acoustic wave are temporarily ignored, and one concentrates on examining the various paths the rays travel within the plate, and calculating the amplitude of these paths relative to the incident wave. It will be shown that due to the plate structure of the sample, that as the acoustic wave traverses each layer in the plate it travels a path segment with properties (specifically the time of flight, horizontal distance, and total distance in traversing a layer of the plate) which are independent of the direction of travel of the wave, as well as the previous path travelled by the wave. Because of this equivalence in the path segments, the examination of the various possible paths along which the acoustic waves can travel finds that many of these paths will be equivalent in total. That is, after undergoing a number of reflections (and transmissions), two (or more) acoustic waves may have travelled the same total horizontal distance, and travelled the same time of flight to this point. As the acoustic waves now lie coincident on the same path in space-time, it is possible to combine the multiple acoustic rays into a single acoustic ray via superposition; thus reducing the

number of acoustic waves to consider. Without considering the superposition of the equivalent paths the problem of calculating the multiple reflections of the acoustic waves within a plate quickly becomes impractical to consider. For example, in the case of an acoustic wave travelling within a single layer solid plate at non-normal incidence the number of rays would double after each reflection. Thus, after only 20 reflections over 1 million rays would exist inside the plate. For each of these rays it would be necessary to make calculations describing additional reflected and transmitted rays, as well as being required to store the data describing these rays. In contrast, in the situation presented in this thesis the number of rays to consider increases in a linear manner, and after 20 reflections only 42 unique wave paths exist. Thus this analysis of the wave paths, and the resulting utilizations of the principle of superposition is able to reduce the overall number of waves to track, which in turn reduces the number of calculations needed to produce a numerical solution, and allows the problem to be solved in a time efficient manner.

In addition to reducing the complexity of the problem, the technique presented in this thesis also presents an advantage in that the acoustic waves in the plate are treated as rays, where only the initial considerations only consider the amplitude, time of flight, angle of travel, and distance travelled through the plate of the acoustic ray. This produces initial results which are independent upon the frequency, physical size, and time domain properties of the incident acoustic wave. A second set of calculations can then be used to extend the acoustic rays into more realistic waves by considering the spacial and time domain changes of the acoustic waves, and consider any additional superposition effects due to the waves overlapping in the time and space domains. This use of two separate

sets of calculations allows the theory to test a variety of acoustic sources using one set of results (under the condition of constant sample structure).

1.3 Literature Review

In this section we will briefly overview some of the relevant literature which relates closest to the situation presented in this thesis. Examined will be options where authors have investigated the multiple reflections of an acoustic wave in the plate structure via a variety of methods; such as restricting the sample to consider only liquid layers, thin layers, or restricting the case to examine normal incidence, or analyzing only those reflections with the largest amplitude. In addition, we will examine the commonly used plane wave methods, which simplify the description of the multiple acoustic waves in the plate structure to a finite number of plane waves (waves of infinite size in the time and space domain). Finally we will briefly overview the idea of boundary conditions due to their usage, and importance, in this theory.

1.3.1 Overview of Multiple Reflection Calculation Methods and Solutions

The coupling between longitudinal and shear vertical (transverse) waves in an isotropic solid, creates a problems in analyzing a single, or multilayer, plate due to the large number of wave paths to consider. Thus many studies of waves in layered media, and multiple scattering problems, consider cases with liquid layers [4,5], shear horizontal waves [6–10],

or waves with normal incidence [11,12]. Such situations eliminate the possibility of mode conversions between the acoustic wave polarizations, thus only one polarization is allowed to propagate in the sample and overall the problem becomes simpler to analyze. While these situations may only consider the propagation of a single acoustic wave polarization, and may only examine a single layered structure, these papers do have their advantages in that they obtain analytical solutions, analyze specific experiments or experimental features, or are usable in situations not suitable for this theory such as anisotropic media, or cylindrical samples. Those studies which choose to deal with solid materials, and allow for mode conversions, often utilize a infinite plane waves approach [13–15] to aid in the analysis the problem. (Section 1.3.2 gives details on this literature, and Section 1.4.3 gives a comparison of the plane wave and ray technique methods.) Alternate approaches exist as well, some authors choose to calculate only the reflections and mode conversions which are deemed important to the specific problem being considered [16], or make approximations such as literature dealing with thin bonding layers [17–20]. In the following sections we will briefly examine some of these options which have been used to the calculate the multiple reflections in a multilayer plate.

1.3.1.1 Literature Noting Equivalent Paths or Superposition of Paths

While some authors [21,22] have pictured the intersecting pairs and coincident rays for acoustic waves in a single layer plate via ray diagrams similar to the ray diagram shown in this thesis (Figure 2.3 in Section 2.1), neither of these authors have used this observation to their advantage in their theories, or expand their considerations to a multilayer plate.

Instead both authors consider alternative plane wave methods to examine the existence and propagation of Lamb waves in a plate.

The importance of examining all ray paths, and the superposition of the ray paths is found in a series of papers Blonigen and Marston [23–25]. Here the authors discuss the case of theoretically modelling and experimentally observing the backscattering contributions from cylindrical shells immersed in water. In cases with air filled cylindrical shells the authors note that a helical wave may make successive circumnavigations around the sample and that one must consider these superpositions theoretically and experimentally. In cases with air filled cylindrical shells the authors find cases where the length of the tone bursts of the incident wave are of sufficient duration ($150\mu s$) to require the consideration of the superposition of helical waves' contributions which travel successive circumnavigations of the cylinder [23]. The authors also examined the case of a fluid filled cylinder and found it was important to consider the possibility of rays crossing the the fluid filled interior exciting additional helical rays. These results superposed with the helical paths travelling in the cylinder, are found to produce larger backscattered waves [24]. In short these authors find it is important to consider all wave paths, and the superposition of these paths. In the results section of this thesis similar situations are observed where the superposition of multiple wave paths must be considered to fully explain the results.

1.3.1.2 Single Polarization Cases

As previously mentioned, by restricting the problem to examine cases which deal only with shear horizontal waves [6–10], liquid layers [4, 5], or normal incidence [11, 12]; one is able examine situations where mode conversion is no longer an issue, and only a single reflected and transmitted wave is created when an acoustic wave interacts with the interfaces of a plate structure. With the reduced number of waves to track it becomes easier to analyze the problem at hand, and as well provide an opportunity to form an analytic solution for the reflection or transmission coefficient, especially in those cases dealing with a single layer plate. Such studies of single polarizations within a multilayer structure are of course not limited to only the traditional flat plate [5, 11, 12], but also include cylindrical samples such is shown by Cai [6–8].

Caviglia and Morrow [11] examine the case of normal incidence waves in a multilayer plate with an arbitrary number of layers, where the layers are formed from isotropic or anisotropic, homogeneous, linear materials. The authors repeatedly use the continuity conditions of perfectly bonded boundary conditions to find a system of time domain equations yielding the reflected and transmitted waveforms in the half-space surrounding the plate structure. The authors provide closed form solutions for this system equations for the specific case of a single layer of material, and as well provide an algorithm which is able to solve the general system of equations in a finite number of steps. The authors note that by using a time domain solution (rather than a frequency domain solution common in plane wave methods), the equations provide for a description which, in their own words

"is often the most direct and natural representation of a material behaviour and can be expected to provide results and insights which may be hard to arrive at in the frequency domain through the eventual inverse Fourier transform." While the authors are able to provide symbolic results via a system of equations, and closed form solutions for specific cases, it should be noted that this does not mean that these results can be easily analyzed by visual inspection. In this case these closed formulas are quite detailed, even for the simple cases.

Bamberger and Greenwood [5] also examine the case of acoustic waves at normal incidence, but consider a situation with both solid and liquid media. The authors consider a case where a liquid, or slurry, flows through a pipeline, and are interested in the creation of a system to measure the properties (density, velocity, and attenuation) of the liquid or slurry in the pipe. To do this the authors only consider the major paths with in the sample; those travelling multiple reflections in the steel plate only, or those travelling multiple reflections in the liquid only. To obtain the measurement of the impedance of the liquid (where $Z = \rho c$ with Z: impedance ρ: density, and c: velocity) the authors consider a sensor placed at normal incidence on the steel plate, effectively treating the system as a steel plate located between the sensor and liquid half-space. Using a pitch catch mode to obtain 20 echoes of the multiple reflections in the steel plate, the authors examine the ratio of the amplitudes of the multiple pulses, and use this to measure the impedance of the liquid, via the known reflection coefficients for the case of normal incidence. By using the ratio of the pulses, and not the absolute size of the pulse, the results are independent of the sensor's initial voltage and the system becomes self-calibrating. In addition the

authors also examine the multiple reflections within the liquid layer. Here an examination of the time of flight of the multiple reflections is used to measure the velocity of the liquid, while an examination of the amplitude of the reflections within the liquid layer is used to measure the attenuation of the media relative to water flowing through the pipe. Any additional reflections in the steel plate are ignored, and the system is analyzed as a single layer of liquid between the two half-spaces of the pipe

Greenwood et. al. [9,10] also consider the case of a measuring the properties of a liquid using the information from solid-liquid boundary, but utilize shear horizontal waves, as they are interested in discerning the viscosity of the liquid. Such a measurement is possible in cases with shear horizontal waves, because the impedance of the liquid used in the reflection coefficient is related to the liquid's viscosity (here $Z = \sqrt{\omega\rho\eta/2}$ with Z: impedance ω: angular frequency, ρ: density, and η: viscosity). Similarly to the case examined by Bamberger and Greenwood [5] the ratio of the multiple reflections of the shear wave within the solid sample is used to create a system independent of the transducer's voltage. (Here the experimental system uses the results of 28 echoes). It should be noted that the authors are not using a typical plate system, but examine the multiple reflections in a triangular wedge made of silica. Here the reflections proceeded starting at the transducer on one side of the triangular wedge, travel to the base of the triangle immersed in a liquid, reflect off the silica-liquid interface at an angle, and then travel to the opposite side of the triangular wedge. Here the acoustic wave is incident at normal incidence with the wedge, and reflects, returning to the transducer on the same path. With such a system the acoustic wave will interacts twice with the liquid interface,

thus removing the square root from the analysis in the amplitude of the wave, making for a simpler symbolic analysis.

Finally, in a series of papers Cai [6–8] considers the case of a solid layered cylinder, embedded in a linear elastic half-space, where the cylinder acts as a scatter of the incident shear horizontal waves. Here the cylinder possesses one layer for the outer circular ring, and a second later forming a solid cylindrical core; where Cai considers the multiple reflections in the cylinder's outer ring, and chooses to ignore those waves travelling through the cylinder. The usage of the shear horizontal wave simplifies the analysis of the system such that Cai is able to repeatedly use the results for the reflection of waves incident on a cylindrical interface, and is able show the repeating pattern from the application of these coefficients caused by the multiple reflections within the sample. This pattern is able to be used to find the overall symbolic format of the waves leaked from the media. While the final result is a symbolic equation, this result must be examined numerically to be of practical use as its constituent parts are too complicated for easy symbolic analysis. In the final paper [8] Cai is able to expand the results from a single scatterer into an regularly spaced array of scatterers.

1.3.1.3 Thin Layers

Technically here one does not attempt to calculate the multiple refections in the thin layer, but instead uses plane waves and the restriction of a very thin layer of material to simplify the calculations of the multiple reflections. While Sadler et. al [17, 18] use

perturbation methods, Rokhlin and Huang [19,20] use the transfer matrix method to deal with the problem at hand. Both analysis find that it is possible to create an approximation where the multiple reflections from a thin layer of material between two half-spaces can be accounted for via a single waveform. Here the obvious restriction is that one is restricted to a thin layer of material, which typically is defined to be of a size much less than an acoustic wavelength. A second, less obvious restriction, is that these theories are not initially suited for a multilayer plate situation. Because the assumption is that there exists a single layer located between two half-spaces, any additional reflections with the interfaces between the two bonded plates and the outside-world (transducers, additional plate layers, or the external environment (air or water)) of a real world experimental sample are not considered. In this way one must place restrictions on the experiment such as examining a shorter time domain, or requiring the use of thicker plates; or alternatively expanding the theory or calculation models to consider these reflections. The advantages, in comparison with the theory presented here, is these theories present the option of being able to consider a thin layer which is anisotropic [17–20] and nonlinear [17,18,26], and as well the theories provide a symbolic result to analyze.

1.3.1.4 Examining only Reflections Deemed Important

A final approach relies on calculating only reflections and transmissions which are deemed important for the situation in question. The disadvantage of such a method is that a case by case approach is required, where eliminating certain mode conversions for one case may not be appropriate for another case. As well, there is the possibility

that one may eliminate waves which are deemed negligible, but the superposition of many seemingly negligible waves could produce a non-negligible result. The advantages however include the possibility of gaining further insights to the problem by being able to describe the problem in a more detailed mathematical form, as well as possibly yielding a final analytical solution to the problem.

One useful example for this method is found in an article by Chapman and Chapman [16], whose area of interest is the study of ocean acoustics. In this paper the plate structure is designed to mimic the sea floor and is composed of the following layers: a half-space water, a sediment layer (of known thickness), and a half-space bedrock 'basement'. The authors choose to eliminate ray paths which, in their own words, "contribute insignificantly to the final results", by viewing multiple reflections as perturbations and eliminating the high order terms. Physically the authors note their mathematical restrictions would cause no mode conversion at the sediment-water boundary, here the longitudinal wave is reflected the same as at a liquid-liquid boundary. As well, at this interface the restrictions cause a shear vertical polarized wave to be fully reflected with a phase inversion. The approach however does allow for mode conversions at the sediment-bedrock interface, but no more than two mode conversions are allowed on any ray path. The authors find such an approach provides a method which is easy to both visualize and understand, and reproduces the thin sediment effects of a real world thin floor created due to evanescent waves and interface waves. As well this approach also is able to provide an approximate closed form analytical expression for the reflection coefficient. While such an approach of removing selected ray paths may not be usable in all cases, here the

authors have a mathematical basis for the the removal of these waves, corresponding to a perturbation sequence where higher order (smaller terms) are neglected. The approach also corresponds back to the physical interpretation of the problem where the sediment layer has very low longitudinal velocity (close to that of water), and nearly zero shear velocity. This gives nearly full longitudinal reflection at the sediment-water interface, and only a small mode conversion is possible at the sediment-bedrock interface, This allows for a neglection of these terms, and thus the mathematical assumptions are physically validated.

1.3.2 Plane Wave Methods

A typical method for dealing with a multilayer plate made of solid isotropic media, which includes the possibility of mode conversions, is to consider the acoustic wave as a plane wave. Here the situation is simplified as the acoustic plane wave exists in all locations in space and time, in all layers of the plate. This allows the acoustic waves in the plate to be simplified into a total of at the most four waves[1], or acoustic potentials, in each layer of the media [13–15]. In these theories [13–15] one obtains a transfer matrix relating the displacement and stress of the acoustic waves at one side of a layer of the plate to the displacement and stress of the acoustic waves on the other side of the layer. Next, by considering the boundary conditions (Section 1.5.1) at each interface, the multiple transfer matrices can be combined into a single matrix which relates the acoustic waves

[1]The possibility of four waves comes from the case of a solid plate, where there exists one longitudinal, and one shear vertical polarized wave travelling away from both interfaces in each layer of the plate.

on one side of the sample, to the acoustic waves on the opposite side of the sample. In most cases the perfectly bonded interface is examined [13–15], and the final transfer matrix is formed by a series of matrix multiplications of the individual transfer matrices. Other cases examine the necessary alterations for using the imperfectly bonded boundary conditions [27], and as well extensions of the plane wave theories have been created to allow for the consideration of anisotropic layers [28, 29], and considering the effects of material damping [13].

The results from the plane wave theories are typically examined in the frequency versus wavenumber domain (or frequency vs. phase velocity domain), this produces dispersion curves which when examined indicate which Lamb modes can be excited by the multilayer structure. The location of these Lamb modes in frequency-wavenumber space varies depending on the plate structure and can aid in the non-destructive evaluation of the material. Such a discussion of Lamb waves and their use in NDE evaluation is well beyond the scope of this thesis and we defer the reader to other literature reviews [13, 30] and texts [14, 15, 31, 32] for more information on these subjects. In addition to the Lamb modes generated in the plate structure, it is also possible to examine the change in the amplitude of the reflected wave with angle (or frequency, or material parameters) yielding the reflectance function. This reflectance function can be used in further theoretical calculations, such in the calculation of V(z) curves, where the response of the acoustic wave reflected from a plate is analyzed as the distance of the transducer from the plate is changed [33, 34].

The advantage of these plane wave approaches is that the simplification of dealing

with a small number of waves, allows one to produce such theories as those by Lowe [13], Brekhovskikh [14], or Briggs [15], where in certain cases one can obtain a closed form solution for the reflectance function, and a mathematical formula from which one can find the Lamb modes in a plate structure. As well, in these transfer matrix methods, the number of layers can be increased indefinitely as the addition of each layer typically only causes a matrix multiplication to be added. It should be noted there can be problems with the transfer matrix method computations at high frequency-thickness combinations, this however is a problem with the computer driven calculations, not the theory itself. Alternate theories using a similar idea to the transfer matrix method, but with altered mathematics, known as global matrix methods [13] do not have this computational problem at high frequency-thickness combinations, but become more computationally difficult as the matrices generated increase in size with the number of layers. In addition, recent literature by Rokhlin and Wang [35] propose using a stiffness matrix method, which is found to be able to consider anisotropic media, and is stable at high frequency and layer thicknesses.

There are of course also disadvantages to using such plane wave methods. While the approximation of the multiple reflections of the acoustic waves in the plate via four plane waves has simplified the problem to yield a manageable solution, this approximation has caused the physical details of the multiple reflections, and multiple leaky waves to be effectively lost from the results. In addition the plane wave methods require recalculation for each frequency of the acoustic wave, making the examination high bandwidth waveforms computationally intensive, and as well requires calculation of the results over multiple

angles of incidence to alter the space domain properties of the wave. Alternatively the technique presented in this thesis allows for a point by point expansion of the wave in both space and time as described in Section 5.3.1, as well as allows for the results of a more realistic acoustic wave to be approached from the superposition of plane waves.

1.3.3 General information on Boundary Conditions

The location of the change between the two regions with different acoustic impedances[2] in a material is referred to as an interface or boundary. This boundary could be an alteration in the material's acoustic properties, or a connection between two different materials. As an acoustic wave travels from the first region to the second it interacts with this interface producing reflected and transmitted waves with propagate away from the interface. The amplitudes of these wave are in general dependent on the relative impedances of the two media, as well as the incident angle[3] of the acoustic wave interacting with the boundary. Via the process known as mode conversion, different polarizations of the acoustic wave may also be generated at the boundary depending on the angle of incidence of the acoustic wave on the boundary, as well as the polarization of the incident wave, the states of the material (liquid or solid) on each side of the boundary, and the symmetry of the material (isotropic or anisotropic). The exact relation between the amplitudes of these reflected and transmitted waves is dependent upon the boundary in question, and is found via a set of equations referred to as boundary conditions. These

[2]The acoustic impedance of a material is the product of the material's density and velocity.

[3]The incident angle measures the angle between the incident acoustic wave, and the normal to the interface.

conditions mathematically describe the interface connecting the two media, and take into account the type of interface formed between the two media; for example, metallurgical solid-state bonding, dry contact, or lubricated contact, all affect the structure of the interface differently and determine the exact boundary conditions that must be considered. In general O'Neill et al. [26], Rokhlin and Wang [36], and Rokhlin and Marom [37] all agree on two different general categories to describe the boundaries, and associated boundary conditions, for an interface connecting two solids. The first case describes the situation when the materials are fully bonded, and is the situation which will be examined in this thesis. This situation, and the associated set of boundary conditions will be discussed in more detail in Section 1.5.1 and Appendix A. The second case describes the situation when the two materials are not bonded; here the two pieces of material creating the boundary may connect and disconnect in a clapping manner [26,38] (a kissing or clapping interface), or the two materials may remain connected and move in a sliding motion alternating between sliding and sticking motions at an interface with friction [26, 39] (a slipping or sliding interface). These solutions for the clapping and slipping interfaces are not limited to boundary condition method only. Richardson [40] has developed a solution to the clapping interface using the acoustic equation of motion with the boundary conditions used to determine the initial conditions of the open and closed state. In addition more advanced boundary conditions also exist Rokhlin and Wang [36], Rokhlin and Marom [37] both note that the slipping interface is an ideal form for two solids with a thin layer of ideal liquid between them, which is examined by Hedberg and Rudenko [41]. As well O'Neill, Sadler, Severin, and Maev [42] use a boundary condition approach in one dimension to show that boundary conditions can describe an interface with a nonlinear thin layer.

Further details on such thin layer cases are discussed in Section 1.3.1.3.

1.4 Comparison of the Various Theoretical Methods with the Ray Based Technique

As one of the the goals of this thesis is the creation of a new technique the question arises of how the ray based technique compares to the existing techniques. In this section we will briefly compare the various methods used to analyze and calculate the multiple reflections of an acoustic wave within a plate structure; noting the relative advantages and disadvantages of these methods in relation to the ray based technique presented in this thesis. In particular, because the the plane wave technique has presented a successful method to examine the propagation of acoustic waves in a plate, the ray technique and plane wave techniques will be compared in the most detail (Section 1.4.3). Additional details and references to the theories in question may be found in the literature review section of this thesis (Section 1.3).

1.4.1 Common Factors

The ray based technique, plane wave theories, and the alternate methods utilized to examine the propagation of an acoustic wave share a commonality in their overall setup, and restrictions in examining the problem. Here the theories work under a similar set of theoretical considerations, briefly outlined these restrictions requires:

- Perfectly parallel plates, with smooth bonded interfaces (usually perfectly bonded).
- Linear, homogeneous, isotropic, non dispersive, non attenuative materials.
- Known layer properties (layer thickness and material parameters).

These restrictions form the base assumptions for a typical multilayered study, and typically the author allows for the opposite effect, most often allowing for cases examining attenuative, or anisotropic materials. In addition the plane wave and ray technique theories share additional commonalities as both techniques become more computationally time consuming as the number of layers increases, and in addition both techniques require calculations to be done for each angle of incidence. It is the requirements on the calculations for the various frequencies of the incident wave, and the ability to deal with the general isotropic solid case, versus specific cases which differ between the theories. These, and other notable differences will be discussed in the next section.

1.4.2 Notable Differences

While the theories all share a common link as they both examine the propagation of acoustic waves in a multilayer plate, the approaches to yield an end result are quite different. For those theories which examine specific cases such as; normal incidence, liquid layers, single layer media, or thin layers, one deals with an overall simpler analysis, where the increased restrictions placed on the model often allow the theories to yield analytic results (typically for a single layer media case), or yield a finite set of equations and a

method to find a numerical solution. In comparison the ray technique does not provide for simple symbolic results, but provides the advantage of allowing for a wider range on the restrictions in plate structure. For those methods, such as examined by Chapman and Chapman [16], where only those important ray paths are examined, such a solution is only valid for a very specific case (here the ocean floor). The ray based technique allows for a more flexible arrangement of layered materials, and in addition it is found in this thesis that many insignificant results, when combined, can yield visible effects on the results, and these waves need to be considered to fully understand the physics of the problem. Finally, there do exist methods which allow for the consideration of flawed materials (thickness variations, surface defects, material defects) which provide for the examination of samples outside of the theoretical limitations of this work (Section 2.3). Techniques to deal with situations often use finite element methods, finite different methods, and hybrid finite element boundary condition analysis. These techniques are significantly different in their nature and work directly with the acoustic equations of motion, and cannot easily be examined within the scope of this thesis.

1.4.3 Ray Technique versus Plane Wave Techniques

When comparing the ray based technique versus the various plane wave theories one should note that the ray theory provides initial results in the space and time domains, where these results are independent on the frequency of the wave. In contrast the plane wave theory provides initial results in frequency-wavenumber space, which must be recalculated for each frequency considered. When combined these considerations create addi-

tional notable differences when one considers the expansion of the ray, or a plane wave, to a more realistic wave with a specific space-time domain (or frequency-wavenumber domain) distribution. The case of expanding the ray based results to more realistic acoustic waveforms will been discussed in Section 5.3. Here the expansion is easily done for both waves with short time domain behaviour (large frequency domain) and long time domain behaviour (small frequency domain). The frequency independence of the results allows the amplitudes of the waves to be calculated once and used for all time domain waveforms. In contrast, while the plane wave technique easily considers the cases examining a small number of frequency cases, but creating a short pulse would require recalculating plane wave results multiple frequencies. By being able to easily operate at both ends the time domain waveform spectrum provides a distinct advantage for the ray technique in comparison to the plane wave method. The case is similar for the space domain as well, here for a short space domain profiles are easily expanded via the discrete point by point method (Section 5.3.1), while the plane wave techniques require multiple calculations over many wavenumbers (or many angles of incidence). For those longer space domain profiles (near plane waves) the ray and plane wave techniques both require calculations for each wavenumber to be considered, and neither technique has a definitive advantage. Finally, by working in the space-time domain, and actively considering the ray paths, the ray technique provides an other important advantage in that one is able to examine the resulting output from the calculations and determine the path through the media a wave has travelled. In comparison the plane wave technique has combined the multiple reflections at the onset of the theory, and such a determination is not possible. This options allows for the ray technique to provide additional physical insight to the results.

The plane wave techniques do provide for some advantages over the ray based method. First, the plane wave techniques are able to consider waves travelling beyond the critical angles (interface waves, and surface waves), while the ray theory currently does not consider waves at, or beyond, the first critical angle. While such an examination of these cases is beyond the scope of this thesis, it may be possible to examine the ray-based technique in the case beyond the critical angle (the cases of one evanescent, and one real wave, or two evanescent waves). Such a study would eliminate this advantage of the plane wave technique. Finally, the performance of the plane wave techniques are independent of the thickness of the layers of the plate, where in comparison the ray technique requires more reflection calculations as the layer size decreases when one wishes to examine a specific time or space. It is these calculation however which provide the additional physical insight to the problem by being able to examine the multiple reflected paths.

1.5 Physical Effects to Consider

In this section we examine the various physical effects in acoustics related to the problem of acoustic waves travelling through a material, as well as the wave's interactions with the interfaces of a plate structure. Differences between properties such as linearity vs. nonlinearity, isotropy vs. anisotropy, are discussed, as well the factors of boundary conditions, and the effects of attenuation and dispersion. It should be noted that all of these factors will not be included in the theory presented in this thesis, but are discussed in order to understand the options which are included, or excluded.

1.5.1 Boundary Conditions

While previously the boundary conditions have been discussed in terms of a general overview (Section 1.3.3), in this section we will examine the boundary conditions in more detail. In particular, we wish to examine the case commonly referred to as the perfectly bonded boundary conditions, as these are the conditions which will be used to describe the interfaces within the multilayer plates in this thesis. These perfectly bonded conditions can be written to describe the interaction between: two solids, a liquid and a solid, two liquids, or cases where one material is a vacuum. Here the most general case is that of the solid-solid interface, whose results can be reduced to include cases where liquids or vacuum layers are present.

The mathematical conditions of these perfectly bonded, or perfectly welded, interface are written such that both the physical displacement and stress caused by the incident, reflected, and transmitted acoustic waves are continuous across the interface [43–47]. By using these conditions one is able to calculate the amplitudes of the various reflected and transmitted waves relative to the amplitude of the incident wave, thus yielding a set of reflection and transmission coefficients. While many texts [43–47] show various methods to solve this particular situation, typically these methods are shown for cases where one material is a vacuum (a liquid-vacuum, or a solid vacuum interface), or at least one material is a liquid (a liquid-liquid, liquid-solid, or solid-liquid interface). However, Schemerr [47] (who in turn cites Ewing et. al. [48] for their approach) provides a general solution for the reflection and transmission coefficients for the perfectly bonded solid-

solid boundary, which can be altered to also solve cases involving cases where either, or both, layers are liquid(s). While the methods shown by most authors [43–47] typically consider only an isotropic solid, the same general procedure can be expanded to consider cases where the solid is anisotropic in nature. In addition, associated with these perfectly bonded conditions are a set of imperfectly bonded boundary conditions [43] which allow the level of continuity in the boundary conditions to vary in both the normal and shear directions via a set of rigidity parameters. These parameters can be altered such that the conditions range from that of a perfectly bonded interface, to one that is fully disbonded. (In this fully disbonded case the end result is equivalent to the situation where the second material is a vacuum).

It is these perfectly bonded, and imperfectly bonded conditions which are the set of conditions that will describe the structure of the interfaces of the multilayer plates considered in this thesis; where most often we will utilize the case of the perfectly bonded situation. Here the method used to solve the boundary conditions follows the same reasoning as these texts [43–47], but considers the general case of a perfect bond between two isotropic solids. A brief overview of the process can be found in Appendix A.

1.5.2 Linearity vs. Nonlinearity

In the linear theory of acoustics the amplitude of the displacement of the media by the acoustic wave does not alter the properties of the material such as the velocity, density, and elasticity [49,50]. Here the stress and strain in the material follows the linear acoustics

version of Hooke's law, and there exists a linear response between the strength of the input and output signals [50]. This linear approach is suitable as long as the amplitude remains small enough that the changes to strain, pressure, and density in the medium remain small [49, 50]. As the acoustic signal increases in amplitude the amplitude dependent effects can no longer be neglected, and the waves in the nonlinear medium must now be described with nonlinear equations [49–51]. Because the work presented in thesis restricts itself to considering those situations where the materials and acoustic waves produce a linear response, these options for the consideration of nonlinear materials will not be discussed further, and the response of the sample will be assumed to follow the linear acoustics form of Hooke's Law.

1.5.3 Isotropy vs. Anisotropy

As a general definition, an isotropic medium can be said to posses identical properties when examined from any direction. This uniformity can be a result of an ideal case where the medium is truly symmetric, or one in which the medium is so random that on average one direction cannot be discerned from another even though there may be localized anisotropic areas. In the specific case of acoustics [34, 52, 53], this property of being identical in any direction refers to the material's acoustic properties (elasticity, velocity) being uniform in any direction the acoustic wave will travel through the media. In contrast, in an anisotropic material the elasticity of the media is directionally dependent due to the material's crystalline structure. This dependence of the material's elasticity with the direction of the wave in turn causes the the acoustic wave's velocity to be

dependent on the waves propagation direction though the medium.

In both isotropic and anisotropic media, there exist three possible polarized acoustic waves, differences in the velocity of these waves, the orientation of the polarization (the polarization is the direction of displacement with respect to the wave's propagation), and coupling between the three polarizations exist for isotropic and anisotropic media. In the case of an isotropic medium the longitudinal and shear vertical polarizations are coupled together, while the shear horizontal polarization is left uncoupled. This coupling causes a longitudinal or shear vertical wave which is incident upon an isotropic medium, to produce both longitudinal and shear vertical polarized waves in the media. Here the direction of the longitudinal polarization is aligned parallel to the wave's direction of travel, while the two shear polarizations are aligned perpendicular to the wave's direction of travel (and perpendicular to each other). While the two shear polarized waves travel at the same velocity, the longitudinal wave travels through the material at a larger velocity (roughly twice the velocity of the shear wave); where as previously stated these velocities are independent of the angle at which the wave travels through the medial. Alternatively, in the case of an anisotropic layer all three polarizations are coupled, thus an acoustic wave entering an anisotropic material produces all three polarized acoustic waves. Here the polarizations are no longer purely longitudinal, or purely shear polarizations, i.e. the polarization is no longer aligned parallel to, or perpendicular to, the wavefront, and the polarized waves are referred to as quasi-transverse and quasi-longitudinal polarizations. Finally all three polarized waves travel at different acoustic velocities, and as previously stated these velocities are dependent on the direction.

1.5.4 Effects of Attenuation and Dispersion

The propagation of an acoustic wave can be altered by attenuation and also dispersion. The attenuation in a material causes the amplitude of an acoustic wave to dissipate as the wave travels through the medium, and is a combination of the factors of scattering (microscopic reflections of the acoustic wave in other directions than its propagation) and absorption (conversion of the energy of the acoustic waves into other forms). For a plane wave with an initial amplitude A_o, the final amplitude of the wave after travelling some distance χ through an attenuative material can be expressed as an exponential decay

$$A = A_o e^{-\alpha\chi}, \tag{1.1}$$

where A is the amplitude of the attenuated wave, and α is the attenuation factor (attenuation coefficient). The attenuation factor (α) is material dependent, and is roughly proportional to the square of the frequency of the acoustic wave for those factors governed by the absorption of the material, while the portion of the attenuation due to scattering factors is dependant of the relative size of the acoustic wavelength to the size of the grains within the sample[4]. While the effects of the attenuation of the material will be considered, this is not a main focus of this thesis. The necessary additional calculations to perform in order to utilize a material with attenuative properties will be discussed in Section 5.1, however, until this point the materials making up the plate will be considered as non-attenuative.

[4]The grains in the material refer to the localized uniform crystalline regions which join together to make up the material.

The final physical effect influencing the propagation of an acoustic wave as it travels through a media which we will discuss is that of dispersion. Dispersion is the dependence of the phase velocity of an acoustic wave due to frequency. This dispersive property of the media is able alter the time of propagation for an acoustic wave to cross a medium, or the angle at which the acoustic wave travels through the medium, as the wavelength or frequency of the wave is changed. In the case of unbounded homogeneous media the dispersion is a weak effect, and is cited [54] to typically be less than a 1% change within a 1 to 10 MHz frequency change, and thus can often be neglected. However, in specific cases, such as in the case of a bubbly liquid, the dispersion becomes a strong effect and must be considered [55]. The effects of dispersion will not be considered in this theory, and thus the materials used will be assumed to be non-dispersive.

1.6 Uniqueness and Scope of Thesis

As previously mentioned the problem of calculating the multiple reflections of acoustic waves in a plate structure is typically avoided by using one, or more, of the various methods discussed in the previous sections. The uniqueness of the technique in this thesis, is that it does not avoid this problem and presents a technique which shows how the problem can be simplified, and allows for this problem to be analyzed in a reasonable time frame. While the thesis discusses the general case of acoustic waves travelling at at non-normal incidence through a single or multilayer solid plate structure, the technique is also valid for the cases where only a single polarization of acoustic wave travels through

a multilayer plate; such as situations only using shear waves, liquid layers, or examining normal incidence. An additional factor in the uniqueness of the technique presented in this thesis are the benefits gained from using the initial ray based prospective. This technique provides initial results which are independent of the space and time variations of a true acoustic wave, and allows one to test a variety of acoustic sources in a separate second set of calculations without needing to recalculate the initial ray based results (provided the theoretical sample in questions remains constant), As well in this second set of calculations one may also consider the attenuation of the materials (Section 5.1), and it is even possible to re-calculate the horizontal position, and time of flight for each of the ray's intersections with the interfaces of the plate based on alternate thicknesses of the layers in the plate (the other material parameters must remain known and constant as they would alter the amplitude of the rays) (Section 5.2).

The scope of the thesis will be limited to examining situations as prescribed within the theoretical considerations of this technique as outlined in more detail in Section 2.3. These include having an ideal plate structure, where the layers of the plate are bonded via the perfectly bonded, or imperfectly bonded, boundary conditions, and the layers are made of materials with known acoustic properties. As is common with many theories dealing with waves in a plate structure the materials in each layer of the plate are assumed to be isotropic, homogeneous, non-dispersive, non-attenuative, and linear in their stress strain relationship. Finally in this thesis we will only consider cases where the acoustic waves travelling through the plate will travel at real angles, thus we will not examine cases with surface waves, or other evanescent waves. Later in the thesis it will be discussed how it is

possible to include attenuative materials using an additional set of calculations (Section 5.1) and not alter the technique used for the ray based calculations in ideal materials. However, until this point the non-attenuative material requirement will remain. Finally while the theory is able to utilize the imperfectly bonded boundary conditions, the results will focus on using the perfectly bonded boundary conditions as they provide the most familiar cases, thus allowing an an easier analysis of the results.

Chapter 2: Preamble

2.1 Description of problem

As previously mentioned, in this thesis we will consider the general case of ultrasonic waves travelling at non-normal incidence through a single, or multilayer, ideal plate structure made of isotropic solids. A typical example of such a multilayer plate structure, and the case most often examined in this thesis, is a sample formed by the bonding of two aluminum plates together with epoxy (i.e. an Aluminum-Epoxy-Aluminum sample). In such a situation the surrounding half-spaces would typically be the natural air layer of earth's atmosphere, or the water in an immersion testing system; although one could use

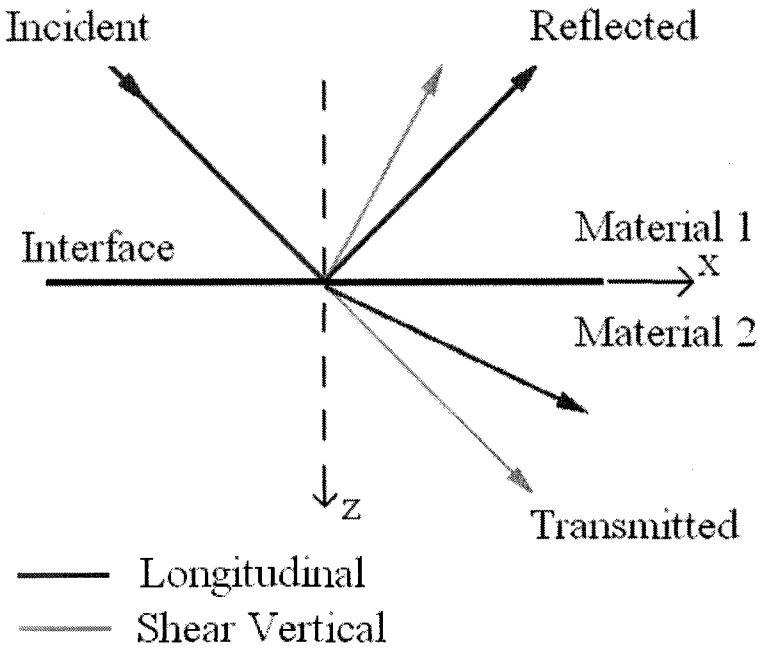

Figure 2.1: Incident, Reflected, and Transmitted Acoustic Wave at a Boundary Between Two Media.

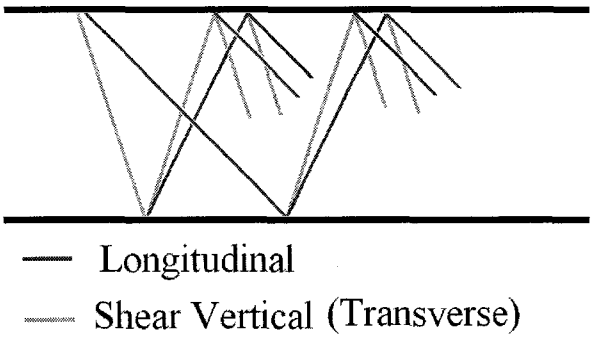

Figure 2.2: Incorrect Ray Model: It appears the number of waves to track will double at each reflection.

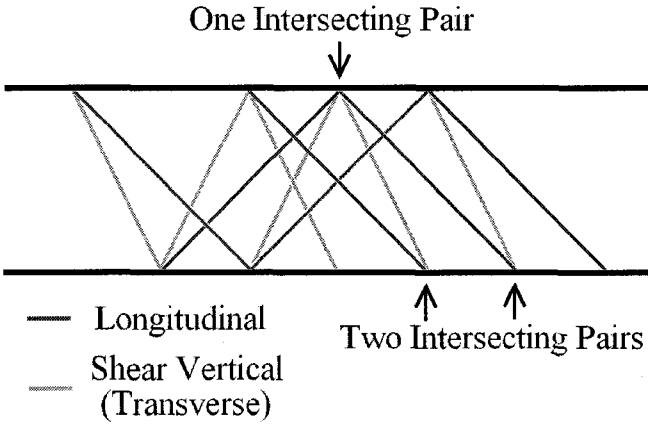

Figure 2.3: Correct Ray Model: By considering the actual paths of the rays many will overlap in time and space. The number of unique paths increases in a linear manner.

the half-space to represent a very thick layer of metal or adhesive, or any material connecting transducer to the sample. An acoustic wave introduced to this multilayer plate sample will travel through the plate structure repeatedly being reflected and transmitted at each of the interfaces. Due to the coupling between the longitudinal and shear vertical (transverse) polarizations in an isotropic solid, a longitudinal (or shear vertical) wave incident on an interface between two isotropic solids will produce two reflected waves (one longitudinal and one shear vertical polarized wave), as well as two transmitted waves

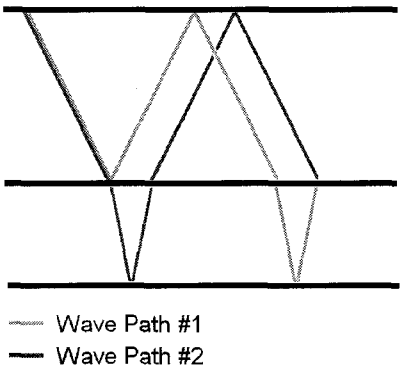

Figure 2.4: An example of two ray paths which intersect in a two layer plate. Here the example only considers waves with a single polarization, but cases with mode conversions are also possible.

(again one of each polarization) as shown in Figure 2.1. Applying only this mode conversion property as the acoustic rays interact with each interface in the plate one would produce the situation seen in Figure 2.2 for the single layer plate. In this case one initially estimates that the number of waves doubles with each internal reflection, and an initial glance the problem of calculating the multiple reflections of an acoustic wave within even a single layer plate appears to be a very time consuming endeavour. However, by carefully considering the paths the acoustic waves travel in both space and time, one finds that many of the ray paths are equivalent in their horizontal distance travelled and time of flight. These rays will travel on coincident paths (i.e. the same path in space and time), and superposition can be used to combine the coincident rays into a single ray. With these considerations the actual ray paths for the single layer plate are as shown in Figure 2.3. This superposition of coincident paths causes the number of waves to consider to be reduced, and in the single layer plate case the number of waves to consider now increases linearly with each internal reflection. The importance of the linear increase in the number

of calculations, relative to the situation where the number of calculations doubles with each reflection, is discussed in the next section on Computational Complexity (Section 2.2). This observation of equivalent paths can also be extended to the case of a multilayer plate, where in addition to the equivalent ray paths in each layer of the plate as seen in Figure 2.3, there also will now exist equivalent paths where the rays travel through the layers of the plate; an example of two such paths is as shown in Figure 2.4. Here it is noted that the example has shown the case of two equivalent paths using only single polarized waves (paths with mode conversion of course also exist). The importance of such an observation is that the technique will also be useful for cases with liquid media, waves travelling at normal incidence, and shear horizontal waves (the three single polarization cases), as long as the sample contains at least two layers.

In the chapters following this preamble the theoretical basis of this technique will examine the idea of equivalent paths in more detail, and prove the existence of these paths as well the coincident paths which as previously mentioned can be combined via superposition into a single acoustic ray. Next the ray based amplitude calculation process will be examined, here by using the perfectly bonded boundary conditions the amplitude calculations can be performed as a series of reflection and transmission calculations (and the superposition of these results). Because these coefficients are independent of the space-time domain properties of the acoustic waveform, the repeated application of these coefficients, and thus the ray based amplitude calculations, also are independent of the acoustic waveform. The additional options for the post ray based calculations will then be examined, here the ray based amplitude results can be extended to more realistic acoustic

waves, also the attenuation of the material can be considered. Also briefly discussed is the possibility to work further with the results and filter the data to consider transducer effects, and the possibility to consider altering the thickness of the layer and recalculating the time of flight, and horizontal position of the ray data. Finally results of the ray technique will be examined, comparing to expected theoretical results, experimental cases, and applying the results to the detection of bonding in a layered Metal-Adhesive-Metal sample.

2.2 Computational Complexity

The computational complexity of a problem, or order of a problem, is a computer science term which measures the growth of the computational difficulty of the problem as the data it needs to deal with increases. Most often this refers to the worst case scenario under which the program will run, but the average case and best case scenarios can also be considered. Overall the computational complexity gives an estimate of the increase in the time taken to execute the program with increasing data size, where this estimate is independent of the processing power of the computer. As well it is also possible to use the order of the problem to measure other important factors in the area of computer science and algorithm development, such as the growth in the amount storage space needed for the current calculations, as well as the final result. A more familiar idea for those studying physics, is the order of an equation as it appears in mathematics. Here one would refer to a polynomial equation such as $y = x^4 + x^3 + x^2 + x^1 + x^0$ as an order x^4 equation, only

the dominant term of the function's growth is considered, and constants are most often ignored. The idea is the same in computer science, but here one examines the dominant factor for the processing speed, or memory use of an algorithm. By comparing multiple algorithms and their complexities one can make a more educated decision upon which method should be used to solve the problem at hand.

In the case discussed in this thesis (calculating the multiple reflections within a multi-layer plate), the computational complexity of the problem is known to increase with the number of acoustic waves one must perform calculations on, which in turn increases with the number internal reflection and transmission in the plate. If one does not consider the paths which the rays travel (Figure 2.2), the number of rays double with each internal reflection creating a problem with 2^N waves at the N^{th} internal reflection. This causes the coinputational complexity of the problem to also grow on the order of 2^N, and as well the amount of memory space needed for calculations, and storage space for the final results would also increase on the order of 2^N.[5] Such algorithms with an order 2^N complexity provide for the second most complex group of algorithms in computer science, where these algorithms only overshadowed by those algorithms with order $N!$ complexity. Typically in these cases one attempts to simplify the problem, or find new techniques to solve the problem. In our case this is achived by considering the paths which the rays travel, and utilizing superposition to combine rays with coincident paths so that the number of rays is reduced to a more manageable scale. Using these considerations, in the case of the

[5]Here one should note that $2^{10} \approx 10^3$(1 Kilo), $2^{20} \approx 10^6$(1 Meg), $2^{30} \approx 10^9$(1 Gig), thus after only 30 reflections one would easily obtain over 10^9 items of ray data to store, where we have not even included an estimation for the memory needed to store the data of the ray itself (i.e. the amplitude, time of flight, distance travelled) in these 10^9 items.

single layer plate there now exists $2N$ unique rays incident at the N^{th} internal reflection, with $2(N+1)$ rays being reflected and transmitted, thus giving an end result where the number of rays increase linearly with each internal reflection. Overall we have created a solution of order N for each set of reflection and transmission calculations, or in total a complexity of order N^2. In addition, the amount of memory space needed for calculations, and storage space for the end results are also reduced to orders of N and N^2, respectively. Thus by combining the coincident paths via the principle of superposition the complexity of the problem has be dramatically decreased (Table 2.1 provides a summary of the complexities for each case), and has reached a level of complexity where the problem is able to be solved in a time efficient manner.

To close we show the actual time of the calculations taken in a single layer plate case in Figure 2.5, here we note this curve does fit an N^2 polynomial as expected (the fit is $t = 9.711\,N^2 + 17.224\,N + 881$, where N is the number of reflections and the time t is in μs). As well we show an estimate of the time that would be taken if one chose to ignore the wave paths yielding an order 2^N calculation (i.e. $t = 9.711 \cdot 2^N$). Figure 2.5 shows that after a number of reflections the time difference becomes very pronounced, at larger numbers of reflections the time difference is not simply a of a few seconds, but potentially hours (or more) of calculation time. Based on this estimate 33 reflections would take just under 1 day to calculate via an order 2^N method, versus approximately 12 μs in the order N method presented in this thesis.

	Calculating All Waves		Considering Ray paths
One iteration:	2^N	vs	N
Overall/Total Complexity†:	2^N	vs	N^2
Memory Space for Calculations*:	2^N	vs	N
Final Data Storage Space:	2^N	vs	N^2

† $\sum_{n=1}^{N} 2^n = 2^{N+1} - 2 = O(2^N)$

* One needs only to keep data from last set of calculations, and may discard data from previous calculations

Table 2.1: Computational Complexity of Calculating Waves in a Multilayer Plate.

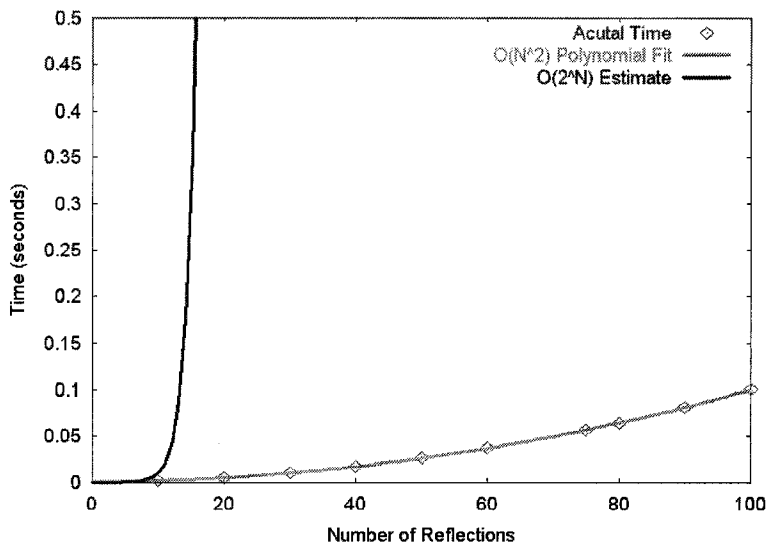

Figure 2.5: Time to obtain results for single layer plate calculations accounting for coincident wave paths (N^2 curve), and not accounting for coincident wave paths (2^N curve).

2.3 Theoretical Considerations, or Limitations

In this section we outline the theoretical considerations, or limitations, on which the technique is based. In the multiplayer plate samples used in this thesis, it will be assumed that the materials for each layer of the plate and the surrounding half-spaces are made of ideal acoustic materials; where such ideal materials are assumed to be: isotropic, homogeneous, non-dispersive, have no attenuation, are linear in their stress strain relationship (i.e. obey the linear acoustics form of Hooke's Law). The layers making up the plate structure are arranged in parallel layers, with smooth flat interfaces, and have known constant thickness and material parameters (i.e. velocity, and density). It should be noted that while this ideal plate structure forms a fairly restricted situation, these are typical considerations for papers dealing with multilayer plates. In fact, in many papers dealing with a multilayer plate the author instead refers to the effect being allowed, i.e. the plate is allowed to be inhomogeneous, anisotropic, non linear, dispersive, or attenuative in its properties. As is also common we will assume that the interfaces connecting the layers of the plate are bonded such that they satisfy the perfectly bounded [43–47]. And as well it is also possible to consider the less commonly examined imperfectly bonded boundary conditions [43], where for these cases the rigidity constants are restricted to be constant along the entire imperfectly bonded interface. (These rigidity constants define the level of imperfection in the bonding ranging from the perfectly bonded condition, to a fully disbonded situation). As the above boundary conditions are developed from acoustic waves with planar wavefronts, the rays in this theory are also restricted to have planar wavefronts. Thus the expansions of these rays to more realistic waves is limited

in accuracy in which one can represent the acoustic source as one or more planar rays. Finally this theory limits itself to currently considering only waves which travel at real angles; that is there are no evanescent waves in any layer (no waves travelling at angles beyond the critical angle), and no interface waves (Rayleigh, Stonely, or Stonely-Sholtze waves). Finally, in Section 5.1 it will be shown how the effects of the of the material's attenuation can safely be considered; this procedure will not alter the technique used for the ray based calculations in the ideal materials, and thus until this point the material will be considered non-attenuative.

2.3.1 Real World Limitations to Theoretical Considerations

The theoretical conditions made in the previous section transpose to some real world limitations when dealing with physical samples and experimental measurements. For each of the factors the exact limitations are difficult to determine for a generic case, and the results of this theory will in reality serve as an approximation of real world results, where the accuracy is limited by how realistically (or irrealistically) the theoretical sample corresponds to the real world case. We will briefly examine each of the theoretical considerations, and when appropriate describe possible methods (from either the theoretical, or the experimental point of view) to overcome the variations due to using the ideal case to describe a real world sample. These ideas are introduced for purposes of discussion only, and none have been tested for application in real world situations.

- Non Linearity: Here one should choose an experimental setup such that the am-

plitude of the acoustic wave does not generate nonlinear responses in the sample. As well one must consider that some materials are more susceptible to produce nonlinear responses than others. In such cases of using materials with very high nonlinearities the experiment may need to be carefully controlled, or the usage of these materials avoided in order to produce the most comparable results between the experiment and the results of this theory.

- Perfect Plate Structure: Here adjustments to the results would depend on the imperfection in the plate (non parallel plates, slightly curved plates, or rough surfaces). Here the best solution may be to experimentally examine results for smaller horizontal sections, possibly averaging results for many sections together to produce more reliable data for the ideal parallel plate structure.

- Anisotropy: While the technique would allow for those materials with very small anisotropy to be treated as isotropic materials, and yield approximate results, those cases of highly anisotropic materials should be avoided. In such cases with anisotropic layers the mode conversions to the shear horizontal waves will not be calculated, and as well the differences between the directions of the phase velocity and energy velocity of the waves would not be considered. With highly anisotropic materials one would be limited to testing at only normal incidence, or at an angle such that the acoustic wave travels on the acoustic axis through the anisotropic material (at this angle the material can be treated as an isotropic material). As well, as an approximation the simulation could examine an anisotropic material using a small range of angles where the material is approximately isotropic in to attempt to

produce reliable data. Here the simulation would still not consider the creation of shear horizontal waves, or the direction of the energy velocity of the acoustic wave, but these effects become more negligible as the material's properties approach the isotropic case. The best option to deal with anisotropic materials may be to extend the technique so that it correctly allows for such situations. Such an expansion requires the examination of alternate problems such as finding the direction of the three polarized waves in the anisotropic material based on the direction of the incident wave, calculating the direction of the energy propagation of these waves, and reliably discerning which polarization the resulting reflected and transmitted waves are so that the appropriate reflection and transmission coefficients can be applied. While the consideration of such problems presents interesting possibilities, such an examination is beyond the scope of this thesis.

- Non Dispersive Materials: As mentioned in Section 1.5.4 most acoustic materials have fairly small dispersive effects, and thus the effects of dispersion can often be neglected. Those remaining materials with high dispersive properties should be avoided, similarly to those with large anisotropy. If such a material were to be tested the results would only be applicable for a specific range of frequencies. To examine such non dispersive materials it may be possible to produce multiple sets of results, where each set of results utilizes approximate material parameters for a small range of frequencies. The results for each frequency could then be combined via the necessary superposition in accordance to the frequency spectrum of the acoustic source, and thus approximate the end result of an acoustic wave travelling

through a dispersive sample.

- Attenuation: Here the real world limitation is the combination the effects of the material's attenuation and thickness, as well as the number of times the wave propagates through the layer, where this in turn creates restrictions on the space and time domain one can examine quantitatively. Without factoring in attenuation, materials with high attenuation would need to be restricted to thinner layers, and limitations on the space and time domain examined by the theory be used. As previously mentioned the necessary additional calculations needed to consider such cases can be used (the are outlined in Section 5.1), thus lifting these restrictions as long as the attenuation of the material is reliably known.

- Inhomogeneous Materials: The accuracy limit of the results here is dependent on how well one can produce a material which is roughly homogeneous over some finite size. One interesting possibility the simulation allows for is the plate like structure could be used to simulate a step like inhomogeneity in the thickness of the plate (i.e. each layer of the plate represents a homogeneous layer in an otherwise inhomogeneous material). However, adding numerous layers of material will continuously increase the complexity of the calculations. Thus approximating an inhomogeneous media as being formed from many homogeneous layers with gradually changing material properties may not provide the best results initially, but combining this technique with methods examining the calculation of multiple reflection methods for inhomogeneous materials [56, 57] may prove to be useful.

- Very Thin Layers: One of the limitations not explicitly set in the theoretical con-

siderations is the situation of a layer so thin (very small compared to an acoustic wavelength) that the real world acoustic wave will not interact or detect such a layer. To accurately correspond this theoretical sample to the real world case such a the thin layer should be excluded from the theoretical setup. We do note that if a thin layer included in the theoretical setup the calculation process will happily provide the results under the assumption that the acoustic wave is reflected multiple times within the thin layer. These results can of course be compared to results from typical thin layer models (See Section 6.1.3); however, even when the layer is thick enough to allow for an interaction with the acoustic wave, these effects of the thin layer are small and can be viewed as a perturbation [17, 18]. Thus again it may be valid to ignore the existence of the thin layer in the theoretical setup of a particular sample containing a thin layer.

Chapter 3: Theoretical Basis of this Technique

3.1 Setup of Problem, and Definitions

To begin we will show the overall setup of the multilayer plate problem, and define the parameters denoting the characteristics of the plate layers. The list of parameters here is not exhaustive, and other parameters may be introduced as is needed in future sections. The multilayer plate structure in question is shown in Figure 3.1, where we define one axis horizontal to the plate layers, and another perpendicular to the layers of the plate. The third spacial direction is out of the page, and will not be considered other than to state the plate's size is this direction is much larger than the acoustic wave, so that the sides of the plate need not be considered. The material in each layer of the plate has longitudinal velocity c, shear vertical (transverse) velocity b, density ρ, and thickness d. A ray in this layer of the plate travels at some angle θ_L (for longitudinal waves), or θ_V (for shear transverse waves, where it will be shown in Section 3.3.1 that these angles are

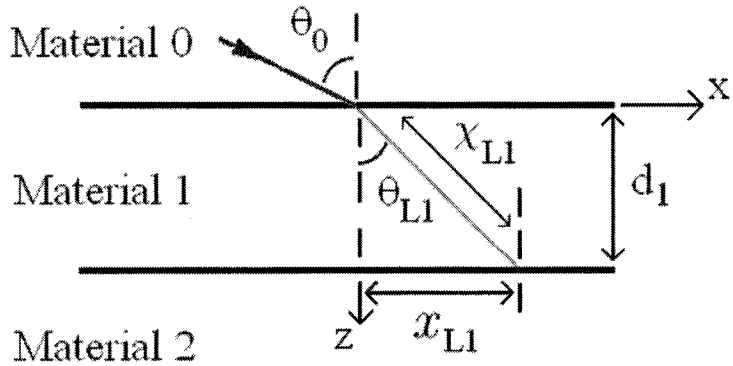

Figure 3.1: General Setup of the Multilayer Plate System.

independent of the path the ray has travelled through the sample, and the direction of travel in the layer of the plate. A numerical subscript (i.e. c_1) will be used to denote which layer of the plate is being referred to. The subscript 0 refers to the upper half-space, where the initial acoustic wave is incident upon the sample from this upper half-space, and the remaining layers are numbered 1 through N for the N layers of the plate; likewise, the interfaces are numbed from 1 to N beginning at the upper half-space. We will also make reference to the time of flight (tof) the ray takes to travel across any number of layers, the horizontal distance (x) travelled by the wave (i.e. the distance the wave travels along the x-axis, which runs parallel to the plate's surface), the total distance travelled by the wave (χ), and amplitude of the wave. This amplitude is the displacement amplitude unless otherwise noted (one can also examine the pressure, or energy (intensity) amplitude); this is measured in proportion to the incident's wave amplitude, so that this amplitude of the wave in reality is the overall reflection-transmission coefficient combination to this point. The above quantities may also be specified by a subscript denoting the parameters as being due to a longitudinal L or shear vertical V paths (i.e. tof_L is the time of flight of a longitudinal ray path). Additionally we may refer the to polarized path in a specific media ($L1$, $V1$, $L2$, ect.), or the total number of such paths to this point (N_{L1}, N_{V1}, N_{L2}, ect.). Any other definitions required will be described as needed.

Path			
1	2	3	4
VVV	VVL	VLL	LLL
	VLV	LVL	
	LVV	LLV	

Table 3.1: Paths of Rays for Third Reflection in a Single Layer Plate.

3.2 The Idea of Equivalent Paths

To begin consider the case of a single layer plate, with two possible polarizations for the acoustic waves and the possibility of each internal reflection creating both reflected longitudinal and shear vertical waves, the exact path the ray has traversed can be denoted by a series of individual longitudinal (L) or shear vertical (V) sections. For example, in a single layer plate after three reflections the possible paths a wave could travel are those listed in Table 3.1. Knowing the material in question, and the angle at which the wave propagates, it is possible to determine the horizontal distance, and time of flight taken as the wave traverses across the thickness of any layer in the plate. By utilizing Snell's Law, and some geometry, it is possible to show (see Sections 3.3.1 and 3.3.2 for details) that these quantities are constant for each polarization, in each layer of material. This makes any longitudinal (and all shear vertical) path segments equivalent regardless of the path the wave has travelled to this point. Because the total horizontal distance, and time of flight for the entire path is calculated by sum of the individual path segments, the order the path is traversed does not matter, only the total number of longitudinal and shear vertical sections. Thus two separate paths, with the same number of each polarized path

segment, will in total travel the same total horizontal distance, and same time of flight. That is, the rays have travelled equivalent paths. As an example, consider the second column of Table 3.1, the paths VVL, VLV, LVV all have the same number of shear vertical, and longitudinal sections, yet only the order in which the paths are traversed is changed. All these rays will have travelled the same total horizontal distance, and taken the same time of flight to this point, i.e. these are all equivalent paths.

In a multilayer plate the idea is the same, but now the rays will travel through multiple layers of media, with each layer having longitudinal and shear vertical paths segments which are distinguishable from other layers. The exact path the ray has traversed can now be denoted by a series of individual longitudinal (L) or shear vertical (V) sections where the layer the wave travels in is noted (i.e. L1, V1, L2, V2, for longitudinal (L) and shear vertical (V) in layers 1 and 2). Again, in each layer of the plate the ray path segments for each polarization are equivalent, and the entire path can be expressed as the total longitudinal and shear vertical sections in each layer. Overall, the order of the polarizations in a ray path is again indistinguishable; and again there exists the possibility that rays will travel equivalent paths in total. One such example of two equivalent paths which travel through multiple layers of a plate structure has been shown in Figure 2.4, where we note that we do not even require a mode conversion to occur within a multilayer plate to create two equivalent paths. (There are, of course, many equivalent paths with mode conversions as well.) And as well, for each layer of the multilayer plate, there will still exist the equivalent ray paths of waves travelling within only one layer of the plate (Figure 2.3). As a final important note for the multilayer plate case is that because the

acoustic wave must traverse the layers of the plate in order there is a restriction in that we can consider only valid ray paths, and not allow the wave to arbitrarily jump between the layers of the plate.

3.2.1 An Analogy with Multistate Systems

It is possible to restate this problem in a form analogous to a multistate problem (such as the familiar two-state problems from thermodynamics and quantum mechanics). In the case of a single layer plate the problem is analogous to the two state problem, here the two states are the two polarizations, and the indistinguishable factor will be the order of the polarizations in which the acoustic rays have traversed a path. Again this makes the three paths VVL, VLV, and LVV equivalent as the overall quantities of time of flight, and horizontal distance travelled are identical (the total value does not depend on the order of the polarizations). This extends as well to the case of a multilayer plate, where the problem could be described as a two-by-N state problem (where N is the number of layers in the plate). However, in the acoustical version, there will exist restrictions on the first states due to the fact that as the acoustic ray must travel through the layers in order. This reduces the number of states possible for the first N refections, i.e listing the number of states in order of reflections and transmissions, there are 1, 2, 3, ... N-1, N, N, N ... possible states. Even with these restrictions, this multistate problem will allow for numerous equivalent states where the order of the polarizations the waves have travelled is indistinguishable. This is of course only an analogy, and is presented only to provide an alternate view in which to show the idea of the equivalent paths; one should

not interpret the acoustic waves travelling in a multilayer plate as a quantum mechanical, or thermodynamic system.

3.3 Proving the Existence of Equivalent Paths

In order to prove the existence of equivalent path segments described in Section 3.2, it is first necessary to show that the angle of travel of each polarized wave, in each layer of the media, is constant. And that in turn these constant angles lead to the time of flight, and horizontal distance travelled as the wave travels across each layer of the media to be constants as well. It should be noted that we are making no assertion that the amplitudes (displacement, pressure, or energy amplitude) of the equivalent ray paths are equal. In fact, as will be discussed in Section 4.2, the opposite is true and that the intersecting ray paths will typically have different amplitudes. Thus, the amplitude from each ray paths must be calculated until two (or more paths) become coincident, only after the ray paths have travelled the equivalent paths can superposition then be used.

3.3.1 Angles of the Waves: Snell's Law and a Little Geometry

To begin, consider the wave incident on the multilayer plate with angle θ_0, it produces two transmitted waves (one longitudinal, and one shear vertical) with angles (θ_L for the longitudinal wave, and θ_V for the shear vertical wave) given by Snell's law

$$1/c_0 sin(\theta_0) = 1/c_1 sin(\theta_{L1}) = 1/b_1 sin(\theta_{V1}), \tag{3.1}$$

where the subscripts 0 and 1 refer to the half-space, and the first layer of the plate, respectively. These two transmitted waves travel through the plate and become the waves incident on the next interface, by using a little geometry (Figure 3.2) it can be seen that these new incident angles are the same as the transmitted angles. These two new incident waves of course reflect and transmit, producing waves at angles again given by Snell's law. Combining two Snell's Law in series the second reflection and transmission ($R2$ and $T2$) can be related directly to the initial incident angle

$$\begin{aligned} 1/c_0 sin(\theta_0) &= 1/c_1 sin(\theta_{L1}) = 1/c_1 sin(\theta_{R2}), \\ &= 1/c_2 sin(\theta_{T2}), \end{aligned} \tag{3.2}$$

where it is noted that equation 3.3 is valid for both longitudinal waves and shear vertical waves. The process continues multiple times, with the reflected or transmitted rays becoming incident waves at the same angle, which in turn produce new rays. At each reflection and transmission Snell's law must be valid, and thus in each layer the angle at which the wave travels can be related back to the initial incident angle. Thus one can write

$$\begin{aligned} 1/c_0 sin(\theta_0) &= 1/c_1 sin(\theta_{L1}) = 1/b_1 sin(\theta_{V1}), \\ &= 1/c_2 sin(\theta_{L2}) = 1/b_2 sin(\theta_{V2}), \\ &\vdots \\ &= 1/c_N sin(\theta_{LN}) = 1/b_N sin(\theta_{VN}), \end{aligned} \tag{3.3}$$

where the subscript numbers 1 through N denote the N layers of the plate (0 is the upper half-space). As one should recall from the theoretical considerations (Section 2.3) the

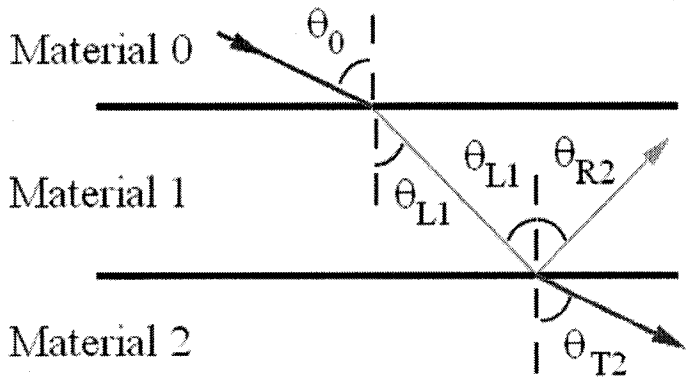

Figure 3.2: Angles of waves within a plate structure. The transmission and incident angle θ_L of the ray in media 1 are equal due to the "Z-Rule" from geometry.

velocity of the material, in each layer of the plate, is constant at all angles travelled by the wave, and throughout the entire layer of the plate, as we have restricted the problem to only examine homogeneous isotropic materials. Thus from equation 3.3 we see the angle of a ray, in any layer of the material, is constant (one angle for each polarization of course) regardless of path it takes. Also one finds that by knowing the incident angle (or any angle in fact), all other waves' angles in the plate are known.

3.3.2 Time of Flight, and Horizontal Distance Travelled

To show the possibility of equivalent paths we need to now examine the horizontal distance, and time of flight of each of the polarizations of acoustic waves as the waves travels through the plate to the opposite interface. These quantities can be related to the angle of travel for each wave polarization, which was shown to be constant (one constant for each polarization, and in each layer of the sample) regardless of the path taken, or direction of travel of the wave through the plate structure in Section 3.3.1. Thus allowing

one to in turn show the time of flight, and horizontal distance travelled are constants as well (again with one constant for each polarization, in each layer of the plate).

To begin, consider an arbitrary layer of the plate (Figure 3.1), here the horizontal distance (x) travelled by each polarization as it travels through the plate to the opposite interface can determined via

$$x_L = d\ tan(\theta_L), \qquad x_V = d\ tan(\theta_V), \tag{3.4}$$

where the thickness of the layer d is assumed to be known. As well the time of flight (tof) taken during this traversal can be determined via

$$tof_L = \frac{d}{cos(\theta_L)\ c}, \qquad tof_V = \frac{d}{cos(\theta_V)\ b}, \tag{3.5}$$

where the velocity of the longitudinal and shear vertical polarizations are c and b, respectively. It should be noted the that the time of fight is of course: $tof = distance/velocity$, where the entire distance travelled by the wave is needed, not the horizontal distance. These distances travelled through the material for the longitudinal and shear vertical polarizations are

$$\chi_L = d/cos(\theta_L) \quad \text{and} \quad \chi_V = d/cos(\theta_V), \tag{3.6}$$

respectively. Because the angle of the wave is constant in each layer of the material (as is the thickness and the acoustic velocities), the time of flight, horizontal position, and the entire distance travelled as the wave propagates across a layer of a plate are also constants.

Thus each of the longitudinal and shear vertical path segments (in each layer of the

material) have been shown to be indistinguishable in terms of their angle of travel, time of flight, and horizontal distance travelled. Because the total horizontal distance and total time of flight is the sum of the individual path segments; two ray paths which have the same number polarized segments will in total travel equivalent paths, intersecting at one of the plate's interfaces.

3.4 Visualizing the Paths and Coincident Waves

In the previous section it was shown that any individual longitudinal and shear vertical path segments are indistinguishable in terms of their horizontal distance travelled, and time of flight taken as they travel through a layer of the plate structure, in each layer of the plate. As the total path is not dependent upon the ordering of the polarized segments there exists the possibility that multiple ray paths will travel equivalent paths and intersect at the same position in space and time after undergoing any number of reflections or transmissions. In this section we will again show the existence of these equivalent paths, but in a more visual manner, as well as examining the coincident rays paths which are produced at the reflections and transmissions of the intersection of the equivalent paths.

To begin we consider the case of a single layer plate; in order to visualize the ray paths more clearly a tree structured digram can be made which shows the various possible ray paths within the plate (Figure 3.3). The tree structure is also able to provide a convenient method to visualize the reflection and transmission calculations. In Figure 3.3 the right

branches of the tree denote longitudinal paths, and the left branches shear vertical paths, with each new level corresponding to an additional internal reflection. The branches which connect represent waves which have travelled equivalent paths (they have the same total number of longitudinal and shear vertical sections), i.e. these waves have travelled the same horizontal distance, and have the same time of flight. From Figure 3.3 we see that the equivalent paths intersect in pairs of opposite polarizations (like polarizations will not intersect at the interfaces as they travel parallel). The waves reflected and transmitted from these intersecting pairs possess the same origin in both space and time, and the waves of like polarizations will travel from this point at the same angle. Thus the multiple longitudinal waves reflected from the intersecting pairs are travelling along the same path in space and time, or in other words, they are coincident. In addition, the same can be said for the shear vertical waves, as well as any transmitted waves of like polarizations. By using superposition it is possible to combine these coincident waves to a single wave. It is noted that because these intersecting pairs of rays have the same time of flight the two rays will be in phase (a sign convention in the reflection and transmission coefficients is used to keep track of any 180 degree phase shifts, or amplitude sign change), thus this superposition need concern itself with only the waves' amplitude, even for waves with complicated time domain behaviours.

For a multilayered plate the tree structure becomes multidimensional and difficult to visualize. However, there still exist rays which travel equivalent paths and intersect at the interfaces of the plate. Again the waves reflected and transmitted from these points will be coincident, and superposition can again be used to combine them into a single ray.

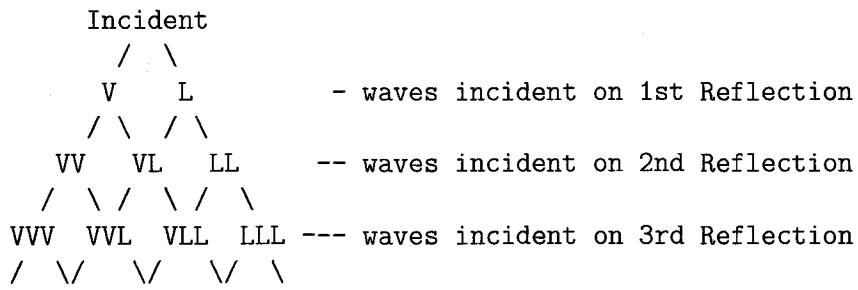

Figure 3.3: Tree Diagram of Wave Paths.

While the rays in multilayered plate becomes difficult to track by hand, a computerized method can easily keep track of the multiple ray paths, as well as the necessary ray path properties; such as the amplitude, time of flight, and horizontal distance travelled. As well the computerized method is also able to combine the necessary rays as each path can be defined, stored, and accessed via the distinguishable properties of the ray's path (i.e the total number of longitudinal or shear vertical polarizations in each media). Thus when two rays become coincident they will share the same storage parameters, and the necessary superposition can be performed.

Chapter 4: Ray Based Amplitude Calculations

4.1 Coefficients at the Interface Between Two Media

Before beginning to calculate the amplitude of the wave as it propagates in the plate structure, it is worth while to briefly overview the details of the reflection and transmission coefficients at an interface as is shown in Appendix A. The important details to note here are that we have set up the polarizations of the reflected and transmitted waves such that the reflection and transmission coefficients are independent of the direction of travel of the incident wave, and are also independent of the space-time domain variations of the incident wave. In addition it is shown that the results of the coefficients for each individual incident wave remain valid, and find that in general the amplitude of the waves reflected and transmitted from the interface between materials 1 and 2 can be calculated via

$$[S]_{\text{total}} = \begin{bmatrix} S_{L1} \\ S_{V1} \\ S_{L2} \\ S_{V2} \end{bmatrix}_{total} = \begin{bmatrix} R_{11}^{LL} \\ R_{11}^{LV} \\ T_{12}^{LL} \\ T_{12}^{LV} \end{bmatrix} A_{L1} + \begin{bmatrix} R_{11}^{VL} \\ R_{11}^{VV} \\ T_{12}^{VL} \\ T_{12}^{VV} \end{bmatrix} A_{V1} - \begin{bmatrix} T_{21}^{LL} \\ T_{21}^{LV} \\ R_{22}^{LL} \\ R_{22}^{LV} \end{bmatrix} A_{L2} - \begin{bmatrix} T_{21}^{VL} \\ T_{21}^{VV} \\ R_{22}^{VL} \\ R_{22}^{VV} \end{bmatrix} A_{V2}. \tag{4.1}$$

Here $S_{\alpha n}$ is the overall coefficient for the acoustic wave travelling away from the media due to incident waves with amplitudes $A_{\alpha n}$, where α denotes the polarization of the wave, and n the media the wave travels in. For each incident wave there exists the original reflection coefficient R, and transmission coefficient T, from the single incident wave case. $R_{cd}^{\alpha\beta}$ (or $T_{cd}^{\alpha\beta}$) describes the coefficient of a wave with incident polarization α in media c

travelling to media d with polarization β. The two negative signs in equation 4.1 are the result of the incident wave in the second medial travelling in the $-z$ direction. With the waveform of the incident wave eliminated in equation 4.1, the reflection and transmission coefficients can be applied in succession as the rays interact with each interface. After these amplitude calculations the waveform can then be reintroduced to the various leak rays as will be outlined in Section 5.3. Before this however it is necessary to examine in more detail the use of these coefficients in the case of a layered plate, rather than an interface.

4.2 Non Equivalence of Equivalent Ray Path Amplitudes

While it is true that the longitudinal (or shear vertical) polarized segments in a ray path are indistinguishable in terms of the time of flight, and the horizontal position travelled as the wave traverses a layer of the sample. And that in addition the total of these quantities are independent on the order a ray traverses the paths. However, it is important to note that this does not make the amplitude of the equivalent paths equal. This non-equivalence is due to the fact that while the rays may travel the same number of longitudinal and shear vertical paths, any two paths may interact with the interfaces of the plate differently. For example, a mode conversion could occur at the reflection of either of the two interfaces of a plate layer, or as well on the transmission of the wave between two layers of the plate. In turn, such a mode converting transmission could occur as the wave travels from layer N to $N+1$, or the in opposite direction, from layer $N+1$

to N. In addition, there is no requirement that the equivalent paths possess the same number of transmissions or reflections, nor the same number of mode conversions. Thus due to the different reflection and transmission coefficients applied as the wave interacts at each interface, the different coefficients for mode converted waves at each interface, and for each transmission direction, the amplitude of the wave cannot be considered equal. As an example consider the case of a single layer plate, and the waves incident on the second reflection. Examining the tree diagram (Figure 3.3), shows that LLV is an equivalent path where a ray could have taken the paths LLV, LVL, or VLL to reach this point. Noting that the first waves are created from a transmission, the first longitudinal and shear vertical waves' amplitudes (displacement, or pressure amplitude) are given by the transmission coefficients T^{LL} and T^{LV} respectively. (Here we have assumed that the incident wave is a unit in size, with longitudinal polarization). In this first section of the path, one of the three ray paths already possess a different amplitude, due to differences in the initial transmission coefficients. Repeatedly applying the appropriate coefficients to the wave's amplitude for the additional reflections, the combined coefficients to this point will be

$$\begin{aligned} &\text{for path LLV: } \mathrm{Amp}_{LLV} = -T_{12}^{LL} R_{23}^{LL} R_{21}^{LV}, \\ &\text{for path LVL: } \mathrm{Amp}_{LVL} = -T_{12}^{LL} R_{23}^{LV} R_{21}^{VL}, \\ &\text{for path VLL: } \mathrm{Amp}_{VLL} = -T_{12}^{LV} R_{23}^{VL} R_{21}^{LV}, \end{aligned} \tag{4.2}$$

Here T denotes a transmission coefficient, R denotes a reflection coefficient, the superscripts denote the polarization of the incident wave and reflected wave (or transmitted wave) respectively, and the subscript numbers denote the incident and transmitted media (1 is the upper half-space, 2 is the plate, and 3 is the lower half-space). Even after two

reflections it is possible that none of these paths have the same amplitude in the case of the upper and lower half-spaces being made of different materials (i.e. $R_{21} \neq R_{23}$ for any polarizations). With the amplitude of the waves being path dependent, it is necessary to create a procedure which tracks the rays through the media, calculates the wave's amplitudes and performs the necessary superpositions.

4.3 Method of Calculation

While this process of calculations can be examined visually for the single layer plate case, this process becomes more difficult to visualize in multilayer plate cases and computerized calculations become essential. The process involves tracing the possible paths of the rays through the multilayer plate, applying the results of the appropriate boundary conditions when a ray is reflected and transmitted at an interface, and keeping track of quantities such as; the number of paths of each polarization in each layer of the plate, the amplitude, time of flight, horizontal position, and current layer and direction of travel of each the ray in the plate. A computerized calculation method can be developed to trace these paths, calculate the necessary quantities, and perform the superposition when two, or more, ray paths become coincident.

The current calculation method occurs in a manner similar to how one would perform the calculations by hand. Beginning with the first iteration of the calculations one defines the angle of incidence for the wave, and define the wave's amplitude to be 1 unit so as to produce results which can be interpreted as relative to the incident wave's amplitude.

Keeping this incident angle constant will define all other angles for the rays in each layer of the plate as discussed in Section 3.3.1, and also allow for the reflection and transmission coefficients to be calculated a single time. With the possibility of waves intersecting from each side of the interface, and with two different polarizations there will exist four sets of coefficients to keep track of per interface, where each set defines the amplitude (relative to the incident wave) of the waves reflected and transmitted from the interface. One can also determine the increments for the time of flight (Equation 3.5), horizontal position (Equation 3.4) for each polarization, in each layer of the media at this time (see Section 3.3.2). Once these factors are known the process of calculating the amplitudes of the ray paths begins. Here each iteration begins with the current group of incident waves; for each incident wave the correct reflection and transmission coefficients is multiplied by the incident wave's amplitude. The amplitudes of the waves which have travelled equivalent paths to this point and reflect (or transmit) as coincident waves, have their amplitudes summed via the principle of superposition. This process of applying the correct coefficients, and performing the necessary superposition can be combined mathematically into a single step as given by Equation 4.1. Recall here that these coincident wave are travelling equivalent paths and posses the same time of flight, and thus are in phase with each other (a 180 degree phase shift is covered by sign convention), allowing the superposition of rays to require only an addition of the coincident waves' amplitude. It is this superposition of coincident waves which reduces the number of rays needing to be considered in further iterations of the problem, and reduces the computational complexity of the problem. At each of the iterations the amplitude of any rays which are transmitted to outer half-spaces are stored for the final numerical solution, and need not

be considered any further, additionally it is useful to output the path travelled by each wave (i.e. the total number of each polarized segments; N_{L1}, N_{V1}, N_{L2}, N_{V2}, and so on) with the amplitude information. (The usefulness of this will become clearer in Sections 5.1 and 5.2 when we discuss altering the results to include attenuation, or altering the thickness of the layers). Those rays which remain in the plate have their time of flight (Equation 3.5), and horizontal distance (Equation 3.4) travelled by each acoustic wave is increased in accordance to the path segment travelled by the ray. As well the ray's path information incremented appropriately (i.e. if the wave now travels a longitudinal path in material 1, the number of $L1$ paths, N_{L1}, would be increased by 1); it is this tracking of this ray path information which allows the computerized calculations to detect the equivalent paths. Here the set of the four possible incident waves used in Equation 4.1 can be grouped in together in the same structure, along with the amplitude, time of flight, and horizontal position information. This structure can be accessed in accordance to the number of of longitudinal and shear vertical paths in each layer of the sample the rays have traversed, thus allowing the information on rays travelling the equivalent paths to be accessed by the algorithm. These grouped sets of waves become the incident waves for the next iteration of calculations and the calculation process continues until some conditions, such as number of reflections, time of flight, or horizontal distance travelled by the waves are met. As these conditions are met for particular ray paths, further reflections or transmission calculations need no longer be considered, and these rays can be excluded from further calculations. When all rays have met the requirements the calculations are finished, the incident wave angle, or material parameters (velocity, thickness) can be changed and the process continued as necessary. While this may sound like a very time

consuming procedure, these calculations usually take only a few seconds on a modern computer.

4.3.1 Possibility of Symbolic Results

While the current computerized calculations have been developed are numerical, it may be possible to adapt the programming to yield a symbolic result for each wave transmitted to the half-spaces. These equations however would continually grow more complicated with every internal reflection. While some paths may create equations which would simplify nicely (in particular those with few mode conversions), most results would likely become too complicated to be of useful for symbolic analysis. For this reason we will concern ourselves with utilizing the numerical results.

Chapter 5: Post Ray Based Calculations

The following sections consider the necessary additional calculations to consider the attenuation of the materials, or extend the ray to a more realistic acoustic wave. It is even possible to alter the thickness of the materials, and recalculate the time of flight and horizontal positions of the rays after the ray based amplitude calculations. Making these calculations a separate process from the ray based amplitude calculations allows for the exploration of multiple cases of attenuation, or various forms for the acoustic waves without recalculating the initial ray based amplitude results.

5.1 Including Attenuation in the Calculations

To increase the realism of the model it is necessary to consider the attenuation of the wave as it travels through the layers of the plate. This is particularly important for the layers of the bonding material, as these have significant attenuation to detect in experimental results. The attenuation will be included by including an exponential decay term in the calculation of the final amplitude of the wave (A)

$$A = A_o e^{-\alpha\chi}, \tag{5.1}$$

where A_o is the initial amplitude of the ray (no attenuation), α is the attenuation factor (attenuation coefficient), and χ is the total distance (not to be confused with the horizontal distance x) the acoustic wave has travelled. Here it should be noted that the attenuation factor (α) is material dependent, and is also roughly proportional to the square of the

frequency of the acoustic wave. Thus a conflict quickly arises because, to this point, the ray based calculations have been independent of the spacial and time domain changes of the acoustic waves, allowing for more broad results in our numerical calculations. Of particular interest here is that we have not defined the frequency of the wave, or its time domain parameters, which are introduced via a second set of calculations as will be discussed in Section 5.3. As we wish to keep these results frequency independent the attenuation should also be included within a separate set of calculations. In this section it will be shown that is mathematically possible to delay the inclusion of the attenuation in the wave's amplitude, and thus calculate it after the ray based calculations are finished.

We begin by examining a ray travelling a single longitudinal path through a layer of the media. The ray has some initial amplitude A, travels through the layer some distance χ_L through the layer, and with attenuation α the ray will then have amplitude

$$A\, e^{-\alpha_L \chi_L}. \tag{5.2}$$

Similarly a shear vertical wave will have amplitude

$$B\, e^{-\alpha_V \chi_V}, \tag{5.3}$$

One notes that in equations 5.2 and 5.3, that we have allowed for the possibility different longitudinal (α_L) and shear vertical (α_V) attenuation coefficients to account for the coefficient's dependence on the wavelength of the acoustic wave. After under going multiple reflections and transmissions the wave will travel some unique path $ABC..R$ with N_{L1} longitudinal paths and N_{V1} shear vertical paths in layer 1, N_{L2} longitudinal paths and N_{S2} shear vertical paths in layer 2, and so on. As we assume this path is unique to this

point, the final amplitude is a product of many single path traversals (Equations 5.2 and 5.3), grouping the reflection and transmission coefficients ($ABC\cdots R$) and exponential terms thus yields:

$$\text{Amplitude} = (A\ B\ C\ \cdots\ R)\ e^{(\alpha_{L1}N_{L1}\chi_{L1}+\alpha_{V1}N_{V1}\chi_{V1}+\alpha_{L2}N_{L2}\chi_{L2}+\alpha_{V2}N_{V2}\chi_{V2})+\cdots)}, \quad (5.4)$$

where α_n is the attenuation coefficient of layer n. Next assume it is at this point where the wave intersects with a second wave travelling some path $abc..r$, which is, in total, an equivalent path. As we specify these two paths are equivalent, this means the second ray has travelled the same number of longitudinal and same number of shear vertical paths in each layer of the media as the first. (It has just done so in a different order). Thus the amplitude of the second ray can be expressed as

$$\text{Amplitude} = (a\ b\ c\ \cdots\ r)\ e^{(\alpha_{L1}N_{L1}\chi_{L1}+\alpha_{V1}N_{V1}\chi_{V1}+\alpha_{L2}N_{L2}\chi_{L2}+\alpha_{V2}N_{V2}\chi_{V2}+\cdots)}, \quad (5.5)$$

where we note the exponential terms is the same as in Equation 5.4, as we have defined that the waves have travelled equivalent paths, thus requiring the values for $N_{\alpha n}$ to be equal. (One also notes that the total distance $\chi_{\alpha n}$ for each polarized wave in each layer of the plate has already been found to be a constant in Section 3.3.2, and the attenuation is each layer of the plate is constant as we have assumed the materials are all homogeneous. The two waves now undergo final reflections and/or transmissions, where we factor in coefficients S and s for the two waves to account for this, and they then travel on an coincident path and superposition can be use to combine the two waves. This yields the total amplitude

$$\begin{aligned}\text{Amplitude} = \quad & [(A\ B\ C\ \cdots\ S) + (a\ b\ c\ \cdots\ s)] \\ & e^{(\alpha_{L1}N_{L1}\chi_{L1}+\alpha_{V1}N_{V1}\chi_{V1}+\alpha_{L2}N_{L2}\chi_{L2}+\alpha_{V2}N_{V2}\chi_{V2}+\cdots)}, \quad (5.6)\end{aligned}$$

where here we note the exponential term contains all the information due to the attenuation of the wave, and the remaining multiplication and addition contains the information of the amplitude of the unattenuated rays. Recall that this superposition in equation 5.6 can be expressed as a summation because the two waves have travelled identical paths. That is they have travelled the same horizontal distance and the same time of flight, and thus there is no phase shift to include in the calculations. (Any 180 degree phase shift resulting in an amplitude inversion is taken care of via sign inversion in the reflection and transmission coefficients). The wave now continues its propagation from this point undergoing additional traversals of unique path segments, and additional superpositions when paths become coincident. The first case requires only more products to be included in Equation 5.6; while the second case again uses the superposition of equations of the form of Equations 5.4 and 5.5, which yield an equation of the form Equation 5.6. Because the exponential term, which deals with the attenuation of the wave, has been successfully separated from the ray based amplitudes, the attenuation can be calculated separately from the ray based amplitude calculations, by making certain the total path length travelled by the wave in each layer of the material is known. These totals can be kept track of and output with the leaky wave information during the ray based amplitude calculations. Alternatively, having kept track the total path travelled by each wave (N_{L1}, N_{V1}, N_{L2}, N_{V2}, and so on) these distances are easily calculated after the amplitude calculations as long as the individual χ values are known for each layer of the plate, or the information to find them via Equation 3.6 is known (i.e. the material parameters, and incident angle).

5.2 Altering Layer Thickness, and Re-Calculating the Horizontal Position, and Time of Flight of the Rays

Although the method of calculation (Section 4.3) described calculating the horizontal position and time of flight during the ray based amplitude calculations; having output the the total path travelled by each wave (N_{L1}, N_{V1}, N_{L2}, N_{V2}, and so on) with the amplitude calculations it is possible to also calculate the time of flight and horizontal position separately. Referring back to the equations for the time of flight (Equation 3.5) and horizontal distance (Equation 3.4) travelled by the ray for each path segment, the total time of flight is calculated via the summation of the individual time of flights segments over each polarization (α) in each layer of material (n)

$$tof = \sum_{\alpha,n} tof_{\alpha n} N_{\alpha n}, \tag{5.7}$$

and the horizontal position is the summation of the individual horizontal displacements

$$x = \sum_{\alpha,n} x_{\alpha n} N_{\alpha n}. \tag{5.8}$$

This allows one to alter the material's thicknesses without recalculating the amplitudes, thus adding further flexibility to the results as they are made partially independent of the layers thickness. We specify partially independent, as to examine the space-time domain of the results we will need the thicknesses at some point. To make these recalculations of course requires the tof and x values be known for each path segment, or the information to find them via Equations 3.4 and 3.5 to be known (i.e. the material parameters, and incident angle).

5.3 Extending the Results from Rays to Waves

To this point the acoustic waves have been modelled as rays, and we have calculated only factors such as the time of flight, the horizontal position, and the amplitude of the ray at the interfaces for a particular angle of incidence and material composition. To extend these rays to more realistic acoustic waves, including factors such as the frequency, or time domain properties of the wave, as well the finite physical size of the wave and its space domain properties. These factors will be accounted for via a separate set of calculations than the ray based amplitude calculations. This allows for the theory to find results for a variety of acoustic sources (under the condition of constant samples, and constant angle of incidence of the acoustic source), while only performing the amplitude calculations a single time. While the specifics of this process will differ for the exact incident wave one wishes to consider, this extension of the rays to physical acoustic waves becomes a matter of considering the superposition of the multiple acoustic waves that will overlap in the time and space domains due to the acoustic wave's physical size, and time domain variations.

This process can be can be examined via two methods which provide convenient methods for the expansion for waves with either short or long space-time distributions. The first considers the situation of a wave with a very short pulse length; for the time domain the wave has a short time distribution, but large frequency distribution. This case is very close to the initial perfect spike in space time of the ray based data, and the wave can be expanded via a discrete examination of the space or time domain properties of the

wave. At the other end of the spectrum exist waves with long time domain behaviour, but a small frequency distribution. Here phasor addition will be used to approximate the result of a plane wave, and a combination of these results allows for the easy consideration of waveforms made up of a discrete number of frequencies. Details of both these options follow in the proceeding sections.

5.3.1 Discrete Time Domain Expansion of Ray Data

In this case the time domain signal is considered as a finite number of discrete points, which is initially filled with zeros (to signify no acoustic waves arriving at any point in the time domain). The current ray data is expanded point by point into the time domain according to the acoustic wave's time domain behaviour. The amplitude behaviour at each point in the time domain from this ray is added to the previous time domain results, thus obtaining the appropriate superposition in the time domain. Mathematically one can write this as

$$Amp(t_n) \leftarrow Amp(t_n) + A\, f(t_n - tof) \tag{5.9}$$

where $Amp(t_n)$ is the time domain amplitude at time t_n, $f(t)$ represents the wave's time domain properties, and A is the amplitude of the ray, which arrives at time tof. The above equation only needs to be calculated beginning at the time tof (or the closest discrete t_n point) with the process continuing while the function $f(t)$ exists. (i.e. the point by point evaluation does not need to be evaluated for all points in the time domain). With such a method a more accurate time domain will create a longer calculation process, as will a

longer time domain. For those very long time domain waveforms (plane waves) it is more advantageous to consider the method examined in the proceeding section.

5.3.2 Approximation of Plane Wave Results Via Phasor Addition

A unique option presents itself when one wishes to expand the results of the ray based theory to a plane wave result allowing it to more easily examine waves with long time domain properties in comparison to the method described above. In this case the amplitude of the superposition of the multiple plane waves can be found via phasor addition. Here the amplitude of the n^{th} wave leaked from the plate at time t_n, and position x_n can be written as a typical plane wave

$$Wave_n = A_n cos(\omega t_n - k_x x_n). \tag{5.10}$$

One could of course consider a sine wave, or the complex format $e^{i(\omega t - k_x x)}$. For phasor addition this plane wave is written in terms of a vector with x and y components

$$Amp_x = A_n cos(\omega t_n - k_x x_n), \quad \text{and} \quad Amp_y = A_n sin(\omega t_n - k_x x_n) \tag{5.11}$$

where the angle of the vector is given by the phase $\omega t_n - k_x x_n$. (It is noted that this system is analogous to considering the complex wave format $Ae^{i(\omega t - k_x x)}$ on real (x) and imaginary (y) axis). To find the total amplitude of the resulting superposed plane wave vector addition can then be used. The total of the x and y components are found individually for each leaky wave

$$\sum_{n=1}^{N} Amp_x, \quad \text{and} \quad \sum_{n=1}^{N} Amp_y, \tag{5.12}$$

making the amplitude of the resulting plane wave

$$Amp_{PW} = \sqrt{\left(\sum_{n=1}^{N} Amp_x\right)^2 + \left(\sum_{n=1}^{N} Amp_y\right)^2}. \tag{5.13}$$

Applying the summation over a large number of waves will allow the ray technique to approximate a plane wave solution, and does not require the expansion of the amplitude results in space and time domain. This process can also be repeated for plane waves at different frequencies, thus allowing for the examination of acoustic waves more easily described as a superposition of plane waves, and those with long time domain distributions. Once the frequency domain results are obtained for the specific waveform, an inverse Fourier transform can be used to examine the results in the time domain.

5.3.3 Space Domain Expansion

While the above sections specifically discussed the expansion of the ray data into time domain, the same procedures also can be used for the expansion of the ray data into the space domain. Here knowing the physical profile of the wave in the space domain one can expand via the point by point method outlined in Section 5.3.1 for waves with small space domain properties. As well, the phasor addition method is also valid in the space domain, for examining cases of long space domain distributions. However, instead of examining the necessary frequencies of the planar wave, the wavenumber k_x is altered. Recalling that $k_x = \frac{\omega}{c} sin(\theta)$, to alter the wavenumber requires the results be calculated for various angles of the acoustic wave within the media. (θ, and c are the angle and the velocity of the acoustic wave in a layer of the plate). This does make the process

somewhat more involved because while the results were frequency independent in the time domain method, they are not independent of the angle θ.

5.4 Other Options

5.4.1 Inclusion of Transducer Effects

As well as the above possibilities to expand the results so that they describe more realistic situations, at this time one could also consider factors pertaining to the reception of the acoustic rays by the transducer by filtering the data appropriately, or performing additional calculations. For example, if one wished to consider the response of a planar transducer located at a specific position along the sample, one could filter the results to only include those rays which lie within a specific range of horizontal positions on the plate's surface. Expanding upon this and using multiple such filters one could consider the acoustic waves arriving at each element in a linear array of transducers. More advanced techniques could consider the angle(s) at which the acoustic wave interacts with the transducers. Such considerations are needed to consider the case of a focused transducer receiving the acoustic single, here one needs to consider the angle(s) at which the acoustic wave(s) interact's with the focused transducer's curved surface to properly calculate the transducer's response. In addition, while this thesis has focused on calculating the amplitude of those those waves leaked to the surrounding half-spaces, one could also consider calculating the displacement of the surface of the sample, or the velocity

of this oscillating displacement of the sample. These could even be considered in terms of horizontal, and vertical components (along the sample's surface, and perpendicular to the sample) to examine the results when alternative devices to detect the acoustic wave, such as laser interferometers, or EMAT (Electromagnetic Acoustic Transducer) are used. (Here the laser interferometer detects the vertical surface displacements, and the EMAT detects the horizontal velocity components of the acoustic wave's oscillations).

5.4.2 Data Filtering for Theoretical Uses

As well as the practical uses for filtering the data, there also exist valuable options for filtering the data for theoretical studies, and to present the results. One such example found useful in this thesis is the ability to filter the results of specific ray paths from the theoretical data. This allows one to easily examine the amplitude changes of these results, or to highlight specific data when plotting results.

Chapter 6: Results: Validation, Experimental Comparisons, and Bond Detection Application

6.1 Validation

6.1.1 Conservation of Energy

It is known that each individual reflection and transmission coefficient calculation undergone by a wave as it intersects with an interface in the plate structure satisfies energy conservation. As the calculation technique is made up of a series of these calculations, and the model features no methods for energy loss (except through the effects of the attenuation of the materials in the plate), the results are thus expected to obey the principle of energy conservation (as long as we consider non-attenuative materials). In this section we will utilize the expectation of energy conservation to test the validity of the results of the calculations of the multiple reflected acoustic waves in a multilayer plate

Material	Longitudinal Velocity (m/s)	Shear Velocity (m/s)	Density (kg/m^3)	Thickness	
				Thin Layer Case	All Other Cases
Water	1400	0	1000	-	Half-Space
Aluminum	6420	3040	2700	Half-Space	2.0 mm
Epoxy	2400	1201	1154	10 μm	2.0 mm
Steel	5960	3235	7900	Half-Space	0.5 mm

Table 6.1: Material Parameters for Theoretical Studies.

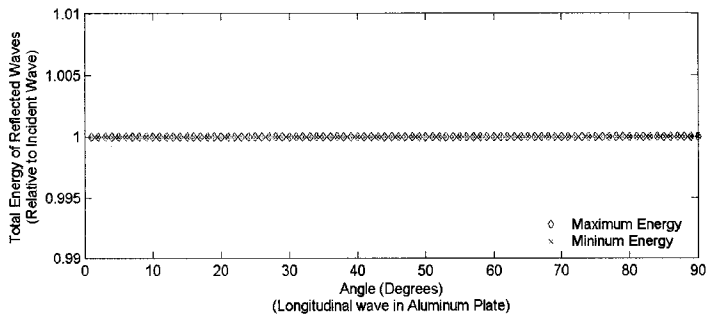

Figure 6.1: Minimum and Maximum Energy of Waves Reflected at the Interfaces of an Aluminum plate. 100 Reflections are calculated and tested.

structure.

6.1.1.1 Conservation of Energy At Each Reflection and Transmission

While the individual reflection and transmission calculations are known to satisfy energy conservation, it is wise to verify that energy is also conserved for the multiple reflection and transmission calculations taking place in each iteration of the ray technique's amplitude calculations. Thus in this section we verify that the total energy of all waves is indeed conserved after each set of the reflections and transmission calculations is made. Here we will examine the cases of a single and multilayer plates surrounded by vacuum half-spaces. In such a situation any acoustic wave introduced to the plate will travel in the plate with no energy loss, thus the total energy of the waves after the first reflection will be the same as the total of the waves after multiple reflections have occurred. For our test we consider a single layer case of an aluminum plate, and in the multilayer plate case of an Aluminum-Epoxy structure. It should be noted that the exact materials in use are not the important part, instead we are concerned with verifying that the reflection and

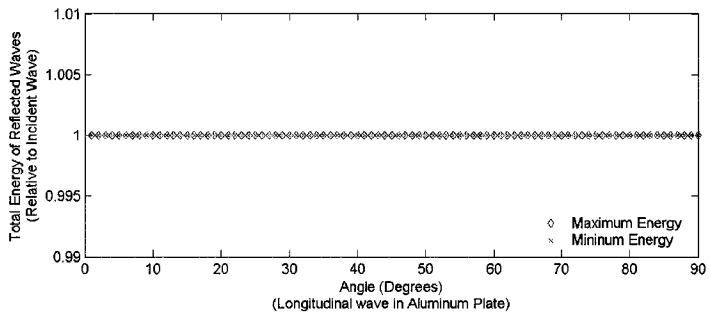

Figure 6.2: Minimum and Maximum Energy of Waves Reflected at the Interfaces of an Aluminum-Epoxy plate. 50 Reflections are calculated and tested.

transmission calculations are energy conserving. In both samples we define an incident longitudinal wave in the aluminum plate with 1 unit of energy, and test a full range of incident angles (0 to 89 degrees, in 1 degree increments, as measured for the longitudinal wave in the aluminum plate, which corresponds to roughly 0 to 12 degrees incidence in the water half-space), finding the minimum and maximum energy of the waves for 100 reflections in the single layer plate, and 50 reflections and transmissions in the multilayer plate case. As this 1 unit incident wave cannot leak to the surrounding media due to the vacuum half-spaces, it is expected that the total energy of the waves after each reflection within the plate to also possess 1 unit of energy. Figure 6.1 and 6.2 show these results for the Aluminum, and Aluminum-Epoxy plate respectively. Here we see that as expected the minimum and maximum energy of waves in the plate, for all angles tested, is identically 1 unit, and with the minimum and maximum wave amplitude being 1 unit, all other calculations are also restricted to be 1 unit in size. Thus it can be safely concluded that the calculation process of tracking the waves, calculating the amplitude, and performing superpositions has maintained an energy conserving state as the number of reflections increases.

6.1.1.2 Conservation of Energy: Examining the Total Energy Leaked to Half-Spaces

With energy conserved after each set of reflection and transmission calculations for an acoustic wave trapped within a single and multilayer plate, the acoustic wave is now allowed to leak from the sample by changing the vacuum half-spaces into half-spaces of water. In these cases, as the acoustic waves reflect multiple times in the sample, waves will also leak to the surrounding half-spaces; where each of these rays carries some fractional amount of the incident wave's energy. By combining the energy of these multiple leaky waves, the total energy is expected to gradually increase to the same level as the incident wave's energy. Because in most cases the wave will be partially reflected and transmitted at the interfaces in the plate structure and the surrounding half-spaces, some energy will remain in the plate, and thus this gradual increase is expected to approach the energy conserving state in an asymptotic manner. Alternatively the energy within the plate is expected to gradually decrease to zero.

To verify the calculations do in fact obey the conservation of energy we choose to examine a few particular cases. Again, the exact materials in use here are not the important part, instead we are considered with verifying that the calculations do in fact approach an energy conserving state as the number of reflections, and thus number of leaky waves accounted for, increases. To begin we consider the case of a single layer plate made of aluminum with two different half-space arrangements. (The material parameters are summarized in Table 6.1). The first arrangement (Figure 6.3) utilizes an upper half-space of

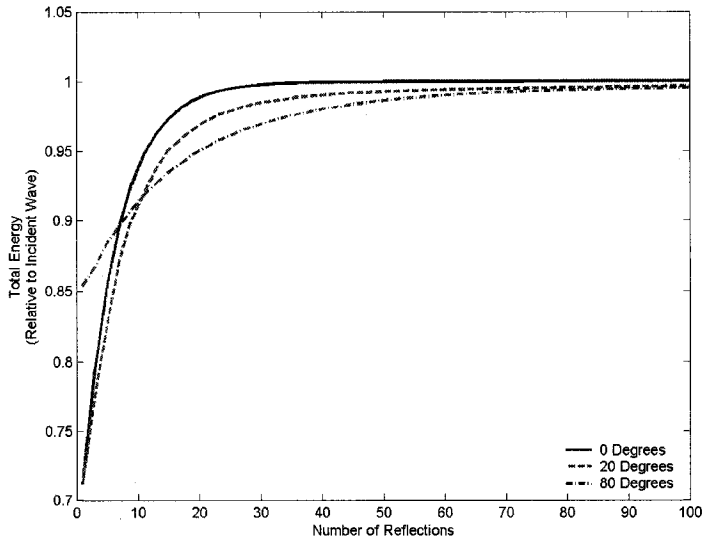

Figure 6.3: Total Energy Transmitted Outside an Aluminum plate with upper Water half-space, and lower Vacuum Half-space.

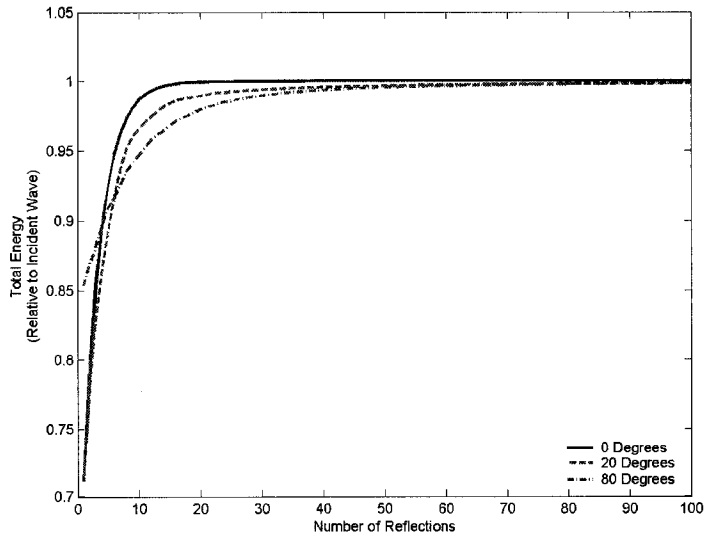

Figure 6.4: Total Energy Transmitted Outside an Aluminum plate with upper and lower Water Half-spaces.

water, and a lower vacuum half-space; and the second (Figure 6.4) utilizes both upper and lower half-spaces of water. In the first arrangement the lower Aluminum-Vacuum interface provides for a 100% reflection of the energy back into the aluminum resulting in the energy only being emitted to the upper water half-space, while the second arrangement allows energy to be emitted to both half-spaces. In both situations the incident wave is a longitudinal wave on the upper water half-space with 1 unit of energy, where this wave is incident on the plate at such an angle that it will generate longitudinal waves in the Aluminum plate travelling at normal incidence (0 degrees), 20 degrees, and 80 degrees. (Shear vertical waves are of course also generated in the plates). These three particular angles are chosen as this provides an opportunity to verify energy conservation exists at normal incidence, a small angle, and a large angle case. In both plate arrangements the energy from the rays are calculated until a total of 100 reflections have occurred in the plate structure to provide ample calculations to verify energy conservation does exist. The results of the energy calculations are as shown in Figures 6.3 and 6.4 for Water-Aluminum-Vacuum, and Water-Aluminum-Water arrangements respectively. As expected the total energy is found to asymptotically approach an energy conserving state as the number of reflections increases for all three angles tested, and in both material arrangements. In addition, in both cases the total energy has reached at least a 99.5% energy conserving state by the time 100 reflections calculations have been made. An examination of the energy remaining in the plate after these 100 reflections finds that the small amount of energy not leaked to the water half-spaces does in fact remain in the plate, and combining the energy remaining in the plate with the energy leaked to surrounding water half-space(s) accounts for 100% of the energy introduced to the sample. As a final note it is observed

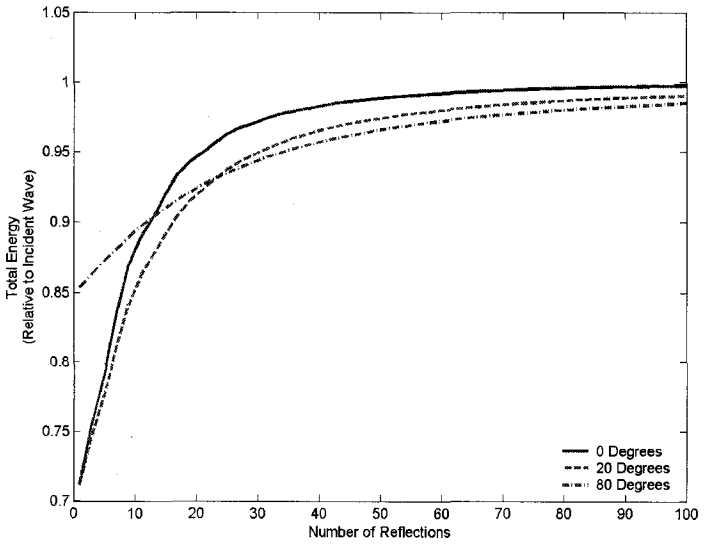

Figure 6.5: Total Energy Transmitted Outside an Aluminum-Epoxy plate with upper Water half-space and lower Vacuum Half-space.

that in the Water-Aluminum-Water arrangement (Figure 6.4) the energy conserving state is approached faster than in the Water-Aluminum-Vacuum case. This is because energy is emitted from the plate at every reflection to a water half-space, rather than every other reflection when the Vacuum half-space is present.

It is of course also possible to consider situations dealing with multilayer plates, where in this case we examine the case of the total energy exiting from an Aluminium-Epoxy plate with an upper half-space of water, and a lower vacuum half space. Where the results are shown in Figure 6.5, and the material parameters are summarized in Table 6.1. Again we have tested the cases an acoustic wave travelling at normal incidence, 20 degrees, and 80 degrees through the Aluminum plate, calculating the energy from rays as the number of reflections and transmissions increases, and a total of 100 reflections have been calculated. Again, as expected, for all three angles tested the total energy

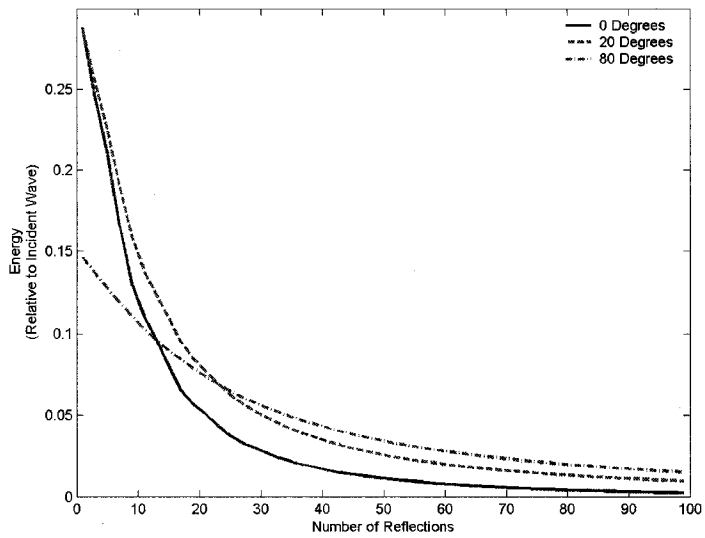

Figure 6.6: Energy Remaining within an Aluminum-Epoxy plate with upper Water half-space and lower Vacuum Half-space.

is asymptotically approaching an energy conserving state as the number of reflections increase. Although the energy leaked to the half spaces continue to rise slightly with additional reflections, by 100 reflections we have obtained a level of at least 98.5% energy conserving state. For completeness, Figure 6.6 shows that the total energy remaining in this Aluminum-Epoxy sample does in fact approach zero as the number of reflections increase. Here, for the 80 degree test angle the sample has 0.015 units of energy in the plate after 100 reflections; when combined with the 0.985 units of energy leaked to the upper water half space one sees that the total energy in the system is indeed 1.0 units; i.e. the total energy is conserved as expected. One could in addition plot the case with two half-spaces of water around the Aluminum-Epoxy sample, here much like in the case when the Aluminum plate is surrounded by water, the energy is able to leak to both half-spaces and the results reach an energy conserving state at a faster rate than seen in

Figure 6.5.

6.1.2 Comparison to Plane Wave Model

In the previous section we examined the total energy leaked from the multilayer plate to ensure the calculations obeyed the principle of energy conservation in situations with non-attenuative materials. This section provides an additional verification for our technique via comparisons to results from plane wave models; in particular the results from the transfer matrix models by by Lowe [13], Brekhovskikh [14], or Briggs [15] which is briefly outlined in Section 1.3.2 of this thesis. To make this comparison the results from the ray based technique must be expanded to approximate a plane wave at various frequencies. This can be done by calculating the amplitude of the waves leaked to the surrounding half-spaces over many reflections, these ray based amplitude results are then considered as the amplitudes of multiple plane waves, and these plane waves can be combined via a series of phasor additions; here the phasor accounts for phase delay in the wave due to both the time delay, and horizontal distance travelled by the waves before they are leaked to the half-spaces. (See Section 5.3.2 for more details.)

In this section we will consider the cases of a single layer Aluminum plate, and a multilayer layer plate with a layer of aluminum bonded to steel (i.e an Aluminum-Steel plate), where in both cases the two surrounding half-spaces are defined to be water. (The material parameters are summarized in Table 6.1). As previously mentioned, the ray based calculations will use phasor addition to approximate the plane wave result by

combining the amplitudes of the waves leaked during 100 reflections for the single layer plate, and 75 reflections for the multilayer plate case. The frequency of the plane waves to be examined range from 0.02 MHz to 4 MHz, in 0.02 MHz increments, where this range and increment size is used as it allows for multiple Lamb modes to be generated and observed, and as well avoids any problems in the transfer matrix calculation process due to large frequency-thickness products. Finally a full range of angles will be tested, examining angles from 0 to 89 degrees (in 1.0 degree increments), where this measures the angle of a longitudinal wave in the Aluminum plate. These frequency and angle considerations are of course the same in the plane wave, and ray technique calculations, and will allow for a quantitative comparison of the two theoretical results.

6.1.2.1 Single Layer Plate

The results for the Aluminum plate can be seen in Figure 6.7 for the ray based result, and Figure 6.8 for the plane wave result. These two figures both show a two dimensional colour scale mapping of the amplitude of the reflectance function for each angle and frequency examined. As well, we also specifically examine the amplitude versus frequency response of the reflectance function at the angle of 50 degrees (Figure 6.9) overlaying the plane wave and ray technique results. In this particular case, Figure 6.9 shows both the amplitude of the reflectance function, as well as the frequency location of the lamb modes[6], match almost exactly between the ray technique and plane wave results. As well,

[6]The locations of the lamb modes correspond to the sudden decreases in the amplitude of the reflectance function see in Figure 6.9

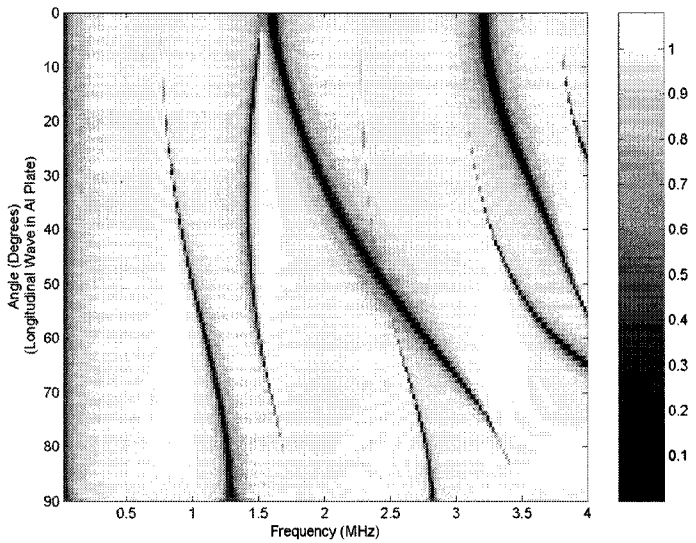

Figure 6.7: Ray Technique results showing the amplitude of the reflectance function versus frequency and angle for an Aluminum plate. (Angle measures longitudinal wave in Aluminum plate).

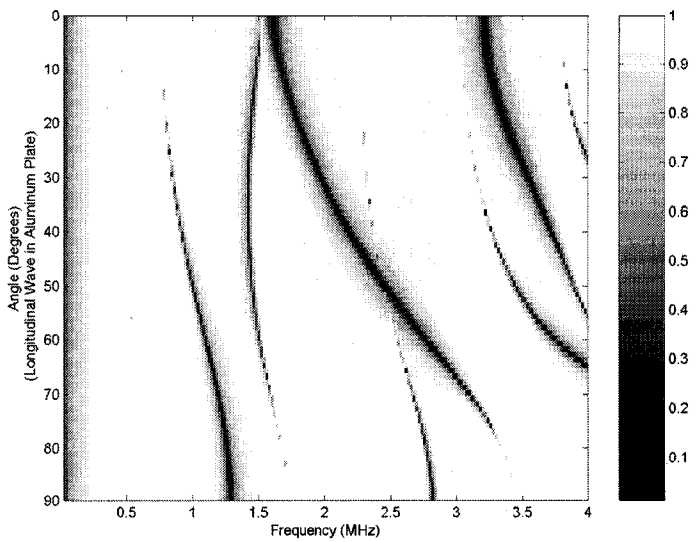

Figure 6.8: Plane Wave results results showing the amplitude of the reflectance function versus frequency and angle for an Aluminum plate. (Angle measures longitudinal wave in Aluminum plate).

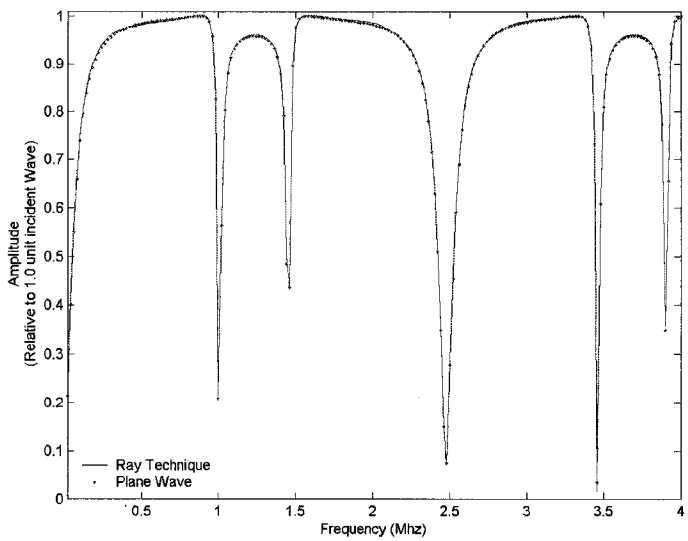

Figure 6.9: Comparison of the Ray Technique and Plane Wave results for the amplitude of the reflectance function versus frequency for a 50 degree angle in an Aluminum plate. (Angle measures longitudinal wave in Aluminum plate).

an examination of the entire frequency versus angle mapping of the reflectance functions (Figures 6.7 and 6.8) finds an overall qualitative correlation in the location of the lamb modes for the Aluminum plate. Because there is a one-to-one correspondence in the frequencies and angles tested in the ray based and plane wave data sets, it is possible to the subtract the two data sets and quantitatively examine the overall difference between the two plots. Figure 6.10 gives a histogram representation of these results showing the distribution of the percentage of data points, where each block represents data within a range of ± 0.0025. Examining these results, it is found that approximately 60% of the results lie within a range of ± 0.0025 from zero, a total of 76% of the results lie within the ± 0.005 range, and a total of 97% of the results within an error range of ± 0.025 from zero. The differences between the two results, though very minor, can be explained by the fact that we have approximated a plane wave result from the ray based calculations by using

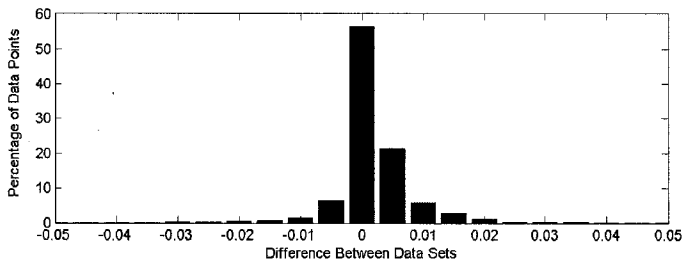

Figure 6.10: Histogram of the difference in the reflectance functions between the ray based and plane wave results for the Aluminum plate.

a finite number of reflection calculations, and the plane wave theory has approximated multiple reflections in the plate via four plane waves. In addition, some accuracy has been lost in the results due to the precision at which the amplitude data from the ray based output, and the calculation process of both theories. If the precision, and number of calculations increased, the error in the results would likely decrease, however data precision and also calculation precision would still be a source of error.

6.1.2.2 Multilayer Layer Plate

The results for the multilayer plate (the Aluminum-Steel sample) are seen in Figures 6.11 through 6.14. A visual examination of the reflectance function for the ray technique (Figure 6.11), and plane wave technique (Figure 6.12), finds an overall very good qualitative match. A very close examination finds the lowest frequency mode intersects the frequency axis at 1.0 MHz in the plane wave case, but below the 1.0 MHz point in the ray technique case. As well, in the plane wave case the two modes located at 3.5 MHz - 70 degrees appear to cross, while in the ray technique case they come very close but

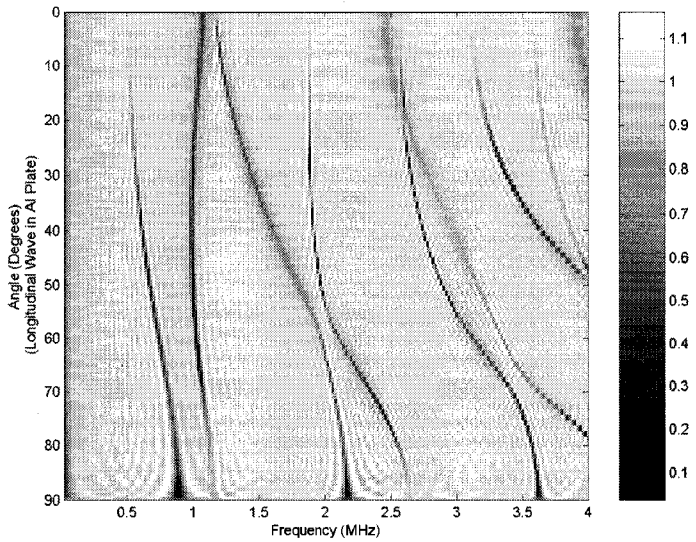

Figure 6.11: Ray Technique results showing the amplitude of the reflectance function versus frequency and angle for an Aluminum plate. (Angle measures longitudinal wave in Aluminum plate).

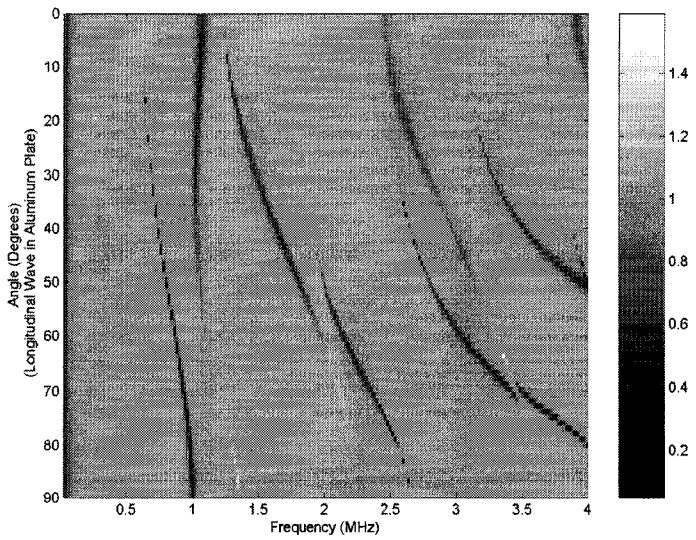

Figure 6.12: Plane Wave results results showing the amplitude of the reflectance function versus frequency and angle for an Aluminum-Steel plate. (Angle measures longitudinal wave in Aluminum plate).

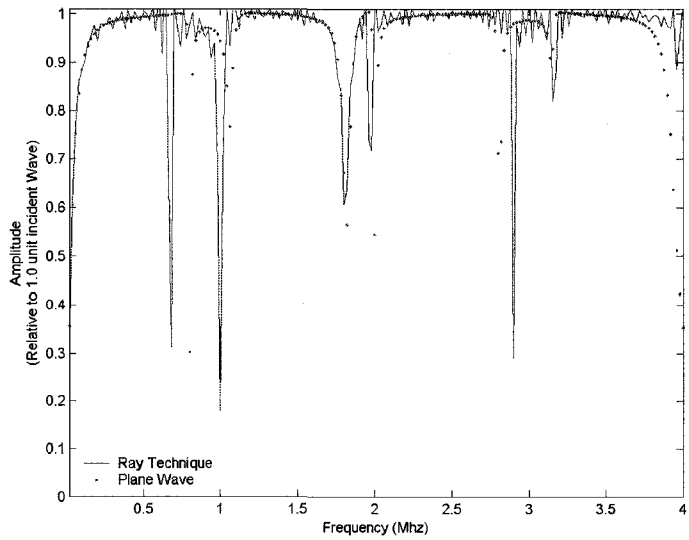

Figure 6.13: Comparison of the Ray Technique and Plane Wave results for the amplitude of the reflectance function versus frequency for a 50 degree angle in an Aluminum-Steel plate. (Angle measures longitudinal wave in Aluminum plate).

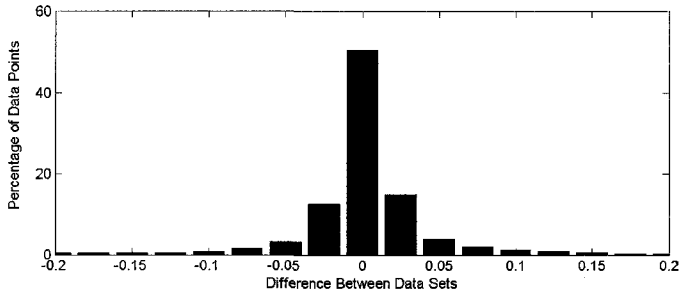

Figure 6.14: Histogram of the difference in the reflectance functions between the ray based and plane wave results for the Aluminum-Steel plate.

do not appear to cross. Examining the case of the 50 degree angle in particular (Figure 6.13) the difference in the frequency location of the first mode is seen more clearly, however the location of the remaining modes in the frequency domain match very well. The examination of this figure also finds the reflectance function's behaviour when not at a Lamb mode (the data near the 1.0 amplitude mark) oscillates in the ray technique result, where this oscillation is generally well centred around the smoother plane wave result. With the slight frequency discrepancies in the location of the Lamb mode, and the oscillating frequency, the difference between the two cases becomes more pronounced in the two layer case. Taking the difference between the results of the two theories, and plotting a histogram (Figure 6.14) of the results finds the error level increases by a factor of about 10. Examining these results, it is found that 50.5% of the results lie within a range of ± 0.025 of zero, a total of just under 70% of the results lie within a ± 0.05 range, and a total of over 91% within a ± 0.25 from zero. While the level of error has increased in this two layer plate case, there is overall a very good match between the two data sets. Here the larger error is attributed the previously mentioned oscillating behaviour of the ray technqiue's reflectance function about the smoother plane wave reflectance function, and as well some observable shifts in the frequency locations of the Lamb modes. Investigating these deviations between the two results further, one finds that recalculating the results, but using fewer reflections to approximate the ray technique's plane wave results, increases the size of the oscillations in the ray technqiue's reflectance function. Thus it is expected that if the number of calculations is increased, beyond the 75 reflection calculations used in these results, the size of oscillations will diminish and the ray based results will follow the plane wave results more closely. However, the change in the number of

calculations does not visibly alter the location of the Lamb modes, and the question of if the location of the Lamb modes are indeed shifted in real world experimental results remains. This question can unfortunately not be easily answered here, but due to the quite comparable results of the two theories any experimental results would be expected to yield results comparable to the ray technique and plane wave techniques. However, because both methods have approximated a real world sample by assuming the ideal case, the real world experimental results will most likely provide a third option for the results of the reflectance function.

Before continuing, one may have observed that the number and location of the Lamb modes in the case of the Aluminum plate (Figures 6.7 and 6.8), is different than the case of the Aluminum-Steel plate (Figures 6.11 and 6.12). Such differences in the Lamb mode structure is already the subject of quantitative and qualitative; experimental and theoretical studies (not all of which use the plane wave approach) in the non destructive evaluation of materials. With such wide usage of the Lamb modes it is very beneficial that this technique is able to produce the expected results, thus aiding in showing the validity of our model.

6.1.3 Comparison to Thin Layer Model

The validation of the results continue, now examining the specific case of a thin layer of material between two-half spaces. The thin layer results used for this validation will be provided from the phase perturbation theory previously examined by Sadler, O'Neill,

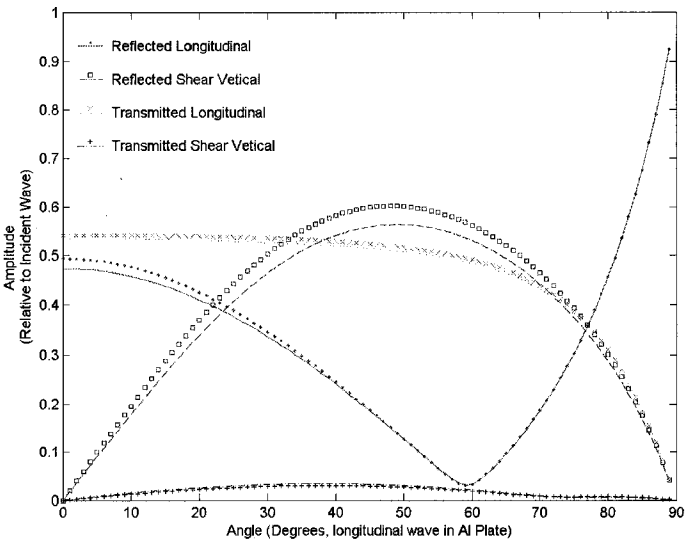

Figure 6.15: Comparison of Phase Perturbation results (symbols) with Ray Technique results (lines) for an Aluminum-Epoxy-Steel sample. Here the epoxy layer is very thin (10 μm, much less than the acoustic wavelength).

and Maev [17,18]. The assumptions of this phase perturbation theory are similar to that in Section 2.3 (requiring a perfect plate, and ideal acoustic materials), and as well require a incident plane wave, and the thin layer of material to have thickness much less than an acoustic wavelength. (It is noted that while some of the restrictions in Section 2.3 are allowed in the perturbation theory, we will of course not examine such situations). Because the phase perturbation theory [17,18] has assumed the incident wave is a plane wave, the results from the ray technique will be again combined using phasor addition to approximate a plane wave as was previously done in Section 6.1.2. As well we must assume that the thin layer used in this section is thick enough so that it is possible for the wave to reflect multiple times within the layer.

Keeping these requirements in mind we examine the case of a $10\mu m$ thick layer of

epoxy bonded between a half space of aluminum and a half-space of steel, and use a 1.0 MHz incident wave with 1.0 unit amplitude. (The material parameters are as in Table 6.1). Using this theoretical setup in both the phase perturbation theory, and ray technique produces the results seen in Figure 6.15, which shows the amplitude of various reflected and transmitted waves as the angle of incidence changes. (In Figure 6.15 the phase perturbation results are denoted with the various symbols, while the ray technique results are denoted with various lines). The results from the two theories are very comparable overall, with the amplitudes following the same curve shape, and having very comparable amplitudes. In this case the results from the reflected shear vertical wave are the most noticeably different at all angles. At its largest the amplitude difference between the two results is approximately 0.04, or 7.2% different for the reflected shear vertical wave at approximatly 40 degrees, and 0.02 (4.2% different) for the reflected longitudinal wave at normal incidence. The differences between the results can be factored in from three major sources; first of all as in the plane wave comparison Section 6.1.2 the ray technique has again approximated plane wave results via a finite number of leaky waves, in this example we have calculated results for 100 reflections. Next it must be noted that the perturbation theory is itself an approximation, where the results of an Aluminum-Steel interface are expanded via a first order perturbation method to include the effects of the thin epoxy layer. This perturbation expansion causes the final source for differences in the results of the two theories; in that this perturbation method does not require that the results satisfy the energy conservation, while in comparison the ray technique results do satisfy energy conservation. Thus as one set of results obeys energy conservation, and the other does not, it is expected, and actually required, that the results of the two cases will not

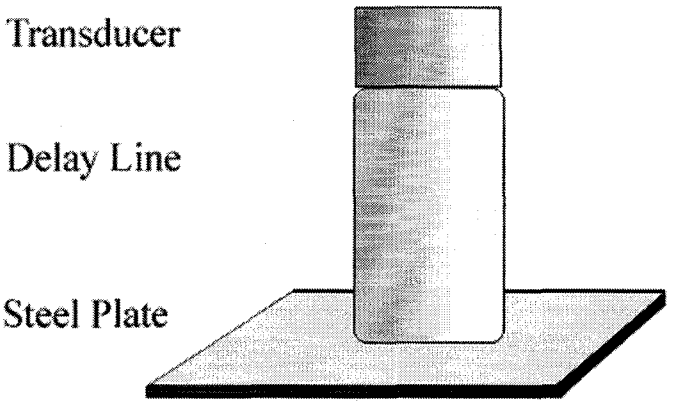

Figure 6.16: Experimental Setup.

match identically.

6.2 Theoretical and Experimental Comparisons

6.2.1 Comparison to an Experimental A-Scan

In this section we wish to compare the theoretical results of the ray based technique with those of an experimental A-Scan from a single layer plate. We wish to not only match the experimental results, but also explain some initially unexpected results obtained in the experimental data due to the assumption that data is obtained at exactly normal incidence. The experiment described in this section and the resulting experimental data obtained is courtesy of Dr. Gilbert Chapman[7] [58]. In the experimental setup shown in

[7]Dr. Gilbert Chapman, Centre for Imaging Research and Advance Materials Characterization, Department of Physics, University of Windsor, Windsor ON, Canada

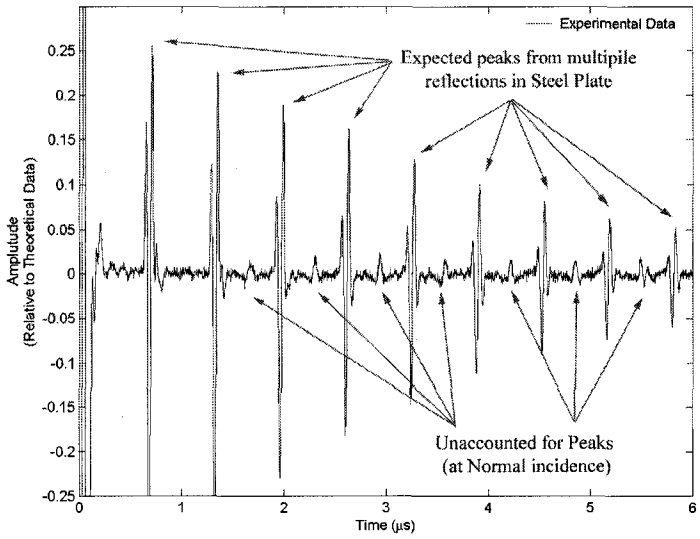

Figure 6.17: Experimental Data: A-Scan of multiple reflected waves within a Steel Plate.

Figure 6.16 a standard planar piezoelectric transducer with delay line (measured to be 7 mm long with a 6.3 μs delay) is used to take A-Scan data of a 1.95 mm thick steel plate. The transducer is ideally at normal incidence with the steel plate sample are the two pieces coupled with glycerin in order to aid the transfer of acoustic waves between the two solids (the layer of glycerin has no appreciable thickness). The transducer is connected to appropriate electronics which create a short wave pulse of approximately 20 MHz, and as well receive the A-Scan data relaying it to a computer for analysis. The resulting experimental A-Scan of a single layer steel plate is shown in Figure 6.17, where the amplitude of the experimental data has been scaled to the theoretical data (discussed below) by matching the amplitudes of the second and third peaks. The experimental data features peaks in the amplitude data that are expected from the multiple reflections of an acoustic wave in a plate at normal incidence. (This includes the peaks being located at the expected time delays, and also with the expected decay in amplitude from

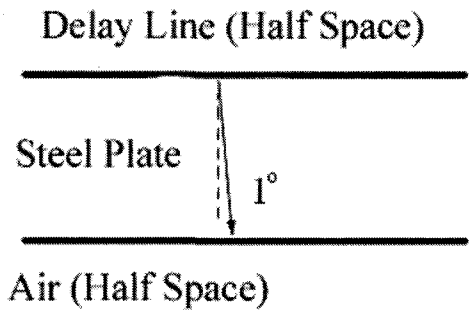

Longitudinal wave at 1° incidence in Steel Plate

Figure 6.18: Theoretical Representation of Experimental Setup.

Material	Longitudinal Velocity (m/s)	Shear Velocity (m/s)	Density (kg/m^3)	Thickness (mm)
Delay	2222	1111	2000	Half-Space
Steel	5909	2954.5	7500	1.95

Table 6.2: Material Parameters for Experimental A-Scan Comparison.

multiple reflections). However, between these expected peaks are smaller peaks, which are unaccounted for at normal incidence, and in addition have an amplitude that slightly increases with time. These peaks were experimentally determined not to be effects of the transducer or coupling material, and were postulated to be due to mode conversions created due to an acoustic wave travelling at slightly non normal incidence. This postulate, however only accounts for the location of the peaks, and does not account for the increase in amplitudes of the peaks with time. In order to test the postulate in a manner which accounts for both the time domain and amplitude properties, specifically the existence of the small peaks, and their ability to increase in amplitude with time, we will now examine the theoretical counterpart of this situation.

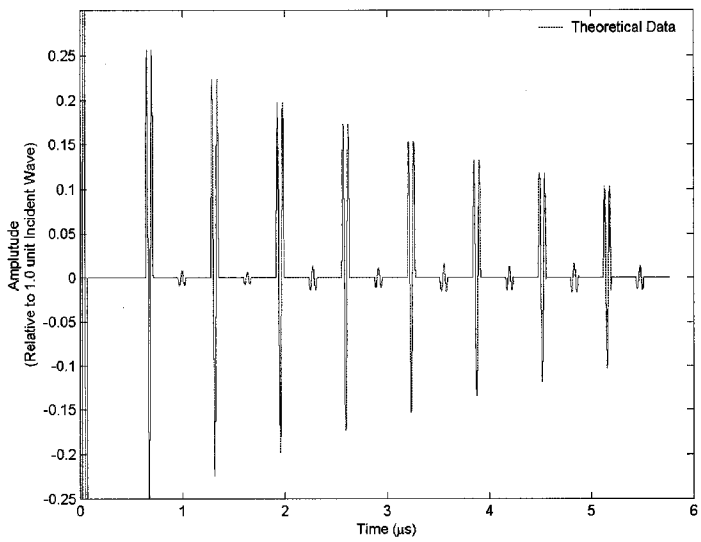

Figure 6.19: Ray Technique results showing acoustic waves leaked from Steel Plate, accounting for the possibility of slightly non-normal incidence waves.

The theoretical interpretation of the experimental setup (Figure 6.18) includes an upper half-space for the delay line, a single layer plate of steel (1.95 mm thick) and a lower half-space of air. It is noted that in this theoretical setup the finite thickness delay line may be safely modelled as a half-space because our time domain examination examines only the first $6\mu s$, and the next reflected path in the delay line itself occurs at approximately $6.3\mu s$. Continuing now, the delay line and steel plate are assumed to be perfectly bonded together (this bonding represents the glycerin couplant), and we define that the longitudinal wave travels at 1 degree in the steel plate to allow for acoustic mode conversions. The material properties of the steel plate and delay line are inferred from the experimental A-Scan data (time of flight, and amplitude of peaks) and thickness measurements of the plate and delay line. As well the results were ensured to match with expected value ranges for the materials in question (see Table 6.2 for material parameters).

The result generated by the theoretical calculations is seen in Figure 6.19 and uses a 20 MHz sine wave of 1.5 cycles in the time domain. As expected the 1 degree off set from normal incidence has allowed for mode converted waves to be generated, and produces the additional small amplitude peaks located between the main reflections in the steel plate; in addition these smaller peaks feature the expected slight increase in amplitude found in the experimental data. Before comparing the theoretical and experimental results in more detail two notes should be made. First we note that in the theoretical data we have not utilized the information about the horizontal displacement of the rays along the surface of the sample. Figure 6.19 considers rays at all positions along the surface of the sample existing at the given times. As well we note that the first peak, a result of the first reflection from the delay-steel interface, is very large (it is nearly a unit in size on the theoretical data), and the amplitude of Figure 6.19 has been set such that the smallest peaks can easily be seen.

Comparing the experimental (Figure 6.17) and theoretical (Figure 6.19) data the position of the all peaks in the time domain match up well qualitatively, and quantitatively between the two data sets. There is some discrepancy between the amplitudes of the two data sets, as the amplitude of the experimental data decreases more quickly with time than the theoretical data. This is easily explained because the theoretical data has not accounted for any attenuation factors, and as well we have considered the glycerin couplant to yield a perfectly bonded interface between the delay line and the steel plate. However, the small peaks in the theoretical data are found to slightly increase in amplitude with time, and have an amplitude in the same scale of that of the experimental data. We

note here it is difficult to provide a quantitative measure of the comparison between the theoretical and experimental data as the we have approximated the experimental wave pulse as a sine wave, and as well only estimated the material properties and influence of the glycerin couplant. Examining the theoretical data finds that these smaller peaks are, as was postulated, the mode converted longitudinal to shear vertical waves created from the reflection off the steel-air interface. In addition, it is found that the multiple reflections and additional mode conversions created on each reflection overlap in the time domain, and the superposition of these peaks cause the peaks to gradually grow in size due to constructive interference. (In this case the shear velocity of the steel has been set to exactly half the longitudinal velocity in order to maximize the number of overlapping multiple reflections.) In addition an examination of the position domain data (not shown) shows that in the time frame examined the acoustic wave has travelled less than 0.5 mm horizontally, allowing the acoustic wave to be able to enter the delay line and be detected by the transducer.

With the unexpected small peaks safely determined to be most likely due to the mode conversions of waves within the steel plate one can ask why such mode conversions may occur in the real world experiment; we thus propose the following possibilities. First the transducer and the attached delay line used to collect the experimental data shown in this section was hand held, and could be easily be held at a slightly non-normal incidence, and as well the delay line may not be cut perfectly square. In our example a 1 degree longitudinal wave propagating in the steel plate corresponds to an acoustic wave incident at 0.38 degrees on the delay line steel interface. Secondly, the sample of the steel plate

is not guaranteed to be of constant thickness, and its interfaces may not be perfectly parallel; this again causes the wave to interact with the plate's interfaces at non-normal incidence. Thirdly, the surface of the plate is not guaranteed to be perfectly flat, and the rough surface of the plates cause the wave to scatter at non-normal incidence. Finally the acoustic wave emitted from the transducer and the delay line is not a perfect beam, the beam typically spreads with a slight angle and a more accurate theoretical representation may thus be to consider the combined theoretical results over a small range of angles. Such a proposition immediately leads to the question of how the amplitude growth of these small peaks changes with the angle of the wave in the steel plate. We examine this in the next section.

6.2.1.1 Amplitude Growth of Mode Converted Paths With Angle

In the above section the theoretical data was tested at an angle of 1 degree for a longitudinal wave propagating through a longitudinal plate. This particular angle was chosen, as it was found to be a good match for the relative amplitude of the main reflections and the smaller additional reflections created due to the possibility of mode conversions. As well, the angle is appropriately small so that the delay line would be at only a 0.38 degree offset from normal incidence to the steel plate, and in addition the acoustic waves will not propagate any significant horizontal distance. The question arises of how the amplitude of these smaller peaks change with the angle of the wave. Examining the results for angles from 0 degrees to 5 degrees (in 0.5 degree increments) and plotting the amplitude of the first, third, and fifth peak due to mode conversions produces the results seen in Figure

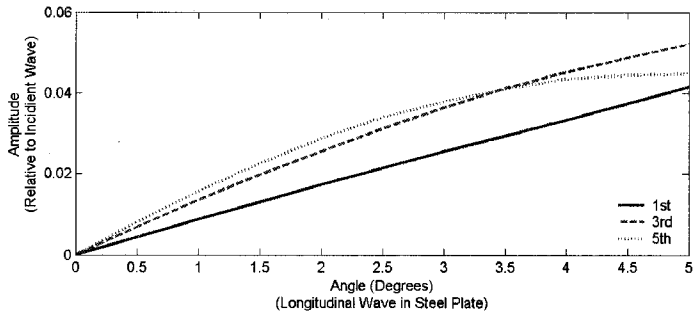

Figure 6.20: Amplitude change of first, third, and fifth peaks due to mode converting paths

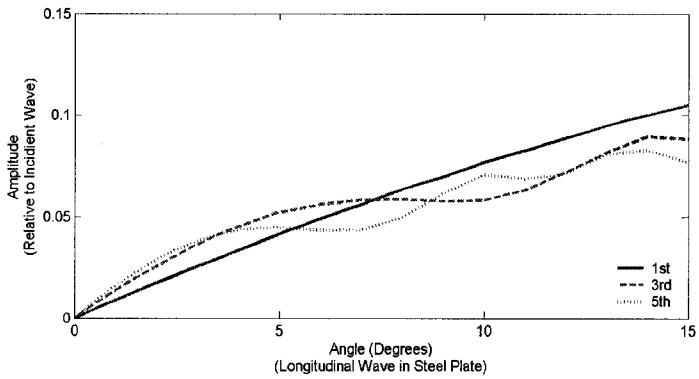

Figure 6.21: Amplitude change of first, third, and fifth peaks due to mode converting paths

6.20. Here one observes that the amplitude of the third, and fifth peaks are linear for low angles, but a noticeable deviation from a linear relation can be seen as the data begins to curve at larger angles. With this roughly linear relation combining the theoretical results over a range of angles within the steel plate thus is expected to produce very similar results to those plotted in Figure 6.19.

While the small angle amplitude change is roughly linear, to see the true relation one must consider a larger range of angles; expanding the consideration to include angles to include data to 15 degrees (additional points are measured every 1.0 degrees) produces

Figure 6.21. Examining Figure 6.21 finds the relation is not a simple curve, but the amplitude is found to oscillate, where the oscillations centre around a generally increasing amplitude as the angle increases. The overall increase in amplitude can be directly related to the tendency of the reflectance coefficients for the longitudinal to shear vertical (and shear vertical to longitudinal) mode conversions to increase with the angle of incidence. The oscillating behaviour is most likely due to the changing time of flight in the waves as the angle increases. Here one must recall that each peak is actually a superposition of multiple waves travelling with approximately the same time of flight, and these waves gradually interact with alternating overall constructive and destructive interference, thus creating the oscillation in the amplitude. (It should be noted these are not the equivalent paths which have already combined via the ray technique, but additional ray paths which simply happen to have the same approximate time of flight due to the material parameters). With further increases in angle the small amplitude reflections begin to separate further, and also interact with the larger amplitude peaks, and the amplitude of the small peaks become more difficult to discern.

6.2.2 Simulation of the Epoxy Curing Process

In this example we simulate the curing process of an epoxy layer in a Polyethylene-Epoxy-Aluminum sample, where the upper half-space is assumed to be a delay line, and aluminum layer forms the lower half-space. Examining such a situation allows for another comparison to a real world experiment, and shows that it is possible to consider situations in which the material parameters are altered slowly (relative to the acoustic scanning pro-

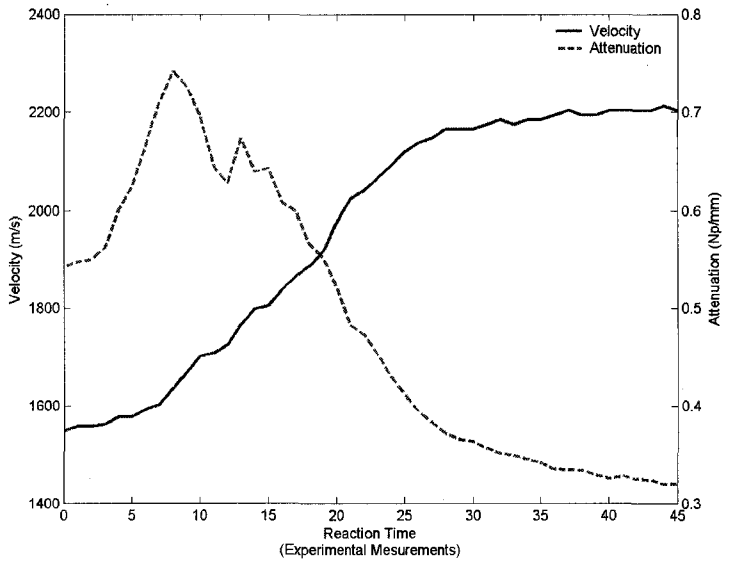

Figure 6.22: Velocity and attenuation of Epoxy layer during the curing process.

cess). In addition, this case also provides an opportunity to examine a problem which includes the effects of attenuation. The ray based technique simulates this curing process by altering the material parameters in accordance to the provided experimental measurements for each iteration of the calculation process. The experimental results used here are provided by Inna Severina[8]and show how the velocity and the attenuation of the epoxy layer are altered during the curing process (See Figure 6.22 for a graphical representation of these changes). Here it is assumed that during the curing process these material properties are altered slowly enough so the parameters of the epoxy layer can be considered as constants for each set of theoretical calculations (i.e. the acoustical scanning process is much faster than the alteration of the material's properties). In addition, during the curing process the thickness of the epoxy layer, and all other material parameters are

[8]Inna Severina, Centre for Imaging Research and Advance Materials Characterization, Department of Physics, University of Windsor, Windsor ON, Canada

Material	Longitudinal Velocity (m/s)	Density (kg/m^3)	Thickness (mm)	Attenuation (Np/m)
Delay	2222	2000	Half-Space	-
Polyethylene	2350	940	1.1	-
Epoxy	See Figure 6.22	1220	3.0	See Figure 6.22
Aluminum	6320	2640	Half-Space	-
Note: Shear Velocity is defined as one half of longitudinal velocity for all media				

Table 6.3: Material Parameters for Adhesive Curing Study.

assumed to be constant during this curing process, these parameters are outlined in Table 6.3. Finally for simplicity the experimental and theoretical data will be assumed to be taken at exactly normal incidence.

Performing the ray based calculations for one set of of material parameters of the curing process produces Figure 6.23 which compares the results for when one considers attenuation, to the results when the attenuation of the epoxy layer is not considered. In these figures results are calculated when the velocity of the epoxy layer is 2202.6 m/s, the attenuation of the epoxy layer is 0.32 Np/mm, and the incident wave form is assumed to be a 4.0 MHz sine wave of 1.5 cycles in the time domain. Comparing the two figures one observes, that as expected, introducing the attenuation of the epoxy layer has decreased the amplitude of the resulting waveform for the data which has travelled through the epoxy layer. Here the significant decrease in the amplitude of the second wave pulse is due to the relatively large thickness of the epoxy layer, where the amplitude of the wave is decreased by a factor of $e^{-2\alpha d}$, or numerically a factor of 0.0118 to 0.14 depending

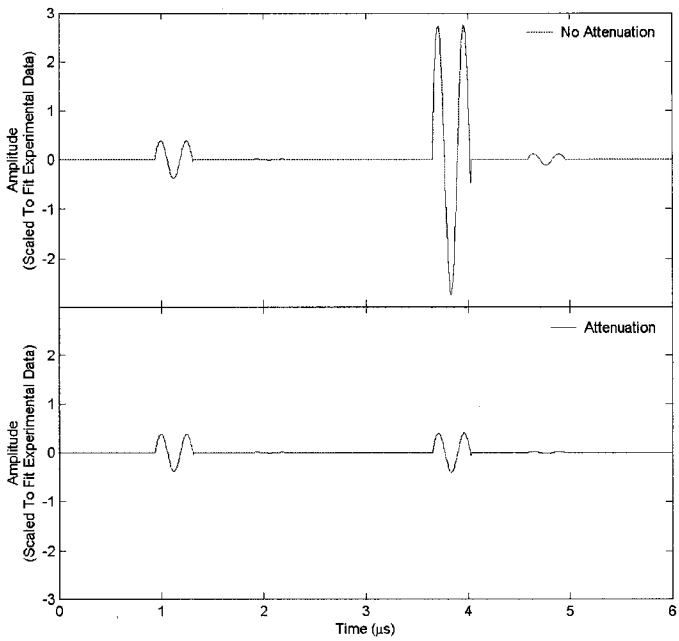

Figure 6.23: Theoretical results of curing process showing difference between data with and without attenuation.

on the attenuation of the epoxy. (The factor of two in the exponential term is due to the acoustic wave needing to travel twice through the thickness of the epoxy to return to the Polyethylene layer.) Meanwhile, there exists no change in the amplitude of the first pulse, because it is created from the reflection off the Polyethylene-Epoxy interface, and thus the wave has not travelled through the attenuating epoxy layer. Here the amplitude of the first pulse is relatively small compared to the second pulse, because the impedance of the Polyethylene and epoxy are of comparable size making the reflection coefficient (and thus the amplitude of the reflected wave) at this interface near zero, and the transmission coefficient near 1.0 unit. Similarly after reflecting from the Epoxy-Aluminum interface the wave again interacts with the Epoxy-Polyethylene interface, and is again mostly transmitted. The small amplitude waves reflecting back into the epoxy

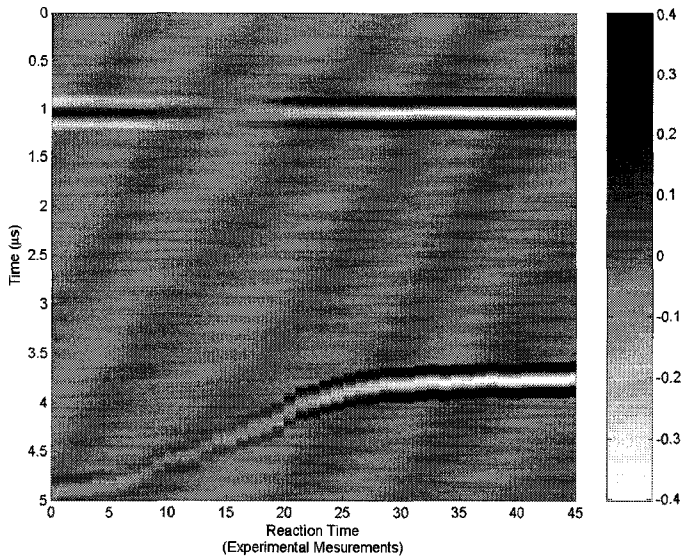

Figure 6.24: Theoretical Results of Curing Process.

layer are subject to even more attenuation, and the subsequent reflections are generally not visible on most measurements. In the case presented here this peak is located after the 6 μ s mark, and is thus not observed on the experimental or theoretical data. An examination of the theoretical data outside of the plotted time domain finds that this peak is indeed of very small amplitude, and is difficult to discern even in the theoretical data.

Combining the results, such as those seen in Figure 6.23, for the various material parameters produces Figure 6.24, where the colour mapping denotes the amplitude of the waves leaked to the upper half-space. Examining Figure 6.24 one can observe the decrease in the time of flight of the waves reflected from the Epoxy-Aluminum interface as the velocity of the epoxy layer decreases during the curing process. When compared to the actual experimental results (Figure 6.25), and provided courtesy of Inna Severina), one

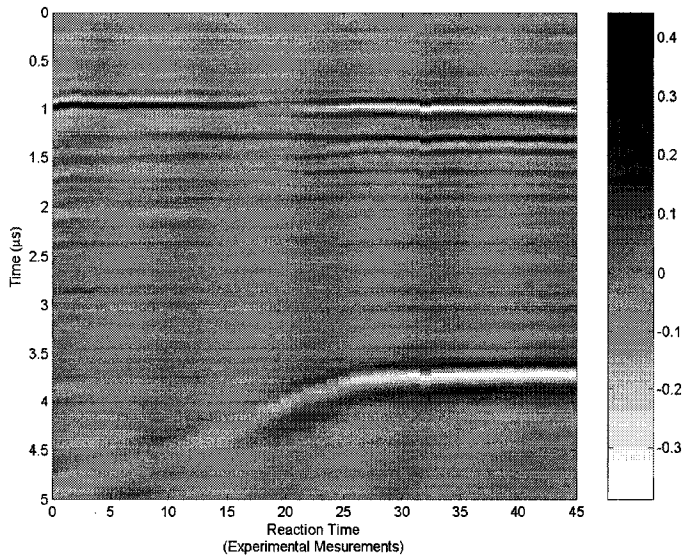

Figure 6.25: Experimental Results of Curing Process.

finds an overall good qualitative comparison between the two sets of results. In particular from both figures one observes the gradual earlier arrival of the reflections from the epoxy layer, located in the 3.5 to 5.0 μs area in both plots, where this change in the time of flight corresponds to the increased velocity of the epoxy layer during the curing process. Qualitatively these timings are nearly identical as the experimental measurements for the timing of these peaks are used to calculate the velocity of the epoxy layer for the theoretical calculations. One can also observe that the first amplitude peaks created from the reflection off the Polyethylene-Epoxy interface (located at roughly 1.0 μs in both plots) passes through a zero amplitude level between the nineteenth and twentieth measurement undergoing a relative sign change. This sign change is due to the impedance of the epoxy layer changing from being lower than impedance of the Polyethylene layer, to being greater than the impedance of the Polyethylene layer. And the point where there is no reflection the impedances of the two materials are equal, making the reflection

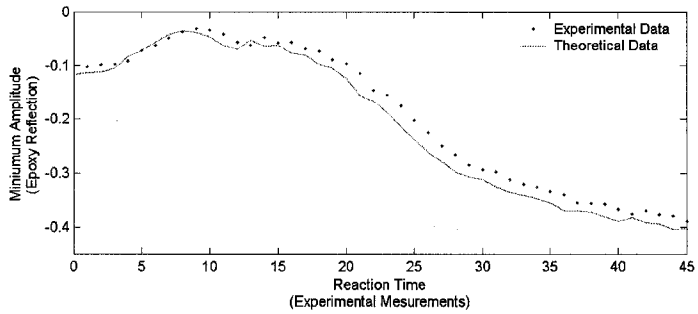

Figure 6.26: Comparisons of the minimum peak amplitude from the Epoxy-Aluminum interface for experimental and Theoretical results.

coefficient theoretically equal to zero. This same feature is present in the theoretical data, but the point where the wave's amplitude passes through zero is predicted to exist slightly earlier in the curing process, thus indicating the while the material parameters for the Polyethylene, or the epoxy layers are relatively close to the real world values, slight adjustments will produce a more exact match between the theoretical and experimental results.

Also present in both the experimental and theoretical data is a change in the amplitude of the waves reflected from the Epoxy-Aluminum interface (the amplitude spike in the 3.5 to 5.0 μs region in both plots). Plotting the minimum amplitude peak of the experimental and theoretical data (Figure 6.26) finds a very good qualitative match between the two sets of results. One is able to infer two results from the similarity between the two data sets. First this indicates the the material parameters of the sample have been correctly inferred from the experimental data, particularly those parameters relating to the velocity of the epoxy layer, and it's attenuation. Second, the results of the ray based calculations are shown to able to be used to describe the curing process and validate the results

of experimental measurements. While in this section the theoretical and experimental results have been used to verify each other, it is possible to use the ray based technique to predict the results of further materials based on an alternate sample structure.

6.3 Bond Detection

These sections will briefly examine the possibilities for the detection of bonding, versus disbonding in the case of a typical multilayered plate made up of two solids connected together via a layer of bonding material. In the preceding sections we will consider the typically used example composed of two aluminum plates bonded with epoxy (the material properties are summarized in Table 6.1). The upper half-space will be assumed to be water so that acoustic waves will leak out of the plate from the upper surface, while the lower half-space varies between each case (this will be discussed when we examine the various bonded and disbonded plate setups). This particular sample arrangement is chosen as it is the common base-line example for many theoretical and experimental uses. While this is one of many possible arrangements for a bonded multilayer plate, overall it provides a structure similar to typical adhesive samples, where two metal materials are used, and have a larger velocity and acoustical impedance than the material used to bond them. Thus while the exact amplitudes of the waves leaked to the surrounding media may be altered, factors such as any sign inversions in the overall wave amplitude (180 degree phase shifts), or relative amplitude changes may be common factors between this example and alternative samples. In the results to be examined, we will be interested

in the detection of the bonding (or disbonding) at the first Aluminum-Epoxy interface, as well as the bonding (or disbonding) at the second Epoxy-Aluminum interface. In both cases the disbonded sample will be created by substituting the unbonded layer with a Vacuum half-space. Thus for the detection of bonding at the first interface we compare the results from a theoretical Aluminum-Epoxy sample, with an Aluminum-Vacuum sample, while in the case of the detection of bonding at the second interface we compare the results from a theoretical Aluminum-Epoxy-Aluminum sample, with an Aluminum-Epoxy-Vacuum sample. It is noted the validity of such a substitution can be seen by examining the equations of the imperfect boundary conditions. Here adjusting the variable bonding parameters to the point of a disbonded state is equivalent to a the case of a layer of material connected to a Vacuum.

6.3.1 Detection of Bonding at First Interface

Here the case of the detection of a disbond at the first interface of the multilayer plate will be examined. As discussed previously this is achieved by comparing the results from the calculations for an Aluminum-Epoxy sample (the bonded case) with an Aluminum-Vacuum case (the disbonded case). In both cases the upper half-space is assumed to be water in order to allow the acoustic waves to leak from the plate, while the lower layer of the plate is considered a half-space. The epoxy layer will then be given a lower interface (an Aluminum-Epoxy-Vacuum case) to examine the changes due to waves reflecting off the lower Epoxy-Vacuum interface. In the next section this Aluminum-Epoxy-Vacuum sample will be compared to an Aluminum-Epoxy-Aluminum case to examine the detection

	Verbal Description	Mathematical Description
Path One	Only longitudinal polarized paths through the Aluminum plate.	$N_{L1} = N = 2, 4, 6$
Path Two	Exactly one shear vertical path through the Aluminum plate.	$N_{V1} = 1$ $N_{L1} = N - 1 = 1, 3, 5$
Path Three	Exactly two longitudinal paths through the Epoxy.	$N_{L2} = 2$ $N_{L1} = N - 2 = 2, 4, 6$
Path Four	Exactly two longitudinal paths through the Epoxy, and exactly one shear vertical path through the Aluminum plate.	$N_{L2} = 2$ $N_{V1} = 1$ $N_{L1} = N - 3 = 1, 3, 5$
Recall that $N_{\alpha n}$ denotes the number of paths in media n with polarization α, while N is the total number of reflections, and must be an even number to make a round trip in the plate structure.		

Table 6.4: Verbal to mathematical description in the particular paths chosen for examination.

of bonding and disbonding at the second interface.

Examining the results of the ray based theory, we consider the amplitude changes for two particular ray paths, where mathematical descriptions of these wave paths refer to Table 6.4. Path one considers rays travelling only longitudinal polarized paths through the Aluminum plate, and produces the results shown in Figure 6.27 for the unbonded case (the Aluminum-Vacuum sample) and Figure 6.28 for the bonded case (the Aluminum-Epoxy sample). Path two considers rays travelling exactly one shear vertical path through the Aluminum plate, with the remaining path segments made up of longitudinal paths. In this

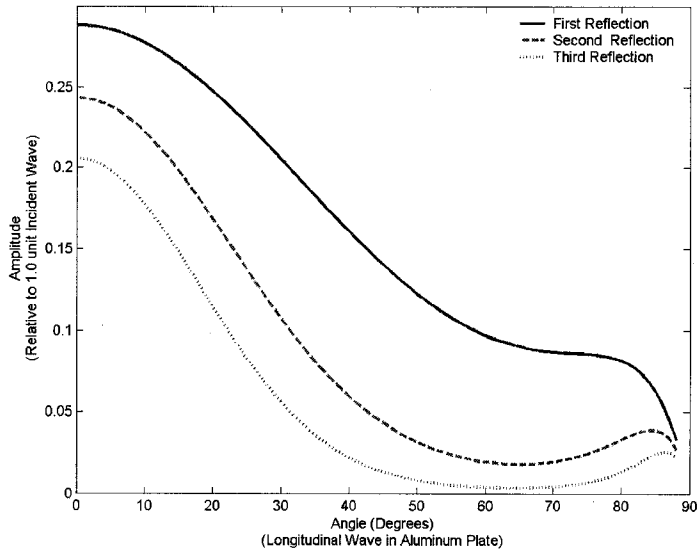

Figure 6.27: Disbonded Case: Waves leaked to upper water half-space from an Aluminum-Vacuum sample. These waves have travelled only longitudinal path segments through the Aluminum plate. (Path One in Table 6.4).

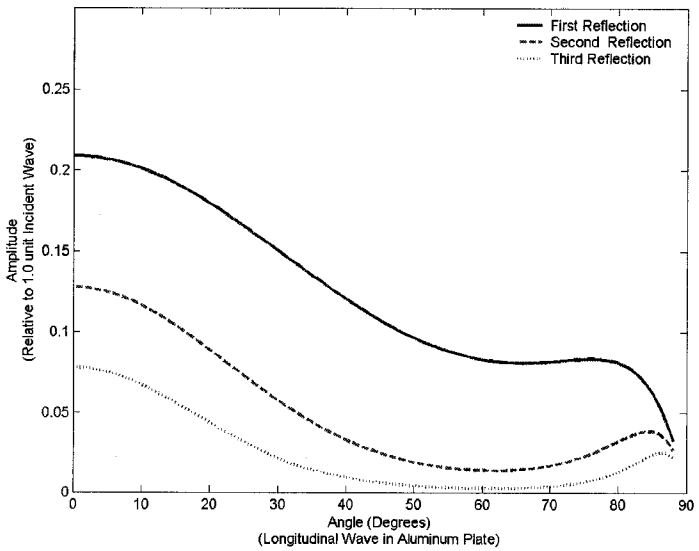

Figure 6.28: Bonded Case: Waves leaked to upper water half-space from an Aluminum-Epoxy sample. These waves have travelled only longitudinal path segments through the Aluminum plate. (Path One in Table 6.4).

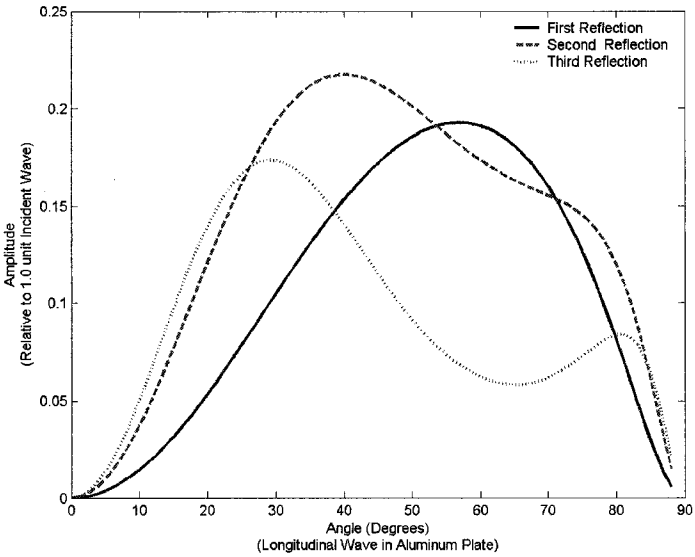

Figure 6.29: Disbonded Case: Waves leaked to upper water half-space from an Aluminum-Vacuum sample. These waves have travelled exactly one shear vertical path segment the Aluminum plate, with the remaining paths longitudinal paths in the Aluminum plate. (Path Two in Table 6.4).

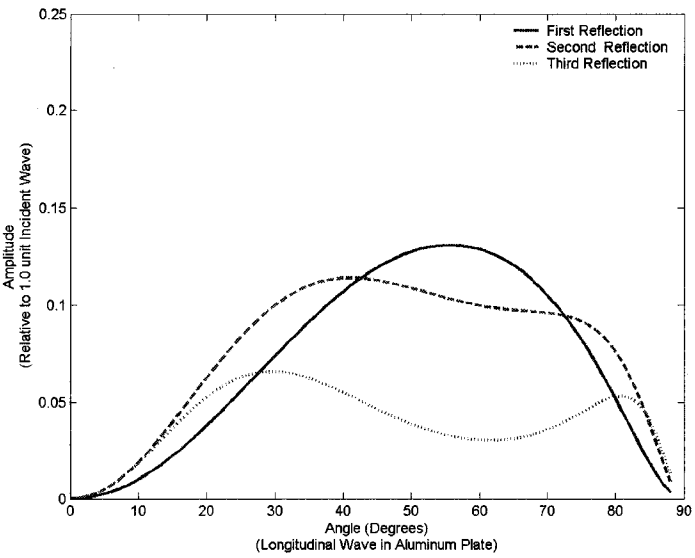

Figure 6.30: Bonded Case: Waves leaked to upper water half-space from an Aluminum-Epoxy sample. These waves have travelled exactly one shear vertical path segment the Aluminum plate, with the remaining paths longitudinal paths in the Aluminum plate. (Path Two in Table 6.4).

situation the results are shown in Figure 6.29 for the unbonded case and Figure 6.30 for the bonded case. These plots examine the first three possible paths fitting these requirements, and show the amplitude of the wave transmitted to the upper water half-space. Recall that this amplitude represents the displacement amplitude relative to the incident wave, or in other words the overall reflection and transmission coefficient for the wave's displacement calculated to this point. Directly comparing the results for the bonded (Figure 6.28 and 6.30) and disbonded cases (Figure 6.27 and 6.29) one observes the presence of the epoxy layer can be detected by an overall decrease in the amplitude of the rays for the entire range of angles tested. In addition, to overall amplitude decrease, the relative decrease between the amplitude of the first, second, and third possible reflections is found to decrease at a faster rate when the epoxy layer is present. These two observations can be explained by the fact that acoustic waves (and the wave energy) is now able to leak into the epoxy layer of the bonded sample. It is possible to consider other paths through the plate structure, where most present similar options for the consideration of the detection of bonding versus disbonding in the plate structure. However plotting the results for many possible paths over a variety of angles creates diagrams which become difficult to discern specific results from easily. In the above examples the two particular paths were chosen as they produced the overall largest amplitude responses. It also should be noted that in real world cases the multiple paths in the plate will often overlap in space and time and thus picking out particular paths may not be possible, here we have simply examined a best case scenario to examine possible options for the detection of bonding versus disbonding.

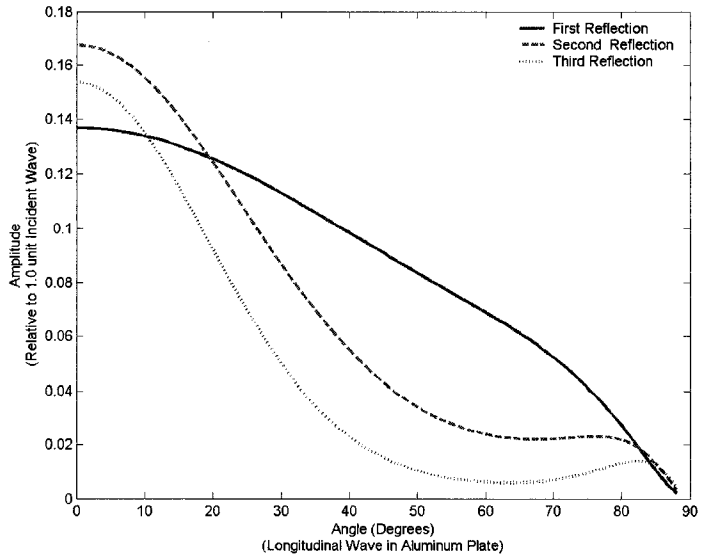

Figure 6.31: Disbonded Case: Waves leaked to upper water half-space from an Aluminum-Epoxy-Vacuum sample. These waves have travelled exactly two longitudinal path segments the Epoxy plate, with the remaining paths longitudinal paths in the Aluminum plate. (Path Three in Table 6.4).

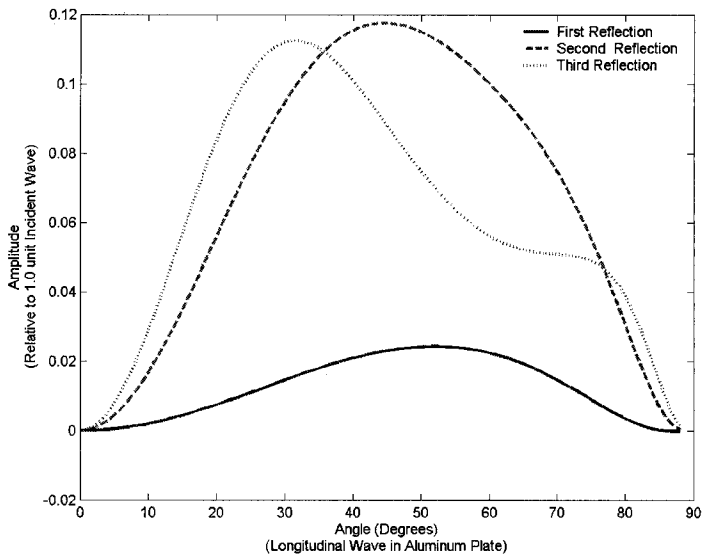

Figure 6.32: Disbonded Case: Waves leaked to upper water half-space from an Aluminum-Epoxy-Vacuum sample. These waves have travelled exactly two longitudinal path segments the Epoxy plate, and exactly one shear vertical path segment in the upper Aluminum plate. The remaining paths are longitudinal paths in the Aluminum plate. (Path Four in Table 6.4).

Adding a lower interface to the epoxy layer and now examining an Aluminum-Epoxy-Vacuum sample allows for reflections to occur at the second interface. The existence of these reflections provides an additional option to detect the existence of bonding at the Aluminum-Epoxy interface, and as well provide an option for the detection of the bonding layer itself, as these reflections are distributed in space time and present a noticeable difference in comparison to the case when the first interface is disbonded and allows only reflections within only the Aluminum plate. This difference in space time distribution will be discussed in further detail in Section 6.3.3 where further options to discuss the detection of the bonding layer itself are examined. Returning now to the examination of the amplitude results, we consider the results for two additional ray paths which now travel through both the aluminum and the epoxy layers. Path three considers rays which travel exactly two longitudinal paths through the epoxy, with the remaining reflections travelling longitudinal wave paths through the Aluminum plate. This produces the results shown in Figure 6.31 for the unbonded case and Figure 6.35 for the bonded case. Finally, path four considers rays which travels exactly two longitudinal path through the epoxy, and exactly one shear vertical path through the Aluminum plate, with the remaining reflections travelling longitudinal wave paths through the Aluminum plate. This produces the results shown in Figure 6.32 for the unbonded case and Figure 6.36 for the bonded case. Again we have considered the first three possible paths with these arrangements, and examined the amplitude of the wave transmitted to the upper water half-space. (For more mathematical descriptions of these wave paths refer to Table 6.4.) Again these particular paths are chosen as they present the highest overall amplitude response, and as well produce unique features to allow for easier detection of the bonding, or disbonding

of the sample. Examining the results, particularly those of Figure 6.32, where the path allows for a mode converted path in the Aluminum plate (the fourth path considered), one finds that the amplitude of the second and third possible reflections is significantly larger than the amplitude of the first possible reflection. This increase in amplitude is caused by the constructive interference in the multiple equivalent paths. Here the second possible reflection is the superposition of 8 equivalent ray paths, and the third possible reflection is the superposition of 18 ray paths, for the mode converted case; meanwhile, the first possible reflection is the superposition of only 2 equivalent ray paths. With such a large difference in amplitude, it would be advised to look for these second and third reflections, which are present later in the time domain, rather than the initial reflections if one were to attempt to detect these waves experimentally. In addition from Figure 6.32 one observes that the optimal angle for peak amplitude is in the 25 to 55 degree range (this measures the angle of the longitudinal wave in the Aluminum plate). In the case examined here of a water half-space this corresponds to an acoustic wave with an angle of incidence from roughly 5 to 10 degrees on the plate surface. Using this information, in collaboration plots for the time of flight (Figure 6.33), and the horizontal position (Figure 6.34) travelled by these specific ray paths reflected off the Epoxy-Vacuum interface, one can determine the appropriate position along the sample, as well as the appropriate time, to detect those waves with the largest amplitude response.

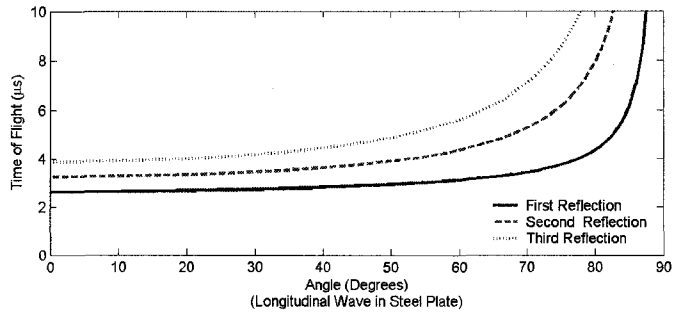

Figure 6.33: Time of Flight for first three possible waves travelling on path four (see Table 6.4).

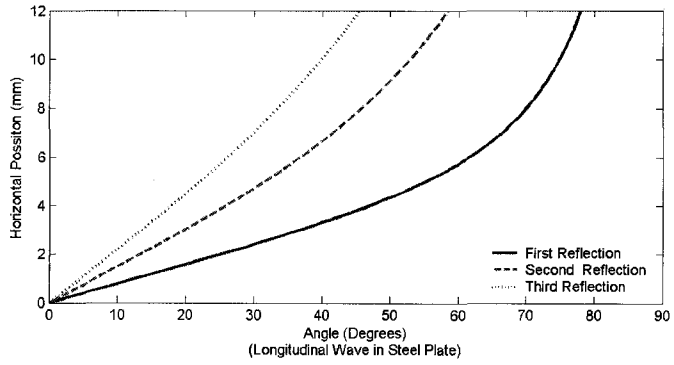

Figure 6.34: Horizontal Position for first three possible waves travelling on path four (see Table 6.4).

6.3.2 Detection of Bonding at the Second Interface

In the previous section we briefly examined the amplitude results for the case of Aluminum-Epoxy-Vacuum sample (Figures 6.31 and 6.32). Here these results represents the situation the second interface is fully disbonded, and we will compare these results to the fully bonded case of an Aluminum-Epoxy-Aluminum sample (Figures 6.35 and 6.36). In these figures the third and fourth sample ray path is considered, where the paths are noted to interact with the second interface in the bonded structure (See Table 6.4 for details of these paths). A comparison of the figures finds that in both paths examined

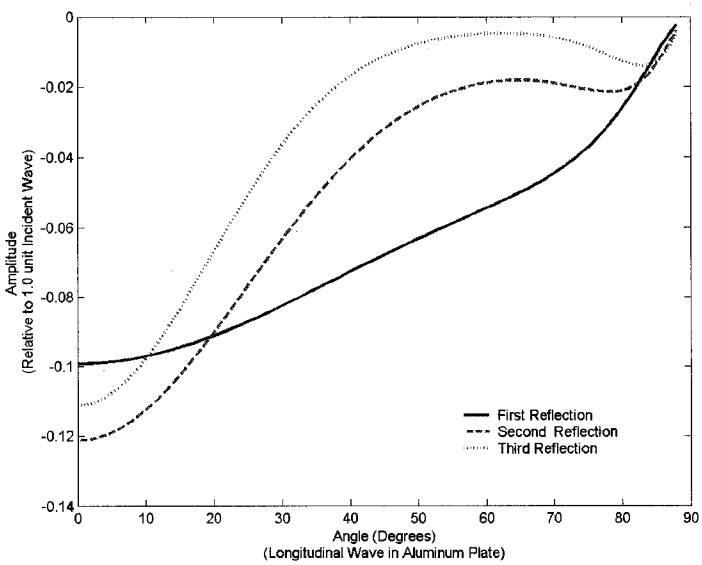

Figure 6.35: Bonded Case: Waves leaked to upper water half-space from an Aluminum-Epoxy-Aluminum sample. These waves have travelled exactly two longitudinal path segments the Epoxy plate, with the remaining paths longitudinal paths in the Aluminum plate. (Path Three in Table 6.4).

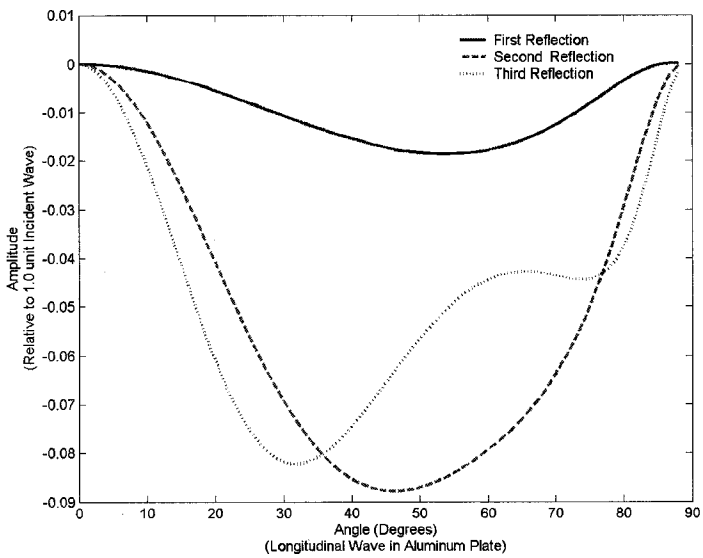

Figure 6.36: Bonded Case: Waves leaked to upper water half-space from an Aluminum-Epoxy-Aluminum sample. These waves have travelled exactly two longitudinal path segments the Epoxy plate, and exactly one shear vertical path segment in the upper Aluminum plate. The remaining paths are longitudinal paths in the Aluminum plate. (Path Four in Table 6.4).

there exists a relative sign inversion between the bonded and disbonded amplitude. This sign inversion is consistent over the entire range of angles tested, and as well exists for not only the first possible reflection of each path, but also the second and third possible reflections. An examination of the reflection and transmission coefficients for each sample discovers that this sign change is due to the phase change of waves reflected from the Epoxy-Aluminum boundary relative to the Epoxy-Vacuum case, and is present at all real angles, and exists for both mode converted, and non mode converted waves reflected from this interface. Again it is noted that the maximum amplitude in the case of Figure 6.31 or 6.35 (path three) is located at normal incidence, while in Figure 6.32 or 6.36 (path four) the amplitude is approximately zero near normal incidence, and increases when there is a non normal incident angle. This offers an additional option for the testing of bonding versus disbonding by using non-normal incidence. As was shown in Figure 6.33 and 6.34, these specific reflections are distributed not only in the time domain, but also in the space domain. This space and time distribution makes interference with other reflected waves less likely, and thus the possibility of detecting the amplitude inversion at non-normal incidence may be better than at normal incidence.

6.3.3 Detection of the Bonding Layer

In the proceeding sections the thesis has examined the methods for the detection of bonded interfaces in a typical Metal-Adhesive-Metal structure, showing options for the detection of a fully bonded versus fully disbonded interface by examining changes the amplitude of the waves reflected from the various interfaces. In this section we will examine

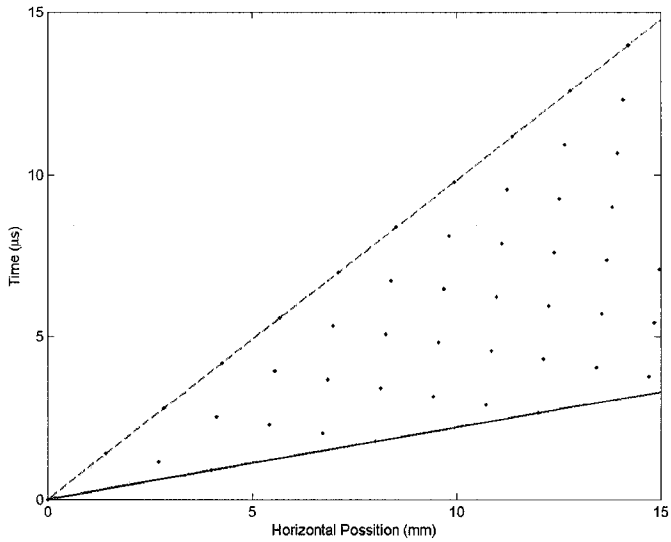

Figure 6.37: Space-Time distribution of ray based results for the Aluminum plate sample. The solid and dashed lines denote the limits of this distribution, with the solid line connecting reflections travelling only longitudinal paths, and the dashed line connecting reflections travelling only shear vertical paths through the Aluminum plate.

possibilities other than examining the amplitude, such as the space-time distribution of the data, and calculating the horizontal velocity (the horizontal position divided by the time of flight) from the ray based data. Such examinations utilize the typically slower material velocity of the adhesive layer to detect the material itself, rather than the existence of the interfaces. It should be noted that while the results presented in this section are able to detect the existence of the bonding layer, and some material parameters of the sample theoretically; it has not been examined if, or how, such observations could be made experimentally, or how accurate such techniques would be.

To begin Figure 6.37 shows the space-time distribution of the ray based data in the case of a single layer Aluminum plate, while Figure 6.38 shows the the space-time distribution

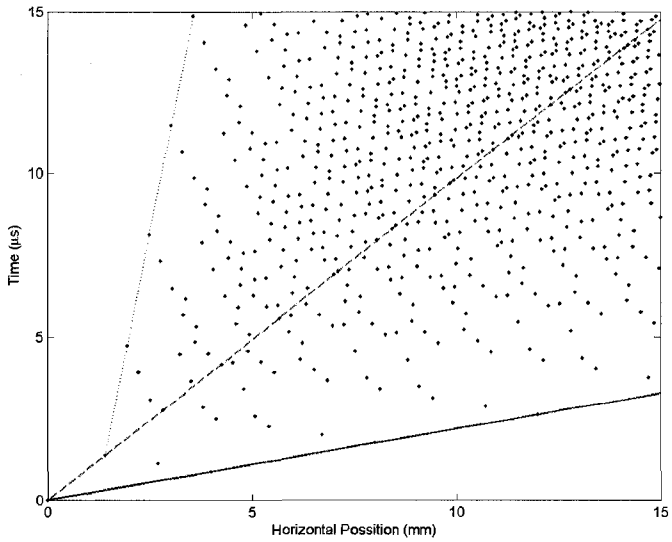

Figure 6.38: Space-Time distribution of ray based results for the Aluminum-Epoxy plate sample. The solid and dotted lines denote the limits of this distribution, and the dashed line the limit for the case of the Aluminum plate sample seen in Figure 6.37.

of the ray based data in the case of the multilayer plate case of the Aluminum-Epoxy sample. In both cases we have considered a wave incident on the plate such that 45 degree angle longitudinal waves are generated within the Aluminum plate, and have shown the space-time distribution of the ray-based results. (Note that the amplitude of the rays is not plotted on these results, thus the absence of any amplitude to colour mapping is intentional.) Comparing the two figures one finds the wave's propagation in the lower velocity of the epoxy layer has created an additional region of data in points as denoted on Figure 6.38 between the dashed and dotted lines. In these figures the solid, dashed, and dotted lines denote the limit of the space-time distribution of the data. The solid line connects reflections travelling only longitudinal paths through the Aluminum plate, and the dashed lines connecting reflections travelling only shear vertical paths through

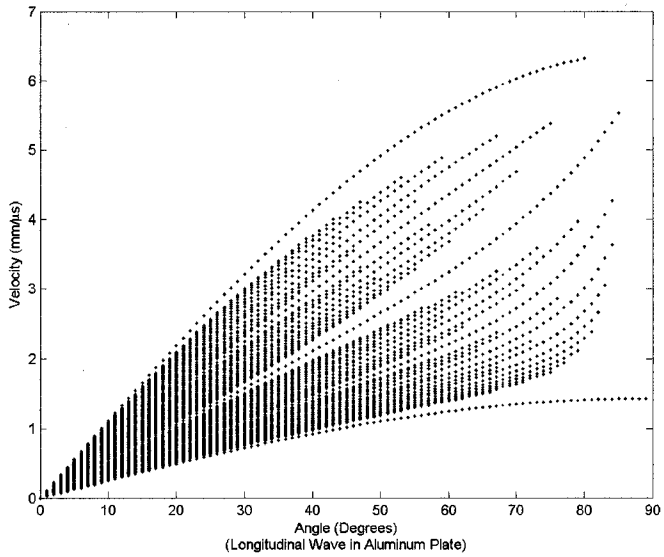

Figure 6.39: Horizontal velocity of the acoustic wave in the case of the Aluminum plate

the Aluminum plate. Thus indicating the fastest, and slowest reflected paths through the Aluminum plate, respectively (Figure 6.37). Likewise the dotted lines connects reflections travelling the slowest path in the entire Aluminum-Epoxy structure (pure shear vertical paths). In addition to this increased space-time distribution, the density of the points has also increased due to the additional reflections in the multilayer plate system. While an experimental system could likely not detect this increase in the density in the number of waves leaked to the upper half-space, the difference in the space-time distribution could be of possible interest in the detection of the epoxy layer, and possibly its properties. While we have shown a case where the material in the second layer of the plate is of lower velocity than the material in the first plate, if in some case this were reversed, and material to be detected was of larger velocity, these additional data points would be located on the opposite side of the original space-time data distribution.

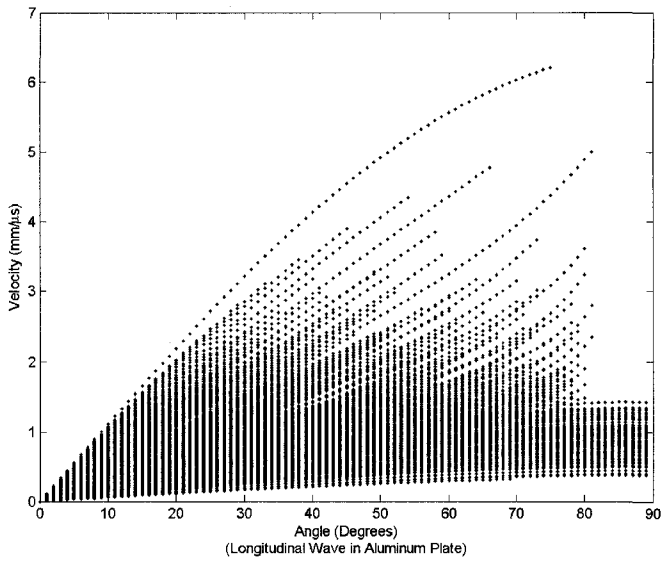

Figure 6.40: Horizontal velocity of the acoustic wave in the case of the Aluminum-Epoxy-Aluminum sample

Next, it is possible to process this ray based data and for each data point find the horizontal velocity (v_x) of the wave via

$$v_x = x/tof, \tag{6.1}$$

where x is the horizontal displacement, and tof is the time of flight of the ray. (It is noted that this is the velocity of the wave's propagation through the plate, and not the velocity corresponding to acoustic wave's oscillating amplitude.) The velocity information can be plotted in the time domain, or the space domain, or in addition by using a Fourier transform examine the data in the frequency domain, or wavenumber domain. All these methods to plot the data yield similar results for the range of horizontal velocities from the media. For the data plotted in Figure 6.37 (the Aluminum plate), the maximum horizontal velocity is 4539.6 m/s, where the minimum is found to be 1017.9 m/s. In comparison when examining the case of the Aluminum-Epoxy layer the epoxy layer lowers the overall

minimum horizontal velocity to 240 m/s. To see how these velocities correspond to the angle of the wave through the plate, and the velocities of the media, the horizontal velocity can be plotted as the angle of incidence is altered. These calculations are performed for rays arriving on the upper Aluminum plate within the limits of 15 mm and 15 μs, and produces the plots as shown in Figure 6.39 for the Aluminum plate, and Figure 6.40 for the Aluminum-Epoxy-Aluminum plate (where the lower Aluminum layer remains a half-space). Examining the results for the Aluminum plate (Figure 6.39) finds that the ray data for the maximum velocity corresponds to rays travelling only longitudinal paths in the Aluminum plate, and follows the curve $v_x = v_L sin(\theta_L)$. Meanwhile the minimum velocity corresponds to rays travelling only shear vertical paths in the Aluminum plate, and follows the curve $v_x = v_S sin(\theta_S)$. (Here v_L is the longitudinal velocity, v_S is the shear velocity, θ_L is the angle of a longitudinal wave in the Aluminum plate, and θ_S is the angle of a shear vertical wave in the Aluminum plate). By using this information in combination with the minimum and maximum horizontal velocities found from Figure 6.37, where the angle θ_L was set to be 45 degrees, it is possible to determine the longitudinal and shear velocity of the Aluminum plate. Finally, comparing these results to the case of the Aluminum-Epoxy-Aluminum sample (Figure 6.40), one can observe the additional low velocity data points due to the slower epoxy layer of the sample. However, the additional velocity data from the epoxy layer is partially obscured due to the presence of the data from rays travelling in the Aluminum plate, and extracting the information of the velocity of the epoxy layer becomes difficult. Although we have not inferred any additional material parameters, the lowest horizontal velocity of the overall sample is quantitatively determined, and will differ if the parameters of the epoxy layer are changed. As well it presents a noticeable

difference to the case of the Aluminum plate, thus allowing for the detection of the epoxy layer.

Chapter 7: Summary and Conclusion

7.1 Ray Based Technique Advantages, and Comparison to Alternate Theories

Before concluding with this thesis we wish to summarize the important advantages, as well as the disadvantages, of the ray technique which have been discussed in the previous sections and utilized in the results section.

7.1.1 Advantages of the Ray Based Technique

The most important advantage of this ray based technique is its ability to calculate the amplitude from the multiple reflections of acoustic waves travelling at real angles in an ideal multilayer plate made of isotropic solids in a time efficient manner. In doing this it does not require simplifications such as assuming plane waves in each layer, calculating only specific reflections, or ignoring those paths deemed unimportant to the results. Instead all reflections for waves travelling at real angles are calculated by using the principle of superposition to reduce the number of wave paths. In addition the ray based technique also provides results which:

- are independent of the frequency, or time domain properties of the acoustic wave.
- are independent on the space domain properties of the acoustic wave.

- are partially independent on the thickness of the layers of the plate (the amplitude of the acoustic waves can be calculated without knowing the thickness of each layer, however the thickness is of course required to obtain results in the time-space domain).

- allow one to discern which polarized paths, and in which layers of the plate, a wave has travelled to provide a specific point of ray data in time and space. The example of using this information is seen in Section 6.3, where particular reflections through the plate structure are examined.

- can be extended to consider the attenuation of the material as discussed in Section 5.1, and applied to the results in Section 6.2.2

- can be extended to consider the specific time and space domain properties of an acoustic wave as discussed in Section 5.3. Such considerations were used to compare to specific experimental cases in Sections 6.2.1 and 6.2.2.

- allow the attenuation of the materials, and the space-time domain properties of the acoustic wave to be considered in a separate set of calculations. Combining this with the frequency independent amplitude results, allows the attenuation and the waveform properties to be altered without recalculating the ray based amplitude calculations.

- naturally consider a short pulse acoustic wave in the time domain as discussed in Section 5.3.1; while in contrast a plane wave theory focus on long time domain pulses, requiring the superposition of results calculated for multiple frequencies to

produce a short pulse.

- can approximate a plane wave case via a phasor addition of the ray based amplitudes based on the frequency of the plane wave as was discussed in Section 5.3.2, and applied for a comparison to plane wave results in Section 6.1.2.

- are also valid for simpler multilayer plate cases, such as the propagation of single polarized in cases with; waves in samples with liquid layers, waves at normal incidence, or shear horizontal waves propagating through the isotropic plate.

7.1.2 Disadvantages of the Ray Based Technique

While there are notable advantages to using the ray based technique there are some notable disadvantages. First, the technique presented is a numerical calculation method, and does not present final symbolic formula for visual analysis. Any symbolic formula created by following the steps in this techniques analytically can quickly produce a quite complicated not suitable for an easy visual analysis. In addition, as is common with other methods dealing with acoustic waves in a multilayer plate, the technique becomes more computationally intensive to use as the number of layers increases. As the number of layers increases it would be wise to consider combining this technique with methods such as shown by Chapman and Chapman [16] and consider limitations on the number of ray paths to be considered by choosing not to examine the lowest amplitude ray paths.

7.2 Conclusion

The first part of this thesis described and examined the theoretical basis of the ray technique, proving the existence of equivalent and coincident paths in the single and multilayer plate structure. In the case multilayer plate structure it was noted that coincident paths are possible for waves travelling both single polarized paths, as well as paths with mode conversions. (In comparison the single layer plate structure requires a mode conversion for two waves to be come coincident). With this observation the technique is useful to examine cases with liquid layers, normal incidence waves, and shear horizontal waves in a multilayer isotropic plate; as well as the intended usage for acoustic waves travelling at angles through solid multilayer plates. In any of these cases the superposition of the coincident paths was found to be able to reduce the number of rays to consider in the plate structure, and allows the problem to be solved in a time efficient manner. The thesis then outlines the method to track the ray paths, calculate the amplitude the rays, and apply the principle of superposition. These calculations apply the reflection and transmission coefficients from perfectly bonded boundary conditions (or the imperfect boundary) from each interface, and as shown in Appendix A these coefficients are independent of the incident waveform. This feature allows the amplitude of the rays to be calculated independently of the frequency of the incident wave, as well as the incident wave's space-time domain profile. After the amplitude calculations, a second set of calculations is then used to: consider the attenuation of the media, recalculate the time of flight and horizontal distances of the rays due to altering the thickness of the layers of the plate, and the ray based results can be extended to a more realistic acoustic wave. By being able to include

these factors as a separate set of calculations adds flexibility to the technique, as these features can be altered without recalculating the initial amplitude results, as long as the other features of the theoretical sample remain constant.

The results from the ray technique are then used to examine various cases for validation, comparison to experimental results, and the examination of options for the detection of bonding or disbonding within a typical bonded plate sample. For validation the results of the ray technique are shown to obey the principle of conservation of energy after each reflection and transmission of waves in the plate, and as well for cases of waves leaked outside the plate. The ray technique's results are also shown to provide results comparable to the existing plane wave theories, for both single layer plates and multilayer plates; and as well provides results comparable to techniques examining a thin layer between two half-spaces. Also examined were two comparisons to two specific experiments. The first situation provides a comparison to the case of a single layer plate at ideally normal incidence. Here the ray technique is found to be able to explain additional peaks created from shear vertical waves in the experimental data created due to slightly non-normal incidence, non parallel plates, or rough surfaces in the experimental setup. As well as explaining those peaks which are initially unexpected, the theoretical results provide an overall qualitative match to the experimental results. In the second comparison with real world experimental results, the ray technique is utilized to simulate the results of the curing process of an adhesive layer. Here the two results share many similar feature such as a sign changes in the amplitude of wave reflected from the upper adherent-adhesive interface, and overall quantitative match for the amplitude of the waves travelling through

the adhesive layer and reflecting from the lower adhesive-adherent interface. Finally, the specific case of examining the detection of bonding, or disbonding at both interfaces in a typical Metal-Adhesive-Metal sample was considered. Options to detect this bonding were found for not only the expected normal incidence cases, but also for non-normal incidence. It was shown that while the first reflection from the Adhesive-Metal interface may be minimal, the second and third reflections had significantly increased amplitudes due to the superposition of waves. This observation was most noticeable for waves travelling at non-normal incidence, and when combined with the examination of the space and time domain provides an opportunity to detect these reflections which may be obscured due to interference effects when examined at normal incidence. Finally, the examination of detecting the bonding layer itself was shown to be possible by examining the space-time distribution of the data, as well as the horizontal velocity of the waves reflecting within the plate. Here the lower velocity of the adhesive layer is found to produce additional data in the space-time domain which may be possible to detect experimentally.

In conclusion, a technique has been developed to examine the problem of calculating the multiple reflections of an acoustic wave in isotropic plate. This is done without the need to approximate via plane waves, limit the number of wave paths, or examine specific situations (liquid only, thin layers only, normal incidence only ect.), but still allows the calculations process to be done in a time efficient manner. The results provided by the method allows for physical interpretation of the problem, and as well provide flexible results which can be extended to include attenuation, alteration of the material thicknesses, and consideration of the space-time domain properties of the acoustic wave.

With the properties the technique provides a useful utility to predict and verify real world results, as well as being a useful theoretical tool

Bibliography

[1] E. Hecht. *Optics, Third Edition.* Addision-Wesley, New York, 1998.

[2] J. Sadler and R. Gr. Maev. Ray technique to calculate the multiple reflections and leaky wave propagation from a single or multilayer plate for the detection of critical disbonds in layered media. *Proceedings of the 9th European Conference on Non-Destructive Testing*, pages 1–9, 2006.

[3] J. Sadler and R. Gr. Maev. Utilizing a ray technique to calculate multiple reflections and transmitted waves from layered plates and examine the detection of critical disbonds, and lamb modes generated. *Proceedings of 2006 IEEE International Ultrasonics Symposium*, pages 2246–2249, 2006.

[4] G. Maze, J. L. Izbicki, and J. Ripoche. Transient acoustic scattering from layers and plates. *J. Acoust. Soc. Am.*, 80(1):295–301, 1986.

[5] J. A. Bamberger and M. S. Greenwood. Measuring fluid and slurry density and solids concentration non-invasively. *Ultrasonics*, 42:563–567, 2004.

[6] L. Cai. Multiple scattering in single scatterers. *J. Acoust. Soc. Am.*, 115(3):986–995, 2004.

[7] L. Cai. Scattering of antiplane shear waves by layered circular elastic cylinder. *J. Acoust. Soc. Am.*, 115(2):515–522, 2004.

[8] L. Cai. Evaluation of layered multiple-scattering method for antiplane shear wave scattering from gratings. *J. Acoust. Soc. Am.*, 120(1):49–61, 2006.

[9] M. S. Greenwood, J. D. Adamson, and L. J. Bond. Measurement of viscosity-density product using multiple reflections of ultrasonic shear horizontal waves. *Ultrasonics*, 44(Suppliment 1):e1031–e1036, 2006.

[10] M. S. Greenwood and J. A. Bamberger. Measurement of viscosity and shear wave velocity of a liquid or slurry for on-line process control. *Ultrasonics*, 39:623–630, 2002.

[11] G. Caviglia and A. Morro. A closed-form solution for reflection and transmission of transient waves in multilayers. *J. Acoust. Soc. Am.*, 116(2):643–654, 2004.

[12] R. Gr. Maev, F. Severin, B. O'Neill, E. Maeva, and B. B. Djordjevic. Ultrasonic inspection of interfacial adhesive bonding in thin metal-metal sheets. In R.E. Green Jr, B.B. Djordjevic, and M.P. Hentschel, editors, *Nondestructive Characterization of Materials XI*, pages 781–787. Springer, 2002.

[13] M. J. S. Lowe. Matrix techniques for modeling ultrasonic waves in multilayered media. *IEEE Trans. Ultr. Ferr. Freq. Contr.*, 42(4):525–542, 1995.

[14] L. M. Brekhovskikh. *Waves in Layered Media*, Chapter 1: Plane waves in layers, pages 1–134. Academic Press, New York, 1960.

[15] A. Briggs. *Acoustic Microscopy*, Section 10.2: Waves in layers, pages 212–223. Oxford Press, New York, 1992.

[16] N. R. Chapman and D. M. F. Chapman. A coherenet ray model of plane-wave reflection from a thin sediment layer. *J. Acoust. Soc. Am.*, 94(5):2731–2738, 1993.

[17] J. Sadler, B. O'Neill, and R. Gr. Maev. Ultrasonic wave propagation across thin nonlinear anisotropic layer between two half spaces. *J. Acoust. Soc. Am.*, 118(1):51–59, 2005.

[18] J. Sadler, B. O'Neill, and R. Gr. Maev. Characterization and imaging of thin, highly oriented layers: Theory and experiment. *Acoustical Imaging*, 27:341–348, 2003.

[19] S. Rokhlin and W. Huang. Ultrasonic wave interaction with thin anisotropic layer between two anisotropic solids: Exact and asymptotic boundary condition methods. *J. Acoust. Soc. Am.*, 92(3):1729–1743, 1992.

[20] S. Rokhlin and W. Huang. Ultrasonic wave interaction with a thin anisotropic layer between two anisotropic solids ii. second order asymptotic boundary conditions. *J. Acoust. Soc. Am.*, 94(6):3405–3420, 1993.

[21] V. Dayal and V. Kinra. Leaky lamb waves in an anisotropic plate. I: An exact solution and experiments. *J. Acoust. Soc. Am.*, 85(6):2268–2267, 1989.

[22] J. L. Rose. *Ultrasonic Waves in Solid Media*, Appendix E.4: Experiment 4: Waves in Plates, pages 410–422. Cambridge University Press, New York, 1999.

[23] F. J. Blonigen and P. L. Marston. Leaky helical flexural wave bascksattering contributions from tilted cylindrical shells in water: Observations and modelling. *J. Acoust. Soc. Am.*, 112(2):528–526, 2002.

[24] F. J. Blonigen and P. L. Marston. Leaky helical flexural wave backscattering contributions from tilted water-filled cylindrical shells. *J. Acoust. Soc. Am.*, 113(1):309–312, 2003.

[25] F. J. Blonigen and P. L. Marston. Leaky helical flexural wave scattering contributions from tilted cylindrical shells: Ray theory and wave-vector anisotropy. *J. Acoust. Soc. Am.*, 110(4):1764–1769, 2001.

[26] B. O'Neill, J. Sadler, F. Severin, and R. Gr. Maev. Theoretical and experimental study of the acoustic nonlinearities and an interface with poor adhesive bonding. *Acoustical Imaging*, 26:309–317, 2002.

[27] A. Pilarski, J. L. Rose, and K. Balasubramaniam. The angular and frequency characteristics of reflectivity from a solid layer embedded between two solids with imperfect boundary conditions. *J. Acoust. Soc. Am.*, 87(2):532–542, 1990.

[28] L. Wang and S. I. Rokhlin. Stable reformulation of transfer matrix method for wave propagation in layered anisotropic media. *Ultrasonics*, 39:413–424, 2001.

[29] L. Wang and S. I. Rokhlin. A simple method to compute ultrasonic wave propagation in layered anisotropic media. *Review of QNDE*, 23:59–66, 2004.

[30] J. Sadler and R. Gr. Maev. Experimental and theoretical basis of lamb waves and their applications in material sciences. review. *Canadian Journal of Physics*, 85(7):707–731, 2007.

[31] J. L. Rose. *Ultrasonic Waves in Solid Media*, Chapters 7: Surface and Subsurface Waves, 8: Waves in Plates, 9: Interface waves, 10: Layer on a half-space, 15: Horizontal shear, pages 90–142, 241–261. Cambridge University Press, New York, 1999.

[32] L. W. Schemerr. *Fundamentals of Ultrasonic Nondestructive Evaluation*, Chapter 7: Propagation of Surface and Plate Waves, pages 141–155. Plenum Press, New York, 1998.

[33] A Briggs. *Acoustic Microscopy*, Chapter 7: Contrast Theory, pages 104–126. Oxford Press, New York, 1992.

[34] A Briggs. *Acoustic Microscopy*, Chapter 11: Anisotropy, pages 232–259. Oxford Press, New York, 1992.

[35] S. I. Rokhlin and L. Wang. Stable recursive algorithm for elastic wave propagation in layered anisotropic media: Stiffness matrix method. *J. Acoust. Soc. Am.*, 112(3):822–834, 2002.

[36] S. I. Rokhlin and Y. J. Wang. Analysis of boundary conditions for elastic wave interaction with an interface between two solids. *J. Acoust. Soc. Am.*, 89(2):503–515, 1991.

[37] S. Rokhlin and D. Marom. Study of adhesive bonds using low frequency obliquely incident ultrasonic waves. *J. Acoust. Soc. Am.*, 80(2):585–590, 1986.

[38] M. Comninou and J. Dundurs. Reflextion and refraction of elastic waves in presence of separation. *Proc. R. Soc. Lond. A*, 356(1687):509–528, 1977.

[39] M. Comninou and J. Dundurs. Interaction of elastic waves with a unilateral interface. *Proc. R. Soc. Lond. A*, 368(1732):1979, 141-154.

[40] J. Richardson. Harmonic generation at an unbonded interface - i. planar interface between semi-infinite elastic media. *Int. J. Engng. Sci.*, 17:73–85, 1979.

[41] C. M. Hedberg and O. V. Rudenko. Pulse response of a nonlinear layer. *J. Acoust. Soc. Am.*, 100(5):2340–2350, 2001.

[42] B. O'Neill, J. Sadler, F. Severin, and R. Gr. Maev. Development of a nonlinear boundary condition approach as a new model for the nonlinear acoustic interface problem. *ISNA 16: Nonlinear Acoustics at the Beginning of the 21st Century*, 1:29–32, 2002.

[43] J. L. Rose. *Ultrasonic Waves in Solid Media*, Chapters 4: Reflection and Refraction, 5: Oblique Incidence, pages 40–81. Cambridge University Press, New York, 1999.

[44] J. D. N. Cheeke. *Fundamentals and Applications of Ultrasonic Waves*, Chapter 7: Reflection and transmission of ultrasonic waves at interfaces, pages 115–141. CRC Press, New York, 2002.

[45] B. A. Auld. *Acoustic Fields and Waves in Solids 2nd Ed., Vol 2*, Chapter 9: Reflection and Refraction, pages 63–220. Kriezer, Florida, 1990.

[46] A Briggs. *Acoustic Microscopy*, Chapter 6: A little elementary acoustics, pages 79–103. Oxford Press, New York, 1992.

[47] L. W. Schemerr. *Fundamentals of Ultrasonic Nondestructive Evaluation*, Chapter 6: Reflection and Refraction of Bulk Waves, pages 91–140. Plenum Press, New York, 1998.

[48] W. Ewing, W Jardetsky, and F. Press. *Elastic Waves in Layered Media.* McGraw-Hill, New York, 1957.

[49] I. Solodov and R. Gr. Maev. Overview of opportunities for nonlinear acoustic applications in material characterization and NDE. *Emerging Technologies in NDE*, pages 137–144, 2000.

[50] Y. Zheng, R. Gr. Maev, and I. Solodov. Nonlinear acoustic applications for material characterization: A review. *Canadian Journal of Physics*, 77(12):927–967, 1999.

[51] L. A. Ostrovsky and P. A. Johnson. Dynamic nonlinear elasticity in geomaterials. *La Rivista Del Nuovo Cimento della Societa Italiania di Fisica*, 94(7):1–46, 2001.

[52] J. L. Rose. *Ultrasonic Waves in Solid Media*, Chapters 3:Unbounded Isotropic and Anisotropic Media, pages 24–39. Cambridge University Press, New York, 1999.

[53] J. D. N. Cheeke. *Fundamentals and Applications of Ultrasonic Waves*, Chapter 4: Introduction to the Theory of Elasticity, 5: Bulk Acoustic Waves in Solids, 11: Crystal Acoustics, pages 59–90, 203–209. CRC Press, New York, 2002.

[54] P. He. Measurement of acoustic dispersion using both transmitted and reflected pulses. *J. Acoust. Soc. Am.*, 107(2):801–807, 2000.

[55] M. F. Hamilton, Yu. A. Il'inskii, and E. A. Zabolotskaya. *Nonlinear Acoustics*, Chapter 5: Dispersion, pages 151–175. Academic Press, New York, 1998.

[56] D. M. Pai. Wave equation solution by a coupled mode multiple reflection series method. *J. Acoust. Soc. Am.*, 88(6):2871–2875, 1990.

[57] R. A. Tenenbaum and M. Zindeluk. An exact solution for the one-dimensional elastic wave equation in layered media. *J. Acoust. Soc. Am.*, 92(6):3364–3370, 1992.

[58] G.B. Chapman, J. Sadler, R. G. Maev, S. Titov, E. Y. Maeva, I. Severina, and F. Severin. Ultrasonic pulse-echo NDE of adhesive bonds in sheet-metal assemblies. *Proceedings of 2006 IEEE International Ultrasonics Symposium*, pages 902–905, 2006.

[59] W. N. Mathews Jr. Superposition and energy conservation for small amplitude mechanical waves. *Am. J. Phys.*, 54(3):234–238, 1986.

Appendix A: Reflection and Transmission Coefficients

In this section we briefly look at how one derives the reflection and transmission coefficients; specifically we will examine the process of obtaining displacement coefficients, however the pressure coefficients could also be examined in a similar manner. Here we follow a similar argument as is presented in many texts [43–47] for the acoustic interface, but consider the most general case of multiple incident waves on a solid-solid interface. Figure A.1 shows the setup for the interface, along with the incident and reflected waves, and their polarizations. In our case the incident wave may arrive at the interface travelling in either of the two media, and with either longitudinal or shear vertical polarization. We will first deal with the incident wave in material 1, then examine the changes when the wave is incident from the opposite direction, and arrives at the interface via material 2. Finally we will consider the case of multiple incident waves on the interface and show the results for the combined reflection and transmission coefficients are a superposition of the results of each individual incident wave.

A.1 Perfectly Bonded Boundary Conditions with a Single Incident Wave

To begin we examine the perfectly bonded boundary conditions for a solid-solid interface, this set of conditions is made up of the continuity of displacement (or equivalently

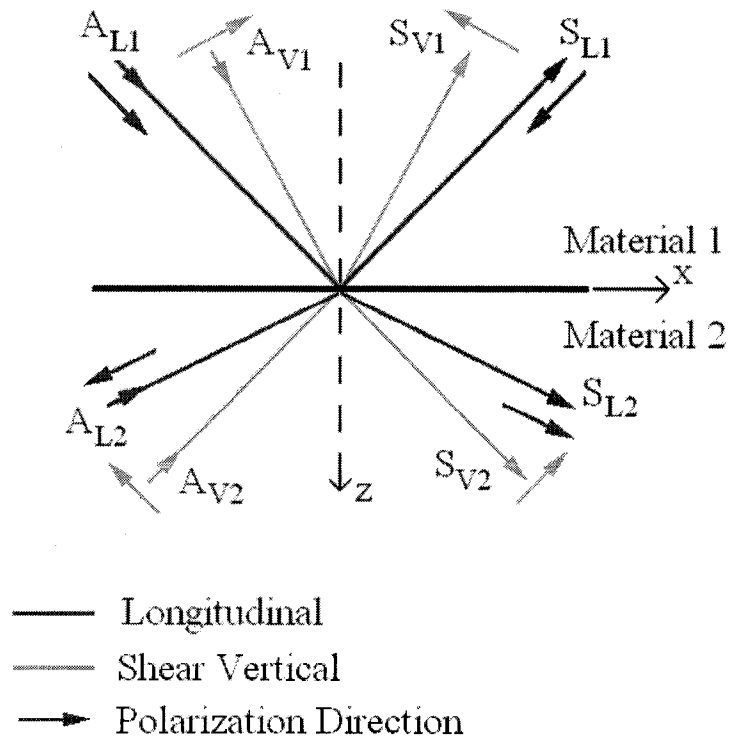

Figure A.1: Setup of Interface showing direction of polarizations

the continuity of velocity) in the directions perpendicular to the plate, and parallel to the plate (the z and x directions, respectively on our axis system)

$$v_z^{(In)} + v_z^{(1)} = v_z^{(2)}, \tag{A.1}$$

$$v_x^{(In)} + v_x^{(1)} = v_x^{(2)}, \tag{A.2}$$

As well the boundary conditions require the continuity of stress across the interface

$$T_{zz}^{(In)} + T_{zz}^{(1)} = T_{zz}^{(2)}, \tag{A.3}$$

$$T_{xz}^{(In)} + T_{xz}^{(1)} = T_{xz}^{(2)}. \tag{A.4}$$

Where the velocity and stress in these equations are evaluated at the interface, which is typically defined to be located at $(x, y, z) = (0, 0, 0)$. In the above equations the

superscripts refer to the incident wave (In), the wave in material 1 (1), and waves in material 2 (2), and the subscripts refer to the Cartesian coordinate system shown in Figure A.1. We note that if one wished to consider shear horizontal polarized waves (SH) there are additional continuity requirements for v_y, and T_{yz} across the interface, where the y axis is perpendicular to the page in Figure A.1. To continue our analysis we will first examine the velocity (v) of the wave:

$$v_i = \frac{du_i}{dt}, \tag{A.5}$$

where the index $i = x, y,$ or z. For an arbitrary polarized wave (travelling in any direction) the displacement is

$$u_i = p_i B \tag{A.6}$$

and thus

$$v_i = w p_i B', \tag{A.7}$$

where p_i is the ith component of the wave's polarization, B and the derivative B' represents the wave form for the reflected or transmitted wave and is related to the incident wave via the reflection and transmission coefficients. That is

$$B = SA, \text{ and } B' = SA' \tag{A.8}$$

where S will be our unknown coefficient (we will concern ourselves with which coefficient this is later), and $A = Af(\omega t - \mathbf{K} \cdot \mathbf{x})$ represents the incident waveform f, with angular frequency ω, and wave vector $\mathbf{K}$, and scaled by amplitude A. (Because the f is intended to denote a generic waveform, ω may more accurately be defined as the central frequency, or other representative frequency, of this waveform). In the above equations the derivative

A' (and B') represents

$$A' = \frac{\partial A}{\partial(\omega t)}. \tag{A.9}$$

Next we examine the stress components (T_{xz} and T_{zz}), for an isotropic media we have:

$$T_{zz} = (\lambda + 2\mu)(\frac{\partial u_z}{\partial x_z} + \frac{\partial u_y}{\partial x_y}), \tag{A.10}$$

$$T_{xz} = \mu\left(\frac{\partial u_x}{\partial x_z} + \frac{\partial u_z}{\partial x_x}\right). \tag{A.11}$$

The constants λ and μ are the Lamé coefficients and are related to the velocities of the media (longitudinal velocity c, and shear vertical velocity b), and the density of the media (ρ)

$$\lambda + 2\mu = \rho c^2, \tag{A.12}$$

$$\mu = \rho b^2. \tag{A.13}$$

Using these relations, and the displacement (Equation A.6) the stress components become:

$$T_{zz} = -\rho c^2 k(p_z \hat{k}_z + p_y \hat{k}_y)B' = \omega \tau_{zz} B', \tag{A.14}$$

and

$$T_{xz} = -\rho b^2 k(p_x \hat{k}_z + p_z \hat{k}_z)B' = \omega \tau_{xz} B', \tag{A.15}$$

where $\hat{k}_i$ is the ith component of unit vector of $\mathbf{K}$, k is the magnitude of $\mathbf{K}$, and the wave form B can again be related via a reflection or transmission coefficient as in equation A.8. The derivative is defined as

$$A' = \frac{\partial A}{\partial(-k_i x_j)} = \frac{\partial A}{\partial(\omega t)} \quad \text{with } i = j = x, y, \text{ or } z, \tag{A.16}$$

In equations A.14 and A.15 we have allowed the angular frequency ω from the factor k to be written explicitly ($k = \omega/c$ for the longitudinal wave, or $k = \omega/b$ for the shear

vertical wave), and have then combined all other variables into a single variable τ for simplicity. Using the results for the velocity components (Equation A.7), and the results for the stress components (Equations A.14 and A.15) in the perfectly bonded boundary conditions (Equations A.1 through A.4) yields the following matrix equation

$$\begin{bmatrix} -p_z^{L1} & -p_z^{V1} & p_z^{L2} & p_z^{V2} \\ -p_x^{L1} & -p_x^{V1} & p_y^{L2} & p_x^{V2} \\ -\tau_{xz}^{L1} & -\tau_{xz}^{V1} & \tau_{xz}^{L2} & \tau_{xz}^{V2} \\ -\tau_{zz}^{L1} & -\tau_{zz}^{V1} & \tau_{zz}^{L2} & \tau_{zz}^{V2} \end{bmatrix} \begin{bmatrix} S_{11}^{\alpha L} \\ S_{11}^{\alpha V} \\ S_{12}^{\alpha L} \\ S_{12}^{\alpha V} \end{bmatrix} = \begin{bmatrix} p_z^{In} \\ p_x^{In} \\ \tau_{xz}^{In} \\ \tau_{zz}^{In} \end{bmatrix}, \tag{A.17}$$

or more simply

$$[M][S] = [In]_{\alpha 1}. \tag{A.18}$$

Here we have now explicitly written the polarization (L and V), and the media (1 and 2) in the superscripts for our variables p and τ, as before the subscripts correspond to our Cartesian coordinate system in Figure A.1. In addition α is a placeholder the polarization of the incident wave, and $S_{cd}^{\alpha\beta}$ is the coefficient of a wave with incident polarization α in media c travelling to media d with polarization β. (Weather the coefficient is a reflection or a transmission will not be specified as we will soon be more concerned with which media the resulting waves travels in). Note in equation A.17 the common factors of ω and A' have been eliminated, and thus equation is independent of the angular frequency, and also the form of the incident wave given by $f(\omega t - \mathbf{K} \cdot \mathbf{x})$.

We have produced Equation A.17 assuming the wave is incident in material 1, if the wave was instead incident in material 2 one simply changes the boundary conditions from

the form

$$In + 1 = 2, \tag{A.19}$$

to the form

$$1 = 2 + In, \text{ or } -In + 1 = 2. \tag{A.20}$$

Thus overall there is a sign change on the incident wave, and no changes in the wave propagating in materials 1 and 2, thus the matrix equation becomes

$$[M] \begin{bmatrix} S_{21}^{\alpha L} \\ S_{21}^{\alpha V} \\ S_{22}^{\alpha L} \\ S_{22}^{\alpha V} \end{bmatrix} = -[In]_{\alpha 2}, \tag{A.21}$$

or

$$-[M][S] = [In] \tag{A.22}$$

where the matrix $[M]$ is the same as the four-by-four matrix in equation A.17. Here we note that the transmission coefficients are now the top two elements of the $[S]$ matrix, and the reflections coefficients are the bottom two elements of $[S]$, so that the coefficients correctly correspond to waves travelling in media 1 and 2, respectively.

A.2 Considering Multiple Incident Waves

Because the matrix $[M]$ is independent of the polarization, and also the direction of the wave, when two (or more) waves are incident on the interface will remain in the form

$$[M][S]_{\text{total}} = [In]_{\text{total}}, \tag{A.23}$$

where $[S]$ and $[In]$ are now a result of the multiple incident waves. This unaltered form allows the matrix equation to be written as a summation of the equations for each individual incident wave. Thus in general for the solid-solid interface where we can have four possible incident waves the equation becomes

$$[M]\left(\begin{bmatrix} S_{11}^{LL} \\ S_{11}^{LV} \\ S_{12}^{LL} \\ S_{12}^{LV} \end{bmatrix}_{+} A_{L1} + \begin{bmatrix} S_{11}^{VL} \\ S_{11}^{VV} \\ S_{12}^{VL} \\ S_{12}^{VV} \end{bmatrix}_{+} A_{V1} - \begin{bmatrix} S_{21}^{LL} \\ S_{21}^{LV} \\ S_{22}^{LL} \\ S_{22}^{LV} \end{bmatrix}_{-} A_{L2} - \begin{bmatrix} S_{21}^{VL} \\ S_{21}^{VV} \\ S_{22}^{VL} \\ S_{22}^{VV} \end{bmatrix}_{-} A_{V2}\right) \tag{A.24}$$

$$= [In]_{L1}A_{L1} + [In]_{V1}A_{V1} + [In]_{L2}A_{L2} + [In]_{V2}A_{V2}$$

Where the amplitude of the incident wave (A, with subscripts denoting media, and wave polarization) may not be related, and thus cannot be eliminated. The importance of equation A.24 is that the total coefficient ($[S]_{\text{total}}$) from multiple incident waves, can be written a sum of the solutions for each incident wave. In addition equation A.24 is independent of factors relating to the incident waveform, and thus allowing the calculation of the reflection and transmission coefficients (i.e. the calculation of the relative amplitude of the rays) to require no knowledge of the incident waveform. While this equation has been derived via the displacement coefficients, a derivation for the pressure coefficients would follow an analogous procedure and thus would yield a similar conclusion for this set of coefficients. However, when examining the energy in a superposition of waves the energy coefficients are not a summation as shown in Appendix B. Finally while we will not attempt to derive the solution for the coefficients of the solid-solid interface, one can calculate the results via the inversion of the matrix $[M]$. As well we will note that Schemeer [47] has produced the solution for the solid-solid interface, however there may

		Reflected		Transmitted	
	p_x^{In}	p_x^{R1}	p_x^{R1}	p_x^{T2}	p_x^{T2}
Incident L (+z)	+	+	+	-	-
Incident L (-z)	-	-	-	+	+
Incident V (+z)	-	+	+	-	-
Incident V (-z)	+	-	-	+	+

Table A.1: Relative signs for polarizations in the v_x continuity equation.

need to be some sign adjustments to account for due to alternate polarization definitions between our setup, and Schemerr's work.

To close we will briefly examine the relation between the set of coefficients for an incident wave travelling in the $+z$ direction from material A to B ($[S]_+$), versus an incident wave travelling in the $-z$ direction from material A to B ($[S]_-$). Here material A and B are specific materials, so that we are examining the same coefficients, but can show there will be no alterations in the coefficient's values (or signs) due to the wave travelling in the opposite direction. To show this is true, we examine the relative signs of the polarizations in the velocity (v_i) continuity equations (Equation A.7):

$$p_i^{In} + p_i^{LA} S_{11}^{\alpha L} + p_i^{VA} S_{11}^{\alpha V} = p_i^{LB} S_{22}^{\alpha L} + p_i^{VB} S_{22}^{\alpha L}. \tag{A.25}$$

where the superscripts A and B denote the specific material which the wave travels within. Examining figure A.1 shows we have chosen all p_z signs to be uniformly positive for the longitudinal polarizations, and uniformly negative for the shear vertical polarizations. Thus the v_z equations for the same for either incident wave, making the v_z continuity

equation independent on the incident wave's direction. As well, tabulating the signs for the p_y polarizations (Table A.1) shows the continuity equation are the same after an overall sign inversion, and thus again is independent on the incident wave's direction. Thus no adjustment needs to be made for the reflection or transmission coefficients due to the wave's propagation direction, and one can rewrite the equation for the total coefficients without the $\pm$ subscripts.

$$[S]_{\text{total}} = \begin{bmatrix} S_{L1} \\ S_{V1} \\ S_{L2} \\ S_{V2} \end{bmatrix}_{total} = \begin{bmatrix} S_{11}^{LL} \\ S_{11}^{LV} \\ S_{12}^{LL} \\ S_{12}^{LV} \end{bmatrix} A_{L1} + \begin{bmatrix} S_{11}^{VL} \\ S_{11}^{VV} \\ S_{12}^{VL} \\ S_{12}^{VV} \end{bmatrix} A_{V1} - \begin{bmatrix} S_{21}^{LL} \\ S_{21}^{LV} \\ S_{22}^{LL} \\ S_{22}^{LV} \end{bmatrix} A_{L2} - \begin{bmatrix} S_{21}^{VL} \\ S_{21}^{VV} \\ S_{22}^{VL} \\ S_{22}^{VV} \end{bmatrix} A_{V2}, \tag{A.26}$$

or if one specifies the coefficients as reflection (R) and transmission (T) coefficients

$$[S]_{\text{total}} = \begin{bmatrix} S_{L1} \\ S_{V1} \\ S_{L2} \\ S_{V2} \end{bmatrix}_{total} = \begin{bmatrix} R_{11}^{LL} \\ R_{11}^{LV} \\ T_{12}^{LL} \\ T_{12}^{LV} \end{bmatrix} A_{L1} + \begin{bmatrix} R_{11}^{VL} \\ R_{11}^{VV} \\ T_{12}^{VL} \\ T_{12}^{VV} \end{bmatrix} A_{V1} - \begin{bmatrix} T_{21}^{LL} \\ T_{21}^{LV} \\ R_{22}^{LL} \\ R_{22}^{LV} \end{bmatrix} A_{L2} - \begin{bmatrix} T_{21}^{VL} \\ T_{21}^{VV} \\ R_{22}^{VL} \\ R_{22}^{VV} \end{bmatrix} A_{V2}. \tag{A.27}$$

It is noted that if one had chosen an alternative definition for polarization directions some sign adjustments may have been needed. (This is the reason we have chosen the incident $-z$ travelling wave's polarization in the same relative direction to the wave travelling out from the interface in the $-z$ direction.)

A.2.1 Imperfect Boundary Conditions

It has been noted in this thesis that the imperfect boundary conditions [27, 43], also present a set of valid boundary conditions for the ray based technique. These conditions are an alteration of the perfectly bonded conditions, where the continuity of displacement in the directions perpendicular to the plate, and parallel to the plate are altered to

$$u_z^{(In)} + u_z^{(1)} = u_z^{(2)} - \frac{T_{zz}}{K_N} \tag{A.28}$$

$$u_x^{(In)} + u_x^{(1)} = u_x^{(2)} - \frac{T_{xz}}{K_T}. \tag{A.29}$$

While the continuity of the stress components remains the same, thus

$$T_{zz} = T_{zz}^{(In)} + T_{zz}^{(1)} = T_{zz}^{(2)}, \tag{A.30}$$

$$T_{xz} = T_{xz}^{(In)} + T_{xz}^{(1)} = T_{xz}^{(2)}. \tag{A.31}$$

Alternatively these boundary conditions can also be expressed in the form

$$T_{zz} = T_{zz}^{(In)} + T_{zz}^{(1)} = T_{zz}^{(2)} = K_N(u_z^{(In)} + u_z^{(1)} - u_z^{(2)}), \tag{A.32}$$

$$T_{xz} = T_{xz}^{(In)} + T_{xz}^{(1)} = T_{xz}^{(2)} = K_N(u_x^{(In)} + u_x^{(1)} - u_x^{(2)}). \tag{A.33}$$

In these sets of boundary conditions the parameters K_N and K_T are the normal and tangential (parallel to the plate) components of the rigidity of the interface. They range from infinity, the case of a fully bonded material, to zero, the case of a fully disbonded material. This fully disboned case is noted to correspond to the same conditions as those of the interface between a solid media, and a vacuum half-space (i.e we require only $T_{zz} = 0$ and $T_{xz} = 0$). The same method used for the perfectly bonded boundary conditions

can be applied to the find the reflection and transmission coefficients for the imperfect conditions. This again creates coefficients independent of the incident waveform, and the ray based amplitude calculations to be done by now utilizing these new results. While the utilization of the imperfect boundary conditions creates for interesting possibilities the results will focus on utilizing the more familiar perfectly bonded conditions, and examine only the two extremes of imperfect bonding, the fully bonded versus fully disbonded interfaces.

Appendix B: Energy in the Superposition of Acoustic Waves

In this appendix we follow Schemerr's [47] derivation for the energy in an acoustic wave, but now consider the energy in the superposition of two waves. To begin the instantaneous power per unit area (Π) delivered by a wave traveling through a surface S with normal $\hat{n}$ is

$$\Pi = -T_{kl} n_k v_l \tag{B.1}$$

with T the stress, v is the velocity, and the subscripts k, and l are place holders for x,y,z indicies. Note that in equation B.1 we follow the convention where the repeated indicies imply summation. Continuing we consider two waves with longitudinal polarization, traveling in the same media with acoustic velocity c, and on the same path in the direction $\hat{e}$. By superposition the velocity is

$$v_l = V e_l f\left(\omega t - \frac{\omega}{c}(\mathbf{x}\cdot\hat{e})\right) + \nu e_l f\left(\omega t - \frac{\omega}{c}(\mathbf{x}\cdot\hat{e})\right), \tag{B.2}$$

and the stress is

$$T_{kl} = \sigma_{kl} f\left(\omega t - \frac{\omega}{c}(\mathbf{x}\cdot\hat{e})\right) + \tau_{kl} f\left(\omega t - \frac{\omega}{c}(\mathbf{x}\cdot\hat{e})\right). \tag{B.3}$$

Here V, ν, σ_{kl}, τ_{kl}, are amplitudes of velocity and stress of the two waves, where the wave form is described by $f(\omega t - \frac{\omega}{c}(\mathbf{x}\cdot\hat{e}))$. Substituting the velocity and stress into equation B.1 yields

$$\Pi = -(\sigma_{kl} V + T_{kl}\nu + \tau_{kl} V + \tau_{kl}\nu) n_k e_l f^2, \tag{B.4}$$

or more simply

$$\Pi = -(\sigma_{kl} + \tau_{kl})(V + \nu)n_k e_l f^2. \tag{B.5}$$

The acoustic equation of motion

$$\frac{\partial T_{kl}}{\partial x_k} = \rho \frac{\partial v_l}{\partial t}. \tag{B.6}$$

is now used to relate the amplitude of the stresses (σ_{kl}, τ_{kl}) to the amplitude of the velocities (V, ν). (In equation B.6 ρ is the density of the material). Substitution of the velocity and stress of our waves (Equations B.2 and B.3) into the acoustic equation of motion (Equation B.6) yields

$$-(\sigma_{kl} + \tau_{kl})e_k = \rho c(V + \nu)e_l, \tag{B.7}$$

where we have eliminated the constant $f' = \frac{\partial f(u)}{\partial u}$ factor. Substituting this result into Equation B.5 yields

$$\Pi = \rho c[V + \nu]^2 e_l n_l f^2. \tag{B.8}$$

Finally because our surface S was in an arbitrary arrangement relative to the wave, we will now choose it to lie perpendicular to the wave, thus making $e_l n_l = \hat{e} \cdot \hat{n} = 1$, so that

$$\Pi = \rho c(V + \nu)^2 e_l n_l f^2.. \tag{B.9}$$

The superposition of two shear vertical waves yields will yield the same result as in Equation B.9, the derivation though requires the use of dot and cross product identities due to the shear vertical wave's polarization. (See Schemerr [47]). To obtain the energy the instantaneous power per unit area is integrated over the period of the wave form to obtain the intensity (I) of the wave (energy per unit area)

$$I = \rho c(V + \nu)^2 C, \tag{B.10}$$

where

$$C \equiv \int_0^T f^2, \tag{B.11}$$

is the time average of our wave form. The importance of the result in Equation B.10 is that the total intensity (and thus the total energy) is related to the total velocity squared, and not the summation of the squared velocities (i.e. not $V^2 + \nu^2$). Thus relating the amplitude of the total velocity to the amplitude of the incident waves via the reflection and transmission coefficients gives

$$I_{\alpha n} = \rho_n c_{\alpha n} (S_{\alpha n})^2, \tag{B.12}$$

where α is the polarization of the wave, n is the number of the medium in which the wave travels, and $S_{\alpha n}$ refers to the appropriate row is the total reflection and transmission coefficient from equation A.26. To find the energy of the wave, rather than the intensity, it is necessary to consider the area of the wave, examining Figure B.1 one sees that the area for each wave is related by the common area ΔA on the interface by the equation

$$\Delta A = \Delta A_{\alpha n} / cos(\theta_{\alpha n}), \tag{B.13}$$

where θ is the angle of the wave's travel, and again α is the polarization, and n is the number of the medium. We note that in our multilayered plate structure equation B.13 can be applied at each reflection calculation, and thus we can relate the area of all waves back the the incident wave, regardless of the wave's path (It was already shown the angle of the wave is path independent). Using the areas of equation B.13 the energy of the wave is

$$E_{\alpha n} = I_{\alpha n} cos(\theta_{\alpha n}) \Delta A. \tag{B.14}$$

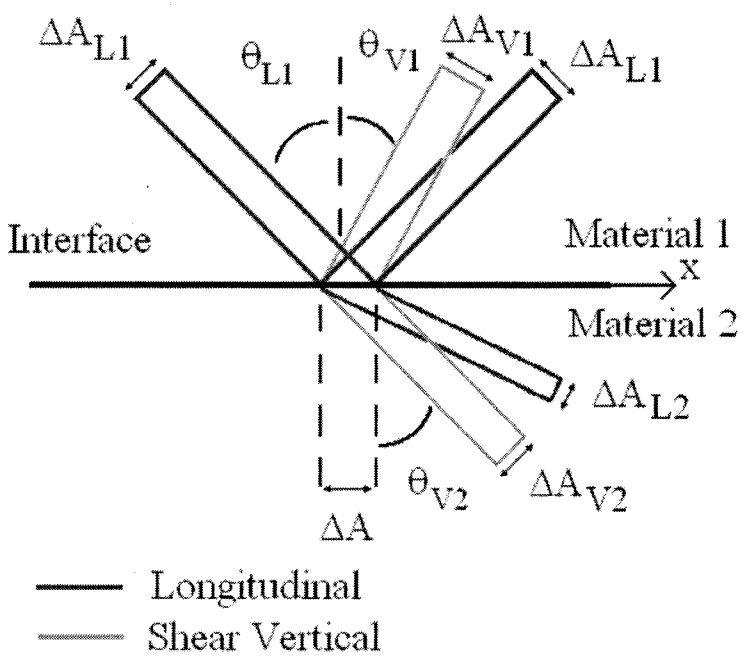

Figure B.1: Examining the relation between the areas of reflected and transmitted waves via the common area ΔA on the interface

Finally as generally energies are typically given in proportion to the energy of the incident wave, both the unknown area (ΔA), and time average of the wave form (the constant C) are eliminated giving

$$E_{\alpha n}^{\text{Relative}} = \frac{\rho_n c_n}{\rho_{In} c_{In}} \frac{cos(\theta_{\alpha n})}{cos(\theta_{In})} (S_{\alpha n})^2. \tag{B.15}$$

Thus we need not worry about the area of the wave, or its time domain properties.

B.1 A Short Word About Conservation of Energy

In the case of a single incidence wave the reflection and transmission coefficients are known to be energy conserving, that is

$$E_{Incident} = E_{Reflected} + E_{Transmitted}, \tag{B.16}$$

or when written in terms or our coefficients and other variables

$$\begin{aligned} 1 =& \frac{\rho_1 c_1}{\rho_{In} c_{In}} \frac{cos(\theta_{L1})}{cos(\theta_{In})} (S_{11}^{\alpha L})^2 + \frac{\rho_1 b_1}{\rho_{In} c_{In}} \frac{cos(\theta_{V1})}{cos(\theta_{In})} (S_{11}^{\alpha V})^2 \\ &+ \frac{\rho_2 c_2}{\rho_{In} c_{In}} \frac{cos(\theta_{L2})}{cos(\theta_{In})} (S_{12}^{\alpha L})^2 + \frac{\rho_2 b_2}{\rho_{In} c_{In}} \frac{cos(\theta_{V2})}{cos(\theta_{In})} (S_{12}^{\alpha V})^2. \end{aligned} \tag{B.17}$$

Where α is incident wave's polarization, and the common $A_{\alpha n}$ amplitude factors have been eliminated

However when we have multiple incident wave the term $(S_{\alpha n})^2$ produces energies in the form of (using the example of the longitudinal wave in material 1)

$$\begin{aligned} E_{L1} =& \frac{\rho_1 c_1}{\rho_{In} c_{In}} \frac{cos(\theta_{L1})}{cos(\theta_{In})} (S_{11}^{LL} A_{L1})^2 + \frac{\rho_1 c_1}{\rho_{In} c_{In}} \frac{cos(\theta_{L1})}{cos(\theta_{In})} (S_{11}^{VL} A_{V1})^2 \\ &+ \frac{\rho_1 c_1}{\rho_{In} c_{In}} \frac{cos(\theta_{L1})}{cos(\theta_{In})} (S_{21}^{LL} A_{L2})^2 + \frac{\rho_1 c_1}{\rho_{In} c_{In}} \frac{cos(\theta_{L1})}{cos(\theta_{In})} (S_{21}^{VL} A_{V2})^2 + \Delta E_{L1}, \end{aligned} \tag{B.18}$$

where the $(S)^2$ portions of the equation are energy conserving when summed over all reflected and transmitted waves. However, there also exists additional energy terms, which have been collected in the variable ΔE_{L1}. (This variable collects the so called 'cross-terms' from the squaring process, i.e. in $(A+B)^2 = A^2 + B^2 + 2AB$, $2AB$ is the cross-term). While the addition of ΔE terms in the energy of each wave would initially appear to cause energy conservation to not be possible, however the interrelation between the coefficients causes

$$\Delta E_{L1} + \Delta E_{V1} + \Delta E_{L2} + \Delta E_{V2} = 0 \tag{B.19}$$

Unfortunately due to the complicated reflection and transmission coefficients in the solid-solid media case it is not trivial to show this is true. However, in the process of validating our results it was verified (Section 6.1.1.1) that the total energy of the waves after each set of reflection and transmission calculations is shown to be conserved. Here it was shown

the maximum and minimum energies were identically 1 unit after each reflection, thus requiring all other energies to also be 1 unit. This was over a full range of possible angles for both a single and multilayer plate case. In addition Mathews [59] has examined the conservation of energy in the case of two waves at normal incidence on a solid-solid interface, showing the interrelations between the coefficients, and verifying energy is conserved.

Vita Auctoris

Jeff Sadler was born in 1976 in Chatham, Ontario. He graduated from Chatham Collegiate Institute in 1995. From there he went on to University of Guelph where he obtained a H. B. Sc. in Physics in 1999, and then obtained a B. Ed. at the University of Windsor in 2000. He then proceeded to obtain his Master's degree in Physics at the University of Windsor in 2003, and his Ph. D. in Physics at the University of Windsor in 2007.